(4)

AD-A201 484

FINAL TECHNICAL REPORT

Contract No. N00014-85-K-0454
$35,936.00 FY88 only
$148,168.00 Cumulative award including FY88

TO MEASURE AND CHARACTERIZE METAL CORROSION IN ELECTROLYTE SOLUTIONS BY EXPLOITING THE PROPERTIES OF SUPERCONDUCTING DEVICES

submitted by:

Professor Margaret L. A. MacVicar, P.I.
Room 8-201, Specialty Materials Laboratory
M.I.T.
Cambridge, MA 02139
(617) 253-6261

to:

Office of Naval Research

August 30, 1988

Objective of the research:

To investigate the feasibility of detecting and monitoring the magnetic field induced by currents flowing in electrolytic corrosion cells by utilizing the extreme sensitivity of Superconducting QUantum Interference Devices (SQUIDS) to magnetic fields. Measurements will be made first on the field due to static currents. However, the primary focus of the proposed research is to characterize the magnetic noise generated by corrosion cells. Not only will this initiation point allow contribution to the understanding of electrochemical noise, but it should provide a framework in which further magnetic measurements on corrosion systems can be better understood.

Technical Report

The Final Technical Report of this ONR contract award is the completed Ph.D. thesis of Dr. James G. Bellingham. The thesis represents a sophisticated scientific framework for approaching the investigation of electrochemical noise in a new manner, demonstrates the power of magnetometry to extract fundamental and practical information from magnetic fields generated by cells, and lays the groundwork for a broad range of future investigative and developmental lines of endeavor.

Presentations and Reports

1. "Detection of Magnetic Fields Generated by Electrochemical Corrosion," J.. G. Bellingham, M. L. A. MacVicar, M. Nisenoff, and P. C. Searson, J. Electrochemical Soc., 133:1753 (1986).

a

2. "Measurement of Magnetic Signatures of Electrochemical Corrosion Reactions", J. G. Bellingham, M.L.A. MacVicar, M. Nisenoff, and P. C. Searson, 170th Electrochemical Society Meeting, San Diego (October, 1986).

3. "Detection of Corrosion Currents by SQUID Magnetometry", J. G. Bellingham, M.L.A. MacVicar, and M. Nisenoff, 1986 Applied Superconductivity Conference, Baltimore (October 1986).

4. "SQUID Technology Applied to the Study of Electrochemical Corrosion", J. G. Bellingham, M.L.A. MacVicar, and M. Nisenoff, IEEE Trans Mag-23, #2: 477 (1987).

5. "Tracing Corrosion's Magnetic Field", SCIENCE NEWS 130: 132 (1986).

6. "Evidence of Corrosion", New York Times C: 10 (April 14,1987).

7. "How to See Unseen Corrosion", Technology Review 90: 80 (1987).

8. "Sensor Looks for Corrosion Damage", High Technology, p.6 (July 1987).

9. "Detecting Rust Before It Can Be Seen", Business Week, p.107 (July 20, 1987).

10. "SQUID Technology helps rust busters", London Sunday Times, p.62 (August 2, 1987).

11. "Rustbusters", Engineering News Report (August 20, 1987)

12. "Taking Corrosion's Magnetic Pulse", Science News, 133: 129 (1988)

13. "Magnetic Detection of Noise and Oscillations in an Electrochemical System", James G. Bellingham and Margaret L. A. MacVicar, Am. Assoc. for the Advancement of Science Meeting, Boston (February, 1988).

14. "Characterization of Electrochemical Reactions Using A Superconducting Magnetometer", J. G. Bellingham and M.L.A. MacVicar, American Physical Society Meeting, New Orleans (March, 1988).

15. "Electrochemical Noise Mechanisms in the Dissolution of Zn in HCl, J. G. Bellingham and M.L.A. MacVicar, American Physical Society Meeting, New Orleans (March, 1988).

16. "Measuring Reaction Rates and Other Electrochemical Parameters Using SQUID Instrumentation", J. G. Bellingham and M.L.A. MacVicar, SQUID NDE Workshop, Harper's Ferry, VA (April, 1988).

17. "Rustbusters ride into town", The Economist 307:87 (1988).

MAGNETIC DETECTION AND CHARACTERIZATION

OF ELECTROCHEMICAL NOISE PROCESSES

by

JAMES G. BELLINGHAM

Submitted to the Department of Physics
on June 17, 1988 in partial fulfillment of the requirements
for the degree of Doctor of Philosophy in
Physics

ABSTRACT

A framework relating fluctuations in an electrochemical cell to fluctuations of the fundamental thermodynamic and kinetic parameters of the system is presented. A method for extracting critical interface parameters via noise measurements, such as the charge transfer resistance, is developed. The technique, called variable load analysis, does not require perturbation of the cell with applied voltage or current. The framework suggests measurements to distinguish between different noise sources superimposed in the same signal, and to determine the mechanisms underlying the observed noise. A cell geometry with two identical electrodes connected through an external resistive load is used. Fluctuations in the current flowing between the two electrodes under "open circuit" conditions (i.e. under no applied external potential) provide the detected signal. Electrochemical Noise. (JGB)

Several fundamental noise sources are reviewed. The author proposes a treatment of catalyst number fluctuation on an electrode surface which yields a Lorentzian spectrum. Computer calcuations of noise processes due to changes in the atomistic morphology of a surface are presented employing the kinetic Ising model. Rates of dissolution demonstrate a $1/f^{0.5}$ dependence at low frequencies under the conditions studied.

Noise in an experimental system, Zn in HCl, has been examined using the developed techniques. The noise is determined to originate from the exposure of active cathodic regions on the electrode by hydrogen bubbles as they release from the surface. The exposure of the cathodic sites initiates an abrupt increase in current, which is throttled by the buildup of a gas film over the site. No evidence is found for fluctuations introduced by area fluctuations of the electrodes or hydrogen bubble induced electrolyte resistance fluctuations. The variable load analysis technique shows agreement with impedance measurements to roughly a factor of two. Variable load analysis measures charge transfer resistances 30 to 50% lower than are measured by impedance techniques for the Zn in HCl system. The experimental results are unambiguous that overall noise power cannot be used as a means to measure reaction rates, except under carefully controlled circumstances.

Thesis Supervisor: Prof. Margaret L. A. MacVicar
Massachusetts Institute of Technology

TABLE OF CONTENTS

Chapter		Page
	Abstract	2
	List of Figures	6
	List of Tables	9
1	Introduction	11
	1.1 Background	13
	1.2 Thesis Outline	15
2	Electrochemical Noise Processes: Background	17
	2.1 The Langevin Method	17
	2.2 Thermal and Shot Noise	18
	2.3 Diffusion Noise	20
	2.4 Complexing Noise	22
	2.5 Gas Evolution Noise	23
	2.6 Catalyst Number Fluctuation	26
	2.6.1 Fluctuations in the Number of Surface Impurities	27
	2.6.2 Fluctuations in γ	28
	2.6.3 A Practical Calculation of Impurity Noise	30
	2.7 Topological Noise	33
	2.7.1 Ising Model of the Interface	34
	2.7.2 Computer Model of Surface	38
3	Introduction: The Two-Electrode System	43
	3.1 General Relations for Interacting Electrodes	44
	3.1.1 Electrochemical Interface with One Reaction Process	45
	3.1.2 Electrochemical Interface with Two Reaction Processes	46
	3.1.3 Two Interacting Electrochemical Surfaces	48
	3.1.3.1 Fluctuation Relations	51
	3.2 Circuit Model For Electrochemical Cell	55
	3.2.1 Electrical Equivalents of Noise Sources	58

3.2.2 Integration of Noise Source into Corrosion Cell Circuit Model 59

3.2.3 Experimental Difficulties in Obtaining $S_m(\omega)$ versus P_t 62

3.2.4 Extracting $Z(\omega)$ via Noise Measurements 65

4 Experimental Method 67

4.1 Electrochemical System Chosen for Study 68

4.1.1 Reaction Scheme of Zn in HCl 70

4.1.2 Zn Dissolution 72

4.1.3 Cathodic Process 75

4.1.4 Experimental Parameters of Corrosion System 77

4.2 Corrosion Cell Design 77

4.2.1 Constraints Imposed by Noise Measurements 78

4.2.2 Constraints Imposed by Electrochemical Processes 79

4.2.3 The Corrosion Cell 81

4.2.4 Variable External Resistor 82

4.3 Noise Current Detection Techniques 84

4.3.1 Magnetic Coupling to Currents 84

4.3.1.1 SQUID Magnetometer 86

4.3.1.2 Coupling to Cell 89

4.3.1.3 Environmental Noise 91

4.3.1.4 Shielding 92

4.3.2 Potentiostat 93

4.3.3 Direct Voltage Measurement 95

4.4 Data Acquisition and Signal Processing of Noise Data 97

4.4.1 Data Acquisition 98

4.4.2 Signal Processing 101

4.4.2.1 Pre-FFT Data Conditioning 101

4.4.2.2 FFT Processing 104

4.4.2.3 Post FFT Power Spectra Conditioning 105

4.5 Impedance Measurement 106

4.5.1 Impedance Apparatus 107

4.5.2 Interpretation of Impedance Spectra 109

5 Results and Discussion 112
5.1 Impedance Measurements 113
5.1.1 Corrosion Rates 116
5.1.2 Temporal Dependence of Interface Parameters 117
5.1.3 Consistency of $R_{ct}C_d$ Product 117
5.2 Noise Measurements 123
5.2.1 Fluctuation Amplitude 124
5.2.1.1 Time Constant of Interaction Current Spikes 126
5.2.2 Simultaneous Measurement of Current and Voltage 128
5.2.2.1 Polarity of Current and Voltage Spikes 132
5.2.3 General Spectral Characteristics 134
5.2.4 Variable Load Noise Analysis 137
5.2.5 Current Noise Power versus Average Current 141
5.2.6 Electrolyte Conductivity versus Interaction Current 143
5.2.7 Cell Impedance versus Interaction Current 146
5.2.8 Scaling of Noise Power with Charge Transfer Resistance 149

6 Conclusions 152
6.1 Noise Processes in the Dissolution of Zn in HCl 155
6.2 Research Opportunities 157
6.2.2 Rotating Electrode Measurements 157
6.2.2 Two Electrode Impressed Current Measurements 159

Appendix A 163

References 165

LIST OF FIGURES

Figure 2.1: Dissolution of a two dimensional solid.

Figure 2.2: Power spectrum of dissolution rate fluctuations calculated using kinetic Ising model of surface.

Figure 3.1: Two electrodes connected via an external resistor.

Figure 3.2: Equivalent circuit of an electrochemical interface.

Figure 3.3: Equivalent circuit of electrochemical corrosion cell.

Figure 3.4: Equivalent circuit with three possible noise sources.

Figure 3.5: Dependence of detected current noise power on R_t.

Figure 4.1: Pourbaix diagram for system Zn-water using data from reference (1).

Figure 4.2: Corrosion rate of Zn versus pH.

Figure 4.3: Epoxy cast containing Zn electrodes.

Figure 4.4: Corrosion cell schematic.

Figure 4.5 Illustration of set-up used to detect current in corrosion cell.

Figure 4.6: Elements of a SQUID magnetometer.

Figure 4.7: A closed superconducting loop consisting of two coils.

Figure 4.8: Apparatus used for measuring corrosion currents with SQUID magnetometer.

Figure 4.9: Schematic of SQUID pickup coils and corrosion cell signal coil.

Figure 4.10: Equivalent current noise of SQUID in mu-metal shields.

Figure 4.11: Potentiostat used for measurements on corrosion cell.

Figure 4.12 Instrumentation noise of potentiostat with OP-27 operational amplifiers.

Figure 4.13: Instrumentation noise level of current measurement by voltage detection of ohmic drop across 10 kΩ resistor.

Figure 4.14: Flow diagram for data acquisition.

Figure 4.15: Attenuation resulting from analog and digital filtering for data acquisition rate of 90 Hz.

Figure 4.16: Flow chart for pre-FFT data conditioning.

Figure 4.17: Corrosion cell configuration for impedance measurement and

equivalent circuit.

Figure 4.18: Illustrations of impedance plots (not real data).

Figure 5.1: Real versus imaginary component of impedance for 6N purity Zn in 0.33 M HCl.

Figure 5.2: Bode plots of impedance of a two-surface Zn cell with 0.33 M HCl.

Figure 5.3: Electrical analog values representing best fit to impedance data.

Figure 5.4: Electrical analog values representing best fit to impedance data as a function of time.

Figure 5.5: Electrical analog values representing best fit to impedance data as a function of time.

Figure 5.6: The RC product as a function of time for the reactions depicted in figures 5.3, 5.4, and 5.5.

Figure 5.7: Current spikes in the reaction of Zn in 3.0 M HCl.

Figure 5.8: Plots of the decay portions of spikes observed for 6N purity Zn in 3.0 M HCl.

Figure 5.9: Experimental arrangement used to measure average potential drop across electrochemical interfaces of identical electrodes.

Figure 5.10: Simultaneous current and voltage measurements of 6N purity Zn reacting in 3.0 M HCl.

Figure 5.11: Power spectra of interactior current fluctuations for three different electrolyte concentrations.

Figure 5.12: Power as a function of external load.

Figure 5.13: Error and best charge transfer resistance fits for active fluctuation model (model A) and passive fluctuation model (model B).

Figure 5.14: Total power in the frequency range from 0 to 2.8 Hz plotted against the average value of the interaction current.

Figure 5.15: Simultaneous measurement of the interaction current and the high frequency impedance of the electrochemical cell.

Figure 5.16: Coherence function for interaction current and high frequency impedance.

Figure 5.17: Simultaneous measurement of the interaction current and the

high frequency impedance of the electrochemical cell.

Figure 5.18: Coherence function for interaction current and cell impedance measured at 1 kHz (top), and for randomly switched resistor (bottom).

Figure 5:19: Power versus observed charge transfer resistance for 6N purity Zn in 0.33, 1.0, and 3.0 M HCl.

Figure 6.1: Design for measuring interaction current between two identical electrodes (also refered to as the working electrodes) while applying a net current to the system.

Figure 6.2: Equivalent circuit for the biased identical electrode cell.

LIST OF TABLES

Table 2.1: Statistics for a 30 x 30 Corroding Surface

Table 3.1: Power at Low Frequencies

Table 3.2: Measured Noise Power as a Function of R_t

Table 4.1: Electrochemical Potential versus Crystalline Orientation

Table 4.2: Resistance of External Circuit in Ohms vs. Switch Positions

Table 5.1: Average Electrical Analog Values

Table 5.2: Average Corrosion Rates

Table 5.3: Deviance of Interaction Current

CHAPTER 1: INTRODUCTION

The primary contribution of this thesis is a framework relating detected noise of an electrochemical cell to fluctuations in the fundamental kinetic and thermodynamic parameters of the system. In particular, differential relations (which the author calls the fluctuation relations) are derived which describe the current or voltage fluctuation resulting from the fluctuation of a parameter like the electrode area or the forward rate of reaction.

The analysis is especially important because the relationships derived suggest a broad range of experiments which are capable of distinguishing between various electrochemical noise sources. For example, the variable load analysis technique, described in chapter three, is able to determine whether fluctuations are from a "passive" source or from an "active" source. Passive fluctuations are fluctuations in parameters like electrolyte resistance or electrode area, which do not directly describe the thermodynamic or kinetic properties of the interface. Parameters which are connected with the thermodynamic or kinetic properties of the interface (e.g. the forward rate of reaction, or the electrochemical potential) are active fluctuations. Furthermore, measurements using noise as a probe to extract critical information about the electrochemical interface such as the charge transfer resistance can be supported by the framework. These measurements have been executed in the experimental section of the thesis.

Noise generated at electrochemical interfaces provides both a probe of, and a signal from a physically complex system. The interface between metal and electrolyte or semiconductor and electrolyte is a region capable of a broad range of physical processes, most of which are poorly

understood. Many of the mechanisms responsible for surface properties at electrochemical interfaces are general mechanisms which are important for surfaces regardless of environment. Since interactions at an electrochemical interface typically influence or participate in charge transfer across the interface, the properties and dynamics of such a surface are readily accessible to experimental measurement. This makes electrochemical systems useful for the study of metal and semiconductor surfaces.

Noise provides a powerful window onto the processes which shape the electrochemical interface. Studies have used electrochemical noise to address basic issues, such as the number of electrons involved in a fundamental reaction step[1, 2, 3]. Fluctuations may also influence the properties of the interface. An example of the latter might be the initiation of pit triggered by the local breakdown of a passivating film.

A more fundamental reason for studying electrochemical noise is that corrosion processes potentially provide a laboratory for the study of non-equilibrium statistical mechanics. In a corrosion system the forward and reverse rates of the component reactions are not equal, thus the system is by definition not in equilibrium. Furthermore, electrochemical reactions are accompanied by current flow, thus fluctuations in reaction rates can be detected directly via electrical measurement. Consequently, corrosion reactions provide experimentally accessible systems for studying non-equilibrium phenomena.

One final motivation for studying electrochemical noise stems from the use of SQUID magnetometers to detect magnetic fields generated by corrosion reactions[4]. Magnetometry has the potential to be a noninvasive technique for the direct detection and characterization of

electrochemical processes. However, the easiest signal to access from the reaction is the component arising from electrochemical noise. Thus, in order to utilize the magnetometer as a practical corrosion detector, one must first be able to extract useful information from electrochemical fluctuations.

1.1 BACKGROUND

Electrochemical noise has been studied since the 1960s. The weight of the literature on the subject has been concerned with empirical examination of noise. In the context of corrosion reactions, effort has gone towards cataloging observed signatures. Attempts have been made to correlate mechanisms which are known to be occuring on electrode surfaces against observed characteristics of the noise signal. The principle reason for interest is that experimental observations have indicated a correlation between the amount of noise generated and the rate of corrosion in a given cell

Corrosion reactions have been observed to generate electrochemical noise, suggesting that noise measurements might provide a unique technique for characterizing these processes[5]. The breakdown of passive films and the initiation of pitting has been studied by several authors[6, 7, 8] as an example of a system in which the initiation of corrosion is associated with an increase in electrochemical noise. Noise has been observed to increase sharply with the initiation of pitting[6], and decrease abruptly with the addition of an inhibitor solution to the electrolyte[8]. Noise has also been studied in systems undergoing generalized corrosion[9, 10], and a trend of increasing noise power with increasing corrosion rate has been observed. Thus a technological motivation for understanding

electrochemical noise stems from the twin desires to understand and detect corrosion.

The wide range of potential noise sources in electrochemical systems invites attempts to catalog them. Gabrielli et. al.[11] suggested that noise sources could be categorized as either "microscopic" or "semi-macroscopic" depending on the amplitude of the resulting fluctuation. An alternative method of categorization is suggested by the observation that noise signals can be generated by stochastic fluctuations in the kinetics of the interface, or via fluctuations in the thermodynamic parameters which define the steady-state. This separation is somewhat artificial since the kinetic and thermodynamic variables are not necessarily independent. However it is useful conceptually, and furthermore suggests the approach the author takes to relating observed noise to fundamental processes at the interface. The author calls the first class of noise processes "rate fluctuations" and second class "parameter driven fluctuations."

Rate fluctuations in basic processes are in a sense the fundamental noise of a system. This is true because they represent the lowest noise level of the system. Shot noise in charge transfer across an interface is an example of a rate fluctuation. Thermally activated noise represent another fundamental source of fluctuations. Practical calculations of noise at a corroding interface are complicated because of the nonequilibrium nature of the reactions.

Parameter driven noise can have many different sources. Basically every variable which helps determine the reaction rate is a candidate for injection of noise to the system. Spatial and temporal variations in the temperature of the interface, and changes in the numbers of impurities at

the surface are examples of parameter fluctuations. Variation in these parameters would in turn cause the reaction rate to change. In the experiments conducted by the author, parameter driven fluctuations were by far the dominant noise source. Rate fluctuations were two to three orders of magnitude below the observed noise levels. Consequently this thesis is primarily concerned with the investigation of parameter driven noise.

Little theory exists describing the origin of electrochemical noise of either class, and that which does exist is primarily concerned with rate fluctuations. Less effort has been made to understand parameter driven noise, with the notable exception of some recent work on hydrogen evolution on electrode surfaces, discussed in chapter two. However even this work is statistical in nature, and does not approach the fundamental mechanism responsible for the fluctuations.

The study of electrochemical noise is complicated by an embarassment of riches: there are so many processes possible at an electrochemical interface that it is difficult to isolate one noise mechanism. To determine the actual source(s) of noise in a given electrochemical system, theory must predict a sufficient range of experimental observables that comparison between alternative sources can be achieved. This poses a problem: characterization of electrochemical noise has to this point consisted only of determining the dependence of noise power on frequency, which is insufficient for the comparison of theory to experiment. The fluctuation relations developed by the author for the identical electrode system provide additional degrees of freedom for such comparison.

1.2 THESIS OUTLINE

The thesis organization covers the three topics central to the study

of electrochemical noise: basic noise theory, the link between fundamental noise sources and electrical noise, and experimental results based on the theoretical framework. First, stochastic models of noise at an electrochemical interface are reviewed and several sources not previously considered in the literature are proposed. Second, relationships are developed relating microscopic fluctuations to fluctuations in the current flowing between the two electrodes. These relationships are shown to provide a particularly rich ground for extracting information about both the interface and noise at the interface. It is demonstrated that noise, in addition to providing a direct window on fundamental processes at the interface, can also be used as a probe of the interface. Finally, experimental results for the study of Zn in various concentrations of HCl are presented. The experimental results support the approach suggested by the theoretical work, and suggest a broad range of experiments for further investigating electrochemical noise.

CHAPTER 2: ELECTROCHEMICAL NOISE PROCESSES

This chapter reviews various noise sources possible at an electrochemical interface. Fluctuation mechanisms discussed in the literature are reviewed, and two new mechanism are proposed.

Two classes of noise processes were introduced in the previous chapter: rate fluctuations and parameter-driven fluctuations. Rate fluctuations are generally of much lower amplitude and are often masked by parameter-driven noise. For the author's experiments measuring current noise generated by Zn in HCl, the noise observed was generally several orders of magnitude higher than that predicted for thermal noise or shot noise. Parameter fluctuations are the obvious candidates for generating the excess noise. The thesis is primarily devoted to the investigation of parameter-driven fluctuations.

The following sections cover three mechanisms whereby the character of an electrochemical interface could be modified. Gas evolution, catalyst number fluctuation, and topography noise are all discussed. The statistics and possible spectral characteristics of each are considered.

2.1 THE LANGEVIN METHOD

The usual approach to calculating noise in electrochemical systems is to utilize Langevin[12,13,14,15,16] type theories. Central to the Langevin approach is the framing of the equation(s) of motion describing the system being considered. The fundamental noise sources are inserted into the equations, and the frequency dependence of the noise amplitude of the experimental observable can be determined after some mathematical manipulation. The utility of the technique is that it allows fluctuations in the observables to be determined from fluctuations in fundamental

quantities.

The classical example of the Langevin approach is Brownian motion[17,18]. The equations of motion for a particle undergoing Brownian motion are:

$$\dot{V} = -\gamma V + L(t)$$

The acceleration of the particle is therefore determined by the sum of a damping term and a random force, L(t). The power of the technique is that only minimal assumptions about the nature of L(t) are required to derive the correlation function for the position of the particle. The approach suggested here is applicable to a broad range of physical systems, including electrochemical interfaces. Application of the Langevin approach to a range of physical probelms is discussed by Van Kampen[12].

In order to utilize the Langevin approach, one must have some knowledge of the noise generated by the "fundamental quantities." For an electrochemical reaction, these quantities are typically the concentration of reactants in the electrolyte, the density of coverage of adsorbate on the surface, and the rate of reaction. Factors determining these quantities are the diffusion of reactants to the interface from the bulk electrolyte, the rate of adsorption, and the rate of desorption. Note that either or both the adsorption and desorption step might involve either chemical or electrochemical reactions.

2.2 THERMAL NOISE AND SHOT NOISE

The charge transfer process at an electrochemical interface generates noise due to fluctuations of the forward and reverse currents. Provided

the interface conditions (i.e. reactant concentration, etc.) remain constant, such noise is relatively simple to predict. Tyagai and Lukyanchikova[1] make the point that the noise will depend whether the surface is in equilibrium, or far from equilibrium. At equilibrium, for a surface with a single charge transfer reaction at the interface (e.g. $M^{z+} \leftrightarrow M + ze^-$), the forward and reverse reaction rates are equal. In this case Nyquist's theorem yields a spectral density of current fluctuations of:

$$S_i(f) = \frac{4kT}{R}$$

$S_i(f)$ is the spectral density of current fluctuations. Far from equilibrium, the current through the interface is sufficiently large that either the forward or reverse reaction rate becomes dominant. In this case, one has:

$$S_i(f) = 2neI$$

For a Zn corrosion rate of 15 μm/hr (typical of the experiments run by the author), the maximum noise density would be about 7×10^{-12} A/√Hz, which is several orders of magnitude lower than the observed noise.

Reactions involving the exchange of more than one electron are usually achieved in several steps. For example, a reaction in which species M is oxidized to M^{2+} might occur in two steps, the first with M going to M^+, the second with M^+ going to M^{2+}. Transfer of atoms from state M to state M^+ is not necessarily accompanied by transfer of an equal number of atoms (or the same atoms) from state M^+ to state M^{2+}. Noise

calculations must account for some degree of independence between the steps[1,20]. Such complications have been considered by Tyagai[12,21], who calculated the noise levels for multi-step reactions.

As an example of a multi-step reaction scheme, Tyagai[12] calculated the noise generated by hydrogen evolution as a function of frequency. Hydrogen was assumed to evolve via the Volmer-Heyrovsky mechanism, in which the process procedes in a discharge and then a desorption step. Tyagai found that at low frequencies the noise is equivalent to a two-electron shot noise source (i.e. $S_i(f) = 4eI$) while at high frequencies the noise is equivalent to that of a one-electron shot noise source (i.e. $S_i(f) = 2eI$). Tygai's treatment of hydrogen evolution noise ignores charging effects of the double layer, an omission corrected in a later paper[21]. Discussion of the consequences of double layer charging is defered until the next chapter.

2.3 DIFFUSION NOISE

Diffusion is the transport of particles due to random Brownian motion, and is another source of noise. Diffusion noise can manifest itself as either fluctuations in rate transport or as concentration fluctuations. If the species concerned are charged (e.g. ions in an electrolyte) the fluctuations in transport rate are detectable as current noise. Concentration fluctuations will be a natural consequence of diffusion noise, since the net flux of species in and out of a given volume fluctuates.

Diffusion noise of charged particles is different from diffusion noise of uncharged particles since space-charge effects must be taken into

account for the former. Deviations in the concentration of a charged species from the mean concentration will generate electrical forces which will tend to smooth out concentration imbalances. Such forces do not exist for uncharged species. Diffusion noise for a charged species has been calculated by Barker[20] using a transmission line model for diffusion[22]. Barker found that space-charge effects reduced diffusion noise levels below that predicted by shot noise. However Barker ignored the consequences of the existence of multiple charged species in an electrolyte. Charge imbalances caused by fluctuations in the concentration of one species could be balanced by redistribution of other charged species.

Van Vliet[23,24] has considered neutral species concentration fluctuations. Neutral species influence electrochemical reactions primarily by their availablity for participation in chemical and electrochemical processes. For example, the concentration of chemical species at the electrode determines the equilibrium electrochemical potential. Van Vliet used a Langevin approach to solve for concentration fluctuations, and therefore derives results valid only for near-equilibrium conditions. A general theory of concentration fluctuations valid for systems far from equilibrium has been advanced by Kiezer[25], but has not been incorporated into descriptions of electrochemical processes.

Experimental measurements of conductivity fluctuations in KCl and $CuSO_4$ solutions have been interpreted in terms of diffusion noise. Some disagreement in the literature exists as to whether the noise is due to mobility fluctuations[26,27] or concentration fluctuations[28,29,30]. Measurements were made across a capillary (1-20 μm diameter) filled with

electrolyte. The authors reporting mobility fluctuations observed a 1/f conductance power spectrum, while those reporting concentration fluctuations did not. de Vos et al.[28] have proposed volume flow of electrolyte as an alternative explanation for the 1/f noise Musha and Sugita[26] interpreted as mobility fluctuations.

2.4 COMPLEXING NOISE

Fluctuations due to complexing of chemical species have been investigated as a mechanism of producing concentration fluctuations, however it has not been considered as a noise source for electrochemical reactions. Investigation of $BeSO_4$[31], KCl, butyric acid, isobutyric acid aqueous solutions[32] have detected conductivity fluctuations with a 1/f spectral dependence. These have been interpreted as evidence as fluctuations in ionic species concentration[31] and as evidence of rearrangement of hydrogen bonds between water and acid molecules[32]. Kolb and Woermann[32] report that as the critical point of the isobutyric acid aqueous solution was reached, the spectral dependence approached $1/f^2$. They argue that this is evidence that the spectrum is associated with complexing of the acid molecules since the relaxation time can be expected to increase near the critical temperature.

The author suggests that complexing noise is a likely mechanism for producing noise at electrochemical interfaces. As a practical example, various zinc chloride complexes are possible for Zn ions in HCl[33]. Complexing noise will influence the interface by changing the relative abundances of the active species in the region immediately adjacent to the interface. Complexing may have a role in the the removal of metal atoms from the surface also. For example, complexing of a weakly attached zinc

surface atom with chlorine ions in the electrolyte could provide a pathway for the removal of Zn atoms in addition to the direct desorption step. The "handoff" of the Zn atom from the surface to a chlorine complex would involve the Zn atom leaving charge behind on the surface. While this thesis does not examine such mechanisms, processes of this sort should be considered.

2.5 GAS EVOLUTION NOISE

Gas bubble evolution at an electrode is possible noise source. The standard three-electrode system (using working, reference, and counter electrodes) has been used to study bubble evolution induced fluctuations. The working electrode is the electrode under investigation, the counter electrode is used for injecting current into the cell, and the reference electrode is used to measure the potential across the working electrode-electrolyte interface. Usually conditions of constant current have been employed. Under such conditions four phenomena are observed[34]. First, the bubbles introduce an additional potential drop at the working electrode surface by decreasing conductivity of the electrolyte. Second, by covering part of the working electrode surface, the bubbles increase the current density at the remaining exposed surface. This increases the overpotential of the surface. Third, the formation of bubbles reduces the solution concentration of the constituent gas, thus reducing the concentration potential. Finally, the growth and detachment of bubbles stirs the electrolyte, alleviating mass transfer problems at the interface.

Gas bubble driven convection at an electrode has been studied by Dees and Tobias[35] using a micromosaic electrode. The micromosaic electrode

consisted of a 10 x 10 array of individual electrodes measuring roughly 0.25 cm^2. Each electrode could be separately controlled and monitored via external electronics. By holding the potential of the electrodes constant through a gas bubble driven event, the fluctuation in current through each element could be monitored. Two basic types of gas bubble events were observed: bubble disengagement, and coalescence of two bubbles. Dees and Tobias noted that coalescence always occurred simultaneously with disengagement. The time for a bubble to rise to one bubble diameter above a horizontal surface is typically a tenth of a second.

Bubble detachment was generally observed to lead to a net decrease in current under the bubble, and a net increase in current near the bubble perimeter. The direction of convection under the bubble was radially in and upwards, away from the electrode. The direction of convection at the bubble perimeter was downwards and radially in. Thus the region near the perimeter of the bubble received electrolyte from the bulk, while the region under the bubble received electrolyte which previously had been at the perimeter.

Dees and Tobias[36] also studied free-convection mass transfer processes with the micromosaic electrode geometry. They were able to observe oscillations with the electrode biased in a regime in which not gas evolution occured. The convection flow rates (about 40 μm/sec) are sufficiently low that bubble driven convection is a much larger perturbation at gas evolving electrodes (convections velocities at least ten times as high ought to occur with bubble release).

Several authors[37,38,39] have noted that the formation of bubbles on the working electrode surface will change the effective electrolyte resistance as measured between the working and counter electrodes.

Theoretical study of the potential drop introduced both individual bubbles on an electrode[40] and by arrays of bubbles[41,42] have been reported. Sides and Tobias[42] have determined that void fractions of 60% will increase the electrolyte resistance by a factor of five in a gas bubble layer. Gabrielli et.al.[43] have made measurements of the impedance of a Fe surface in H_2SO_4 with a glass sphere on the surface to simulate a bubble. Since their simulated bubble had a diameter 80% the diameter of the working electrode, it is doubtful that this measurement relates to the bubbles which are typically a small fraction of an electrode diameter in size.

Gabrielli et al.[43] have constructed a model of noise based on resistance fluctuations introduced by gas evolution under either constant current or constant voltage conditions. The resistance fluctuation was assumed to grow linearly in time for a period u, at which point the bubble was assumed to detach from the surface. So, for a bubble initating at time t = 0 the change in the effective electrolyte resistance, $\Delta R(t)$, is:

$$\Delta R(t) = \begin{cases} k_v t \text{ for } 0 \leq t \leq u \\ 0 \text{ otherwise} \end{cases}$$

Here k_v is a constant reflecting the rate of growth of the bubble. The period of bubble growth, u, is assumed by Gabrielli et al. to be a random variable with a probability distribution:

$$P(u > t) = e^{-\alpha t} \quad \text{for } t > 0$$

This distribution effectively assumes that the probability that a bubble

will release at any given time is independent of the time since initiation. The power spectrum of the voltage fluctuations measured under constant current was calculated to have a frequency dependence as follows:

$$S_v(\omega) = \frac{2\lambda k_v^2}{\alpha^2} \frac{3\alpha^2 + \omega^2}{\left(\alpha^2 + \omega^2\right)^2}$$

Here λ is the nucleation rate. The power spectrum of current fluctuations under constant potential is identical, only with a different constant of proportionality. This Lorentzian-like spectrum has the features of being flat at low frequencies and falling as 1/f at high frequency.

The model proposed by Gabrielli et al.[43] can be summarized as follows. The noise originates from the nucleation and growth of a bubble. A signal from an individual bubble event consists of a linear change in voltage or current, associated with the period of bubble growth, followed by an abrupt reset to the pre-bubble signal level when the bubble releases. The bubble's effect is to change the cell impedance. The resulting power spectrum is Lorentzian-like.

2.6 CATALYST NUMBER FLUCTUATION

Some reactions at electrode surfaces are promoted by the presence of a suitable catalyst. For example, hydrogen reduction at a Zn surface is inhibited by the high hydrogen overpotential of Zn. Consequently, the presence of impurities that are cathodic relative to Zn will provide sites favorable for the hydrogen reduction process, and will therefore act as catalysts. Fluctuations in the number of catalysts on a surface will therefore be a source of noise in the rate of reaction.

Noise driven by fluctuations in numbers of catalytic sites on a surface was first proposed by Barker[20]. However, the spectral dependence of the power fluctuations derived by Barker considered the dominant source of noise to be diffusion of the catalytic species to and from the electrode surface. A flaw in this treatment is that it assumes any interaction between the catalyst species and the electrode surface is of negligible importance. The treatment given below, developed by the author, assumes the random residence time of an impurity on the surface is the dominant noise source in the cathodic reaction rate.

2.6.1 Fluctuation in the Number of Surface Impurities

The fluctuations in the number of impurities on the surface can be calculated from the rate of dissolution of the bulk and by assuming an average residence time for an impurity on the surface. The surface shall be modeled as being composed of N surface sites which may be occupied by either an impurity or a bulk atom. If the rate of anodic dissolution is r_α, and the number of impurities per bulk atom is f, then the probabilities of site transition can be written:

$$p_u = \frac{r_\alpha}{N} \frac{f}{1 + f}$$

$$p_d = \frac{r_\alpha}{\lambda N} \frac{1}{1 + f}$$

The variable p_u is the probability a given site will change from an impurity to a bulk atom, while p_d is the probability of the reverse transition. The possibility that impurities may have a different

residence time on the surface is provided for by including the variable λ. The average number of impurities on the surface is:

$$s_1 = \frac{p_d}{p_u} N$$

Using the relationships outlined above, one can construct a time series for a given site, which will take the value 1 if the site is occupied by an impurity, and 0 if occupied by a bulk atom. This record of the fluctuations of one site can be recognized as a random telegraph signal. The only difference of the above problem from the random telegraph problem solved in most communications theory text books is that the above problem does not have equal probability for an up transition as for a down transition.

In the limiting case that $f << 1$, the power density of the random telegraph wave is:

$$S(\omega) = \frac{p_u}{p_d + p_u} \left(\frac{2\, p_d}{p_d^{\,2} + \omega^2} \right)$$

Derivation of this formula is contained in Appendix A. Substituting for p_d and p_u, and accumulating the spectral density over all N surface sites yields:

$$S(\omega) = \frac{2\, r_\alpha\, f}{\left(r_\alpha / N \lambda \right)^2 + \omega^2}$$

2.6.2 Fluctuations in γ

An additional source of noise associated with impurities will derive

from fluctuations in the rate of cathodic reaction at each impurity, γ. Noise from this source can be calculated fairly easily. First, the square of the deviance is:

$$\overline{\Delta\gamma^2} = \overline{\left(\frac{\Delta n_\gamma}{\Delta t}\right)^2} = \left(\frac{1}{\Delta t}\right)^2 \overline{\Delta n_\gamma^2}$$

Assuming n_γ (the number of cathodic reactions at an impurity in time Δt) obeys Poisson statistics yields:

$$\overline{\Delta\gamma^2} = \left(\frac{1}{\Delta t}\right)^2 n_\gamma = \frac{\gamma}{\Delta t}$$

But this is calculating γ for one impurity, while in reality γ is set as an average over s_i impurities. Consequently the deviance in which one is interested is the deviance of γ averaged s_i times. Provided s_i is a large number, the central limit theorem can be used to argue that the probability distribution of γ is gaussian. Then the average can be written:

$$\overline{\Delta\gamma^2} = \frac{\gamma}{\Delta t\, s_i}$$

The resulting power density is:

$$S_\gamma(\omega) = \frac{\gamma}{\pi s_i}$$

2.6.3 A Practical Calculation of Impurity Noise

The model proposed here will assume that the weight of the cathodic process in the dissolution of the metal is carried by proton reduction, and that the bulk of the proton reduction occurs at impurity sites. Taking the rate of anodic dissolution as α (reactions per second) the anodic current from the surface can be written as:

$$i_\alpha = z\ e\ \alpha$$

The constant z is the valence of the metal ion in the electrolyte. Invoking strict charge conservation (a condition which will be relaxed later) lets the rate of the cathodic reaction be set equal to the rate of the anodic reaction:

$$i_\alpha = -i_\beta$$

Here i_β is the contribution to the current by the cathodic process.

Since the rate of the cathodic reaction is determined by impurities, we can write the simple formula for the rate of the cathodic reaction:

$$\beta = \gamma\ s_i$$

where the number of impurities on the surface is s_i, and γ is the average number of cathodic reactions (i.e. discrete proton reduction events) per second at each impurity. Thus, the cathodic current is:

$$i_\beta = z_\beta e \gamma s_i$$

There are two obvious sources of noise in this equation. First, the number of impurities on the surface can fluctuate. Second, the average number of reactions per impurity, γ, can vary. The following calculations will determine the contributions from each.

To calculate the power spectrum of the cathodic reaction, one must incorporate both of the noise mechanisms described above. The equation for the cathodic current density should be written in terms of its fluctuations:

$$i_\beta(t) = z_\beta e [\gamma_0 + \gamma_1(t)] [s_{i0} + s_{i1}(t)]$$

Here both γ and s_i have been broken into constant and time varying quantities. Making the assumptions:

$$\gamma_0^2 >> \overline{\Delta\gamma_1^2(t)} \quad \text{and} \quad s_{i0}^2 >> \overline{\Delta s_{i1}^2(t)}$$

allows one to ignore the product $\gamma_1(t)\ s_i(t)$ so that the cathodic current becomes:

$$i_\beta(t) = z_\beta e \gamma_0 s_i(t) + z_\beta e \gamma_1(t) s_{i0}$$

The resulting power spectrum is:

$$S_\beta(\omega) = 2\, r_\alpha\, f\, \frac{(z_\beta\, e\, \gamma_0)^2}{\left(r_\alpha / N\, \lambda\right)^2 + \omega^2} + \frac{(z_\beta\, e\, s_\omega)^2 \gamma_0}{\pi}$$

Assuming the cathodic process occurs almost exclusively at impurity sites allows one to write:

$$\gamma_o = \frac{r_\alpha}{f\, N}$$

After substitution into the power density we have:

$$S_\beta(\omega) = \frac{2\, r_\alpha\, (z_\beta\, e)^2}{f\left(1 + N\, \lambda\omega / r_\alpha\right)^2} + \frac{r_\alpha\, (z_\beta\, e)^2}{\pi}$$

One can use experimentally reasonable values in this relationship to determine some noise levels expected for a typical reaction. For example, consider the reaction of a Zn surface 1 mm^2 at a rate of 10 μm / hr with an impurity level (f) of 1×10^{-6}. For proton reduction (the dominant cathodic reaction at a Zn surface) $z_\beta = 2$. The following values can be calculated:

$$N = 1.7 \times 10^{13} \text{ surface sites.}$$

$$r_\alpha = 9.4 \times 10^{13} \text{ atoms / sec.}$$

The power density becomes:

$$S_\beta(\omega) = \frac{1.9 \times 10^{-17}}{1 + \left(\lambda\omega/55\right)^2} + 7.7 \times 10^{-24}$$

The units of power are in Ampere^2/Hz, while the units of frequency are rad/sec. The power is clearly dominated by the fluctuation in impurity number term in the frequency range of interest (<10^3 Hz). For a residence time five times longer than the typical bulk atom (i.e. $\lambda = 5$) the turning frequency of the Lorentzian is 1.7 Hz. The noise level at 10 Hz is 4.4×10^{-9} A/$\sqrt{\text{Hz}}$, which is about 100 time less than the noise level observed in the thesis.

The power will be decreased if the condition that all the cathodic reaction occurs at impurities is relaxed. This can be accomplished by multiplying the power spectrum by η^2. Here η represents the percentage of the cathodic reactions occuring at impurity sites.

The model described above thus provides a framework from which it may be possible to experimentally deduce the influence and statistics of impurities on the dissolution of metals in electrolytes. Both the residence time of an impurity and its "cathodic strength" should be possible to deduce from magnitude and frequency dependence of the power spectrum.

2.7 MORPHOLOGICAL NOISE

Surface morphology is usually quantified in terms of the "roughness factor." The roughness factor is the ratio of the "true" surface area to the "apparent" surface area. The true surface area is that which one might measure with a technique like capacitance measurement, or gas adsorption. The apparent surface area is that which one might measure

with a ruler. Typical roughness factors of surfaces after electrochemical polishing are about two to five. Thus, one expects that electrochemical processes should result in considerable topography on a microscopic and/or atomic scale. Furthermore, authors have noted that it often impossible to reliably electrochemically polish surfaces to the same roughness factor[44]. This would appear to imply that the roughness of the surface is, to some degree, determined by random processes.

For the purposes of the following discussion, surface topology is considered on an atomistic or microscopic scale. An example of microstructure effecting the surface topography is demonstrated by chemically etching a metal to expose grain boundaries. The grain boundaries are exposed because the different crystalline orientations have different electrochemical potentials, and therefore do not corrode at the same rate.

2.7.1 Ising Model of the Interface

An Ising model can be used to model topology dependent kinetics at an electrochemical interface. The model assumes individual surface atoms have free energies determined by the number of bonds by which they are attached to the bulk lattice. In keeping with the Ising formalism, only nearest neighbor interactions are considered. Atoms with fewer bonds are assumed to be more likely to depart, and are therefore described as more active. Thus the scale of an active site is one atom. Surface topology is important since surfaces with high degrees of topography will have more atoms with fewer bonds, and will consequently have a higher free energy.

Use of an Ising model to describe the equilibrium configuration of a monolayer on a crystal surface is described by Huang[45]. Subsequent work

has used a "kinetic Ising model" to investigate crystal growth and evaporation. The kinetic Ising model for crystal growth assumes a probabilty of desorption of an atom from a site to be proportional to exp(E(b)/kT), where E(b) is the energy as a function of the number of active bonds (i.e. nearest neighbors). The probability of adsorption of an atom to a surface site is independent of the site characteristics.

A review of kinetic Ising models is given by Gilmer[46]. Both computer models and analytical models of crystal interfaces have been used to examine growth rates as a function of crystalline orientation[46,47,48]. The consequences of defects[46] (e.g. screw dislocations) and impurities[49] on growth rates have also been investigated. The model can be used to predict relative growth rate of different crystal orientations.

A large body of literature exists on crystal growth models other than the kinetic Ising model. However the kinetic Ising model is particularly attractive for noise calculations since it describes surfaces and their evolution in terms of the fundamental populations and transition rates at the interface. Models describing the interface in more general terms are less useful for the purposes of understanding fluctuations about the steady-state of a given system. Descriptions of interface diffusiveness[50], or adoption or complex accounting techniques for tracking surface roughness[51] are examples of models not lending themselves to noise calculations.

To use the kinetic Ising model to describe an electrochemical interface, several simplifying assumptions are made. First, only the dissolution of species will be considered (i.e the reverse rate of the oxidation reaction will be assumed to be negligable). Second, the

electrolyte environment is assumed to be constant both spatially and as a function of time. Third, the lattice will be assumed to be cubic. Fourth, surface migration will not be considered. Finally, the crystalline structure of the material will be assumed to be unmodified at the surface, so that neither relaxation or reconstruction processes will be important. While none of these assumptions are necessary for the validity of the noise mechanism, they do simplify formulation of the problem.

Two physical consequences of the model can be discerned. First, random fluctuations in the number of active sites on the surface will give rise to fluctuations in the rate of corrosion of the surface. Second, the activity of the surface will be closely coupled with the surface topology (i.e. a surface with a higher degree of topology will necessarily have more atoms with fewer bonds, and will therefore have a higher activity). Since topology can be measured indirectly by measuring the area of an electrode, the model implies a link between the area of an electrode surface and the rate of dissolution. Furthermore the fluctuation in activity of the surface will be accompanied by area fluctuations.

The probability of dissolution of an atom in a time dt is:

$$p(b) = 1 - p_o \exp\left(\frac{-E_b + zeV}{kT}\right)$$

Here p_o is a constant, and E_b is the binding energy of an atom with b active bonds. The simplest form of E_b is $E_b = b\,E_1$ where E_1 is the binding energy of one bond. The energy zeV is the energy imparted on the metal ion by a potential drop of V across the electrochemical interface.

The rate of corrosion of a surface with n_b atoms having b bonds is given by:

$$r\,dt = \sum_{b=1}^{b_{max}} n_b p(b)$$

The variable n_b is the number of surface atoms with b bonds, while b_{max} denotes the largest number of bonds a surface atoms can have. The rate, r, is in units of atoms per unit time.

The method choosen by the author to implement this model is via computer simulation of a surface. A surface is constructed, and its topology is updated as it evolves in time. Two noise mechanisms can be recognized in this system. The simplest to understand is shot noise. This is to say that if the number of atoms dissolving in a time Δt is $r\Delta t$, then the actual number will fluctuate around that value with a standard deviance of $\sqrt{r\Delta t}$. The second noise mechanism derives from the fact that r depends on the values of n_b, and n_b will also fluctuate. This gives rise to noise which is in effect created by fluctuations in the activity of the surface.

Noise due to fluctuations in surface activity is illustrated in figure 2.1. The first part of figure 2.1 depicts a two dimensional solid which is exposed to an agressive medium along its top edge. The initial surface is smooth, however after a short period of time, two atoms leave the surface. Since four of the b=3 atoms have become b=2 atoms, and since $p(2) > p(3)$, the resulting surface has a higher activity. The evolution of a surface will clearly proceed in a random fashion, as will the evolution of its corrosion rate. This class of noise mechanism does not appear to have been studied in the literature, although Gilmer[52] has

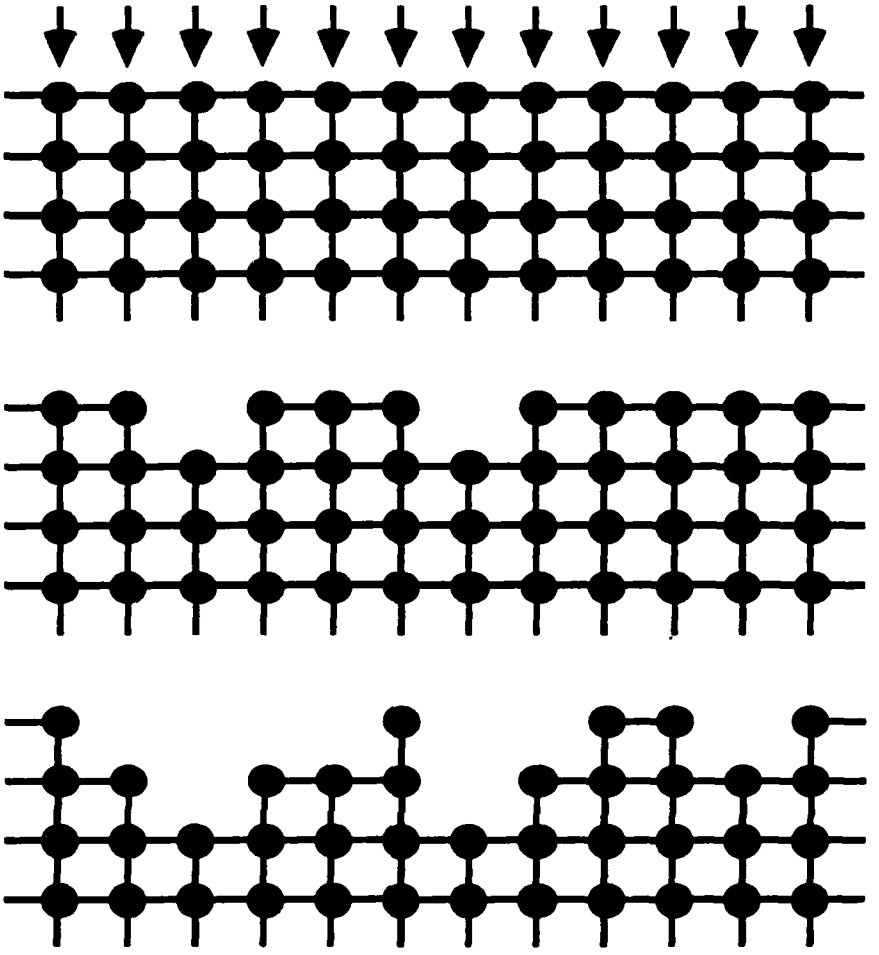

Figure 2.1: Dissolution of a two dimensional solid. Surface under attack is top edge. As reaction proceeds, the degree of surface topography increases until n_b reach steady-state values.

investigated transients in dissolution rate immediately following initiation of attack.

2.7.2 Computer Model of Surface

The author, with the help of UROP student, Scott Lordi '88, implemented programs to generate data for both two and three dimensional solids. The emphasis was on generating enough computer data for surfaces of different sizes to be able to do some statistical analysis.

The computer model simulates the evolution of the surface of a three dimensional bulk solid. The solid has a cubic lattice with all bonds having equal strength. For each time interval, the program polls every atom on the surface to determine if it enters the electrolyte. To establish whether an atom has or has not left the metal, its number of bonds is determined by counting the number of nearest neighbors (if a nearest neighbor is present, then that bond is assumed to be active). A random number is then generated (uniform distribution between 0 and 1). If the random number is less than p(b) then the atom is assumed to have left the surface, and the surface is updated. The form of p(b) which was used is that of equation (3). A value for p(1) was chosen that was sufficiently small that the probability of two adjacent atoms leaving on the same pass was negligible. All atoms with fewer than six bonds are considered. High degrees of surface structure are permitted, even undercutting. However undercutting of surface structures was observed relatively infrequently.

Thus both rate noise and surface activity fluctuations are generated. The data was used to extract the following information

- Determine the average values of n_b and r.
- Generate power spectrum of the rate of corrosion.
- Generate power spectrum from the fluctuations in surface activity.

A surface measuring 30 x 30 atoms was used for the model. Every site on the surface was tested for dissolution once during each time increment (defined as a unit time). The probability of dissolution of an atom with

b nearest neighbors per unit time was $p(b) = 0.4^b$.

Statistics for a run 15,360 time units long are summarized in table 2.1. The number r_b is the number of atoms/time unit entering solutionfrom a given surface site. All the errors are the standard deviation of the indicated quantity (as opposed to the standard error). The column τ_b lists the effective time constants of the different sites as a function of nearest neighbors.

Table 2.1: Statistics for a 30x30 Corroding Surface

b	p(b)	n_b	r_b	τ_b
1	0.4	8.95±3.16	3.61	2.5
2	0.16	61.6±8.4	9.86	6.25
3	0.064	179.1±14.6	11.4	15.6
4	0.0256	319.5±18.6	7.98	39.1
5	0.01024	514.8±19.1	5.27	97.7

Average dissolution rate: 38.21
Average surface population: 1083.9±31.7
Number of open bonds = 1982

The average number of atoms on the surface is 1084, which is 20% more atoms than on a perfectly flat surface. The number of open bonds (i.e. bonds not activated by a nearest neighbor) averages 1982. This represents a factor of two increase over the number of open bonds on a completely flat surface. This last statistic is especially important for adsorption processes. If each inactive bond is a potential adsorption site[53], then surface roughening will double the number of available sites on a surface under the conditions studied here.

Examination of the table shows that a large fraction of the

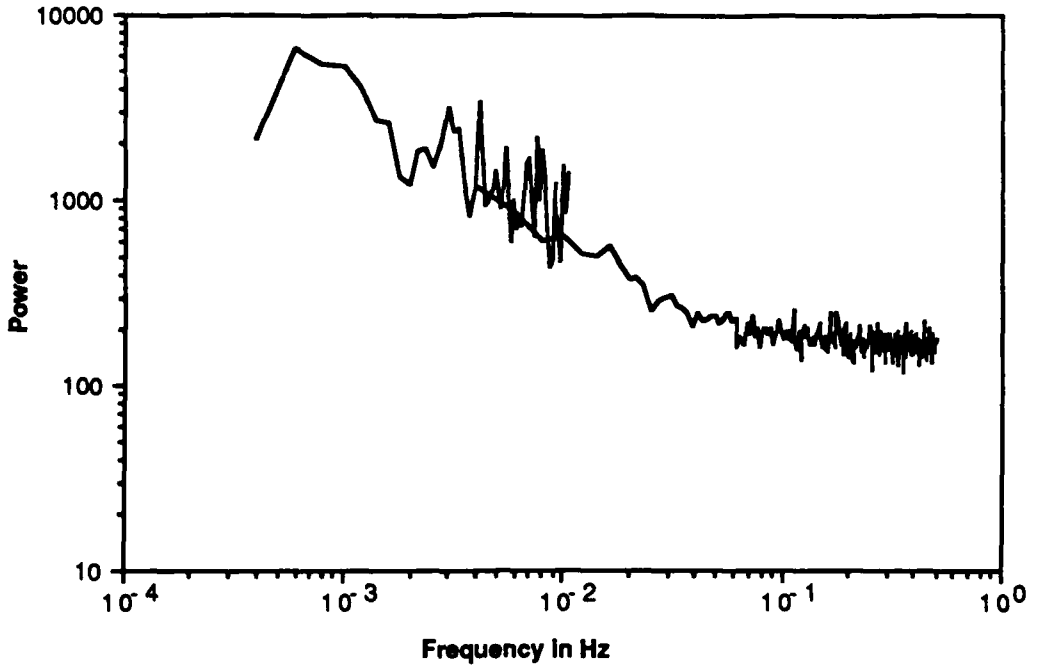

Figure 2.2: Power spectrum of dissolution rate fluctuations calculated using kinetic Ising model of surface. Spectrum was determined from same data set as was used to construct table 2.1. The spectrum shown is the composite of a high frequency spectrum and a low frequency spectrum. The power spectrum for frequencies less than 0.01 Hz was averaged over fewer individual spectra, and consequently is not as smooth.

dissolution rate is carried by atoms with few nearest neigbors. Atoms with three nearest neighbors (i.e. kink sites) contribute the most to the dissolution rate. This is significant because atoms with few nearest neighbors experience the largest fluctuations relative to their respective populations. Consequently low bonded atoms should contribute strongly to the noise process.

The power spectrum for the dissolution rate is illustrated in figure 2.2. For dissolution, shot noise is dominant at high frequencies. However at low frequencies, fluctuations in the activity of the surface appear to become sizable, giving the spectrum a $1/f^{0.5}$ dependence. This noise originates in the fluctuations of the number of active sites (i.e. low bonded atoms) on the surface.

While the kinetic Ising model should not be expected to be an accurate model of the metal surface, it does provide insight into the role atomistic scale topography might play in the production of noise. Further investigation using this model could incorporate redeposition, surface migration, and different crystal lattices.

CHAPTER 3: THE TWO-ELECTRODE SYSTEM

The utilization of a system with two identical electrodes for noise measurements provides unique opportunities for measuring the intrinsic noise of electrochemical reactions. Noise is primarily generated by the electrochemical interfaces, with some noise contribution from the electrolyte between the two electrodes. The fundamental assumption proposed by the author for two electrode systems is that the noise mechanisms at the two interfaces are statistically independent. Thus, the complication of noise injected by reference electrodes and working electrodes is avoided completely. However the relationship between the observed signal (the current flowing between the two electrodes) and the fundamental thermodynamic and kinetic parameters of the system is complicated. Making that connection is the topic of this chapter. This section will attempt to introduce the basic issues.

The relationships governing a two-electrode system are best examined in terms of the anodic and cathodic reaction rates on the two surfaces. If we call the rate (per unit area) of of the anodic process α and the rate of the cathodic process β, we can express the total current from one surface through the electrolyte to an adjacent surface (i_c, the interaction current) as:

$$i_c = 2\ e\ [A_1(\alpha_1 - \beta_1) - A_2(\alpha_2 - \beta_2)].$$

Here the subscripts are used to distinguish between reactions on the first and second surfaces. To arrive at the above formula it is assumed that charge imbalance at the surfaces induced by uneven rates of reaction will

be redistributed by a current through the electrolyte. Of course, a current of equal magnitude but opposite sign will also flow between the surfaces in the metal.

One might expect that if the the two surfaces exposed to the electrolyte were completely identical, and the concentration of the electrolyte uniform, the time averaged reaction rates would be identical on both surfaces. The equation:

$$\alpha_1 + \alpha_2 = \beta_1 + \beta_2$$

for instantaneous reaction rates should also be satisfied. This last condition ensures that there is no net transfer of charge from the metal to the electrolyte on the frequency range of interest (<100 kHz). Note that this means one can write for the time averaged values $\alpha_1 = \alpha_2 = \beta_1 = \beta_2$. Thus the time averaged exchange current should be zero. Consequently, the magnetic signals generated by the generalized corrosion reaction must derive from some electrochemical noise process. The question to be addressed is: what are the fundamental mechanisms underlying the observed noise processes?

3.1 GENERAL RELATIONS FOR INTERACTING ELECTRODES

The following pages are devoted to developing equations for the interaction current between two electrochemical interfaces. Expressions relating changes in the fundamental thermodynamic quantities of the surfaces to changes in the interaction current are developed. As a matter of terminology, the variables describing the surface are broken into two

major categories. First there are variables describing a thermodynamic or kinetic property of a given interface, e.g. the Gibbs free energy or the "jump rate." These are called the interface parameters. The other class of variables describe the electrical prcperties of the interface, e.g. the potential drop across the interface or the net reaction current. These are referred to as the electrical parameters.

A single reaction process at an electrode is considered first. The discussion is then generalized to an electrochemical interface with two reaction processes. Finally the fundamental equations for two electrodes connected via a resistor are developed. These equations are used to evaluate the fluctuation of the interaction current which results from the fluctuation of one of the interface parameters.

Only Faradaic processes at the electrode surfaces are considered in this section. Charging of the double layer is ignored until later in this chapter. Thus, the relationships developed are valid only at frequencies so low that charging of the double layer is not a factor (typically < 10 Hz for experiments described in this thesis).

3.1.1 Electrochemical Interface with One Reaction Process

For a reaction process at a single interface, the net current through the interface (i_{net}) is the sum of the anodic current (i_+) and the cathodic current (i_-). The Butler-Volmer expression is:

$$i_{net} = i_+ - i_-$$

$$i_+ = i_{eq} \frac{C_O}{C_O^*} e^{\frac{\alpha ne}{kT}(V - V_{eq})}$$

$$i_- = i_{eq} \frac{C_R}{C_R^*} e^{-\frac{(1-\alpha) ne}{kT}(V - V_{eq})}$$

The equilibrium potential for this reaction is V_{eq}, the size of the charge transfer step is n, and the equilibrium exchange current with unit concentrations of reactants (C_O and C_R) is i_{eq}. Simplification of the expression can be achieved by defining the following variables:

$$\gamma = \frac{\alpha ne}{kT}$$

$$\gamma' = \frac{(1-\alpha) ne}{kT}$$

$$i_o = i_{eq}\left(\frac{C_O}{C_O^*}\right)^{\frac{\gamma}{\gamma+\gamma'}}\left(\frac{C_R}{C_R^*}\right)^{\frac{\gamma}{\gamma+\gamma'}}$$

$$V_o = V_{eq} + \frac{1}{\gamma + \gamma'} \ln\left(\frac{C_O^* C_R}{C_O C_R^*}\right)$$

The expression for the net current then becomes:

$$i_{net} = i_o\left[e^{\gamma(V - V_o)} - e^{-\gamma'(V - V_o)}\right]$$

3.1.2 Electrochemical Interface with Two Reaction Processes

For a surface with two reaction processes, say reaction a and reaction b, the net current must be written as the sum of the anodic and cathodic currents of both reactions:

$$i_{net} = i_{+a} - i_{-a} + i_{+b} - i_{-b}$$

The subscripts a and b have been used to identify the reactions driving the current contributions. The description can be simplified if the potential of the surface is in a regime in which the anodic current of a given reaction (say reaction a) becomes very large relative to the cathodic current. This happens when V is much less than V_a ($V_a = V_o$ for reaction a). Under these circumstances i_{-a} can be neglected. If V is much greater than V_b, i_{+b} can be neglected also. Thus, the net current through the interface can be approximated by:

$$i_{net} = i_a e^{\gamma_a(V - V_a)} - i_b e^{-\gamma'_b(V - V_b)}$$

For very small excursions of voltage, i_{net} can be expanded in a Taylor series around the average voltage, V. Provided the voltage fluctuations are very small, the expansion need only be carried to first order. The effective resistance of the interface, usually called the charge transfer resistance (R_{ct}) is:

$$R_{ct}^{-1} = \frac{\partial i_{net}}{\partial V} = \gamma_a i_a e^{\gamma_a(V - V_a)} + \gamma_b i_b e^{-\gamma'_b(V - V_b)}$$

The resistance of an electrode to charge transfer is intimately connected to the corrosion properties of the metal. For an electrolyte-metal interface, the mechanism of charge transfer is exclusively electrochemical reactions at the metal surface. This is necessarily true because the conduction mechanism is different for an electrolyte and a metal. An

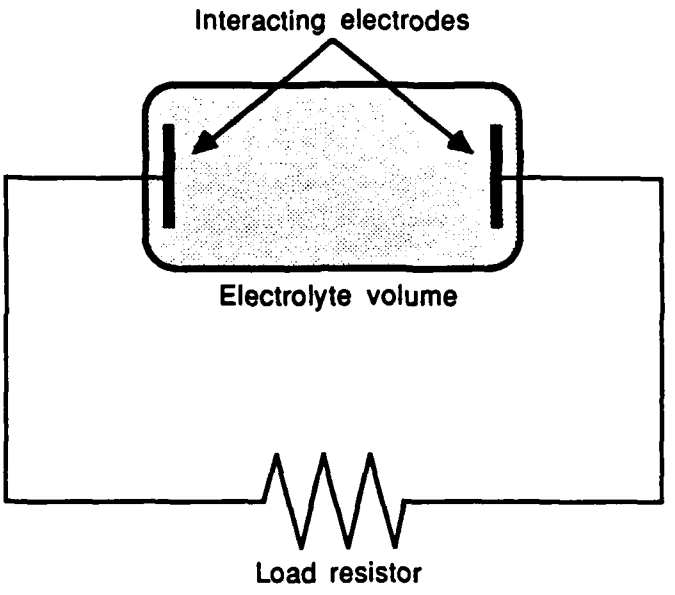

Figure 3.1: Two electrodes connected via an external resistor. Any current which flows between the two electrodes also has to flow through the external load. The electrolyte has resistance R_{aq}.

electrolyte conducts via migration of ionic species as opposed to the conduction via electrons in a metal.

3.1.3 Two Interacting Electrochemical Surfaces

A circuit containing two interacting surfaces is represented in figure 3.1. The connection between the two surfaces contains a load resistor, R_l. In the electrochemical cell the electrolyte has an effective resistance also which is written R_{aq}.

The total voltage around the circuit must be zero (Kirchhoff's voltage law), so one can write:

$$V_1 + i_c R_t - V_2 = 0$$

Here V_1 is the voltage drop across surface 1, V_2 is the drop across surface 2, and i_c is the current through the circuit. The total circuit

resistance, R_t, is equal to the sum of the external load plus the electrolyte resistance. Note that the voltage across surface 2 has a negative polarity compared with surface 1. This occurs because positive polarity is defined relative to the electrolyte-metal interface orientation rather than with respect to the circuit. Since the current through the circuit appears as a net current at each of the interfaces, one can write:

$$i_c = i_{a1}e^{\gamma_a(V_1 - V_{a1})} - i_{b1}e^{-\gamma'_b(V_1 - V_{b1})}$$

$$i_c = i_{b2}e^{-\gamma'_b(V_2 - V_{b2})} - i_{a2}e^{\gamma_a(V_2 - V_{a2})}$$

The subscripts "1" and "2" have been used to identify which surface a given variable "belongs to." The current through surface 2 has a negative polarity compared with surface 1. This occurs because positive current flows from the metal to the electrolyte in the convention for an electrochemical interface defined earlier. However, surface 2 is oriented so that a positive circuit current flows from the electrolyte to the metal. Therefore a positive circuit current corresponds to a negative electrochemical exchange current for surface 2. The same arguments can be utilized to see that the polarity of the current through surface 1 is positive.

The three preceeding equations define the variables V_1, V_2, and i_c in terms of the fundamental thermodynamic and kinetic variables of the system. Since the parameter which is experimentally measured in this system is i_c, the equations should be used to eliminate V_1 and V_2. While this proves to be analytically intractable in exact form, a relatively

good approximation can be determined.

The basic approach is to assume that the interaction current, i_c, is much less than the exchange current levels. Then the exponential parameters in the current-voltage relationships for the two surfaces can be expressed as the first two terms of the Taylor expansion of V_1 and V_2 around $i_c = 0$. The values of V_1 and V_2 at which the respective surfaces pass no net current are V_{10} and V_{20}, which can be evaluated as:

$$V_{10} = \frac{\gamma_{a1}V_{a1} + \gamma'_{b1}V_{b1} + \ln\left(\frac{i_{a1}}{i_{b1}}\right)}{\gamma_{a1} + \gamma'_{b1}}$$

$$V_{20} = \frac{\gamma_{a2}V_{a2} + \gamma'_{b2}V_{b2} + \ln\left(\frac{i_{a2}}{i_{b2}}\right)}{\gamma_{a2} + \gamma'_{b2}}$$

Expanding V_1 and V_2 around V_{10} and V_{20}, the first two non-zero terms are:

$$V_1 = V_{10} + i_c \frac{\partial V_1}{\partial i_c}\bigg|_{V_{10}} = V_{10} + i_c R_{ct1}$$

$$V_2 = V_{20} + i_c \frac{\partial V_2}{\partial i_c}\bigg|_{V_{20}} = V_{20} - i_c R_{ct2}$$

Here the charge transfer resistances of the two surfaces (R_{ct1} and R_{ct2}) are evaluated at $i_c = 0$ for each surface:

$$R_{ct1}^{-1} = -\frac{\partial i_c}{\partial V_1}\bigg|_{V_{10}} = \gamma_{a1} i_{a1} e^{\gamma_{a1}(V_{10} - V_{a1})} + \gamma_{b1} i_{b1} e^{-\gamma_{b1}(V_{10} - V_{b1})}$$

$$R_{ct2}^{-1} = \frac{\partial i_c}{\partial V_2}\bigg|_{V_{20}} = \gamma_{a2} i_{a2} e^{\gamma_{a2}(V_{20} - V_{a2})} + \gamma_{b2} i_{b2} e^{-\gamma_{b2}(V_{20} - V_{b2})}$$

Using Kirchhoff's voltage law for the circuit again, one can determine that the values of i_c, V_1, and V_2 are:

$$i_c = \frac{V_{20} - V_{10}}{R_{ct1} + R_{ct2} + R_t}$$

$$V_1 = V_{10} + \frac{R_{ct1}(V_{20} - V_{10})}{R_{ct1} + R_{ct2} + R_t}$$

$$V_2 = V_{20} - \frac{R_{ct2}(V_{20} - V_{10})}{R_{ct1} + R_{ct2} + R_t}$$

These are the equations determining the interaction current and interfacial voltages of the two electrode system. They become invalid when the interaction current approaches the corrosion currents of the interfaces.

3.1.4 Fluctuation Relations

In a noise experiment the detected quantity is the fluctuation of interaction current: $\Delta i_c(t)$. The fluctuation of i_c is typically driven by variations of some thermodynamic or kinetic parameter of the system. Some useful expressions to determine are the derivatives of i_c with respect to the the thermodynamic and kinetic parameters of the interfaces.

The derivatives allow fluctuations of a given interface variable (say surface parameter x) to be related to interaction current fluctuations. These shall be referred to as the fluctuation relations. Assuming the fluctuations are small enough that i_c has a linear dependence on x over the range of fluctuation Δx, fluctuations of i_c can be written in terms of fluctuations of x:

$$\overline{i_c} + \Delta i_c(t) = \bar{x} + \left.\frac{\partial i_c}{\partial x}\right|_{\bar{x}} \Delta x(t)$$

The barred quantities are the time averages of the indicated variables, and thus have no time dependence. The fluctuation terms, Δi_c and Δx, contain the time dependent information.

One possible source of noise might be a change in V_{a1}. Such a change might be caused by the emergence of a defect on surface 1. The object is to calculate the resulting change in the interaction current. The first step is to calculate the derivative of i_c with respect to V_{a1}. Taking the derivative of the constituent equations for the two interface system with respect to V_{a1} yields:

$$\frac{\partial V_1}{\partial V_{a1}} + R_t \frac{\partial i_c}{\partial V_{a1}} - \frac{\partial V_2}{\partial V_{a1}} = 0$$

$$\frac{\partial i_c}{\partial V_{a1}} = i_{a1}\left(\frac{\partial V_1}{\partial V_{a1}} - 1\right)\gamma_{a1} e^{\gamma_a(V_1 - V_{a1})} + i_{b1}\frac{\partial V_1}{\partial V_{a1}}\gamma_{b1} e^{-\gamma_b(V_1 - V_{b1})}$$

$$\frac{\partial i_c}{\partial V_{a1}} = -\left(i_{a2}\frac{\partial V_2}{\partial V_{a1}}\gamma_{a2} e^{\gamma_a(V_2 - V_{a2})} + i_{b2}\frac{\partial V_2}{\partial V_{a1}}\gamma_{b2} e^{-\gamma_b(V_2 - V_{b2})}\right)$$

The first two equations can be expressed in terms of R_{ct1} and R_{ct2}:

$$\frac{\partial i_c}{\partial V_{a1}} = - i_{a1} \gamma_{a1} e^{\gamma_{a1}(V_1 - V_{a1})} + \frac{1}{R_{ct1}} \frac{\partial V_1}{\partial V_{a1}}$$

$$\frac{\partial i_c}{\partial V_{a1}} = \frac{- 1}{R_{ct2}} \frac{\partial V_2}{\partial V_{a1}}$$

Solving for the derivative of i_c one finds:

$$\frac{\partial i_c}{\partial V_{a1}} = \frac{R_{ct1} i_{a1} \gamma_{a1}}{R_{ct1} + R_{ct2} + R_t} e^{\gamma_{a1}(V_1 - V_{a1})}$$

Utilizing the approximation for V_1 determined previously, one can write the relationship:

$$\frac{\partial i_c}{\partial V_{a1}} = \frac{R_{ct1} i_{a1} \gamma_{a1}}{R_{ct1} + R_{ct2} + R_t} e^{\gamma_{a1}\left(V_{10} + \frac{R_{ct1}(V_{20} - V_{10})}{R_{ct1} + R_{ct2} + R_t} - V_{a1}\right)}$$

Similar calculations can be done to determine the derivative of i_c with respect to the other interface parameters. A summary of the fluctuation relations for i_{a1}, i_{b1}, i_{a2}, i_{b2}, V_{a1}, V_{b1}, V_{a2}, and V_{b2} are given below:

$$\frac{\partial i_c}{\partial V_{a1}} = \frac{R_{ct1} i_{a1} \gamma_{a1}}{R_{ct1} + R_{ct2} + R_t} e^{\gamma_{a1}(V_1 - V_{a1})} = \frac{R_{ct1} i_{a1} \gamma_{a1}}{R_{ct1} + R_{ct2} + R_t} e^{\gamma_{a1}\left(V_{10} + \frac{R_{ct1}(V_{20} - V_{10})}{R_{ct1} + R_{ct2} + R_t} - V_{a1}\right)}$$

$$\frac{\partial i_c}{\partial V_{b1}} = \frac{- R_{ct1} i_{b1} \gamma_{b1}}{R_{ct1} + R_{ct2} + R_t} e^{-\gamma_{b1}(V_1 - V_{b1})} = \frac{- R_{ct1} i_{b1} \gamma_{b1}}{R_{ct1} + R_{ct2} + R_t} e^{-\gamma_{b1}\left(V_{10} + \frac{R_{ct1}(V_{20} - V_{10})}{R_{ct1} + R_{ct2} + R_t} - V_{b1}\right)}$$

$$\frac{\partial i_c}{\partial V_{a2}} = \frac{-R_{ct2}\, i_{a2}\, \gamma_{a2}}{R_{ct1} + R_{ct2} + R_t}\, e^{\gamma_{a2}(V_2 - V_{a2})} = \frac{-R_{ct2}\, i_{a2}\, \gamma_{a2}}{R_{ct1} + R_{ct2} + R_t}\, e^{\gamma_{a2}\left(V_{20} - \frac{R_{ct2}(V_{20} - V_{10})}{R_{ct1} + R_{ct2} + R_t} - V_{a2}\right)}$$

$$\frac{\partial i_c}{\partial V_{b2}} = \frac{R_{ct2}\, i_{b2}\, \gamma_{b2}}{R_{ct1} + R_{ct2} + R_t}\, e^{-\gamma_{b2}(V_2 - V_{b2})} = \frac{R_{ct2}\, i_{b2}\, \gamma_{b2}}{R_{ct1} + R_{ct2} + R_t}\, e^{-\gamma_{b1}\left(V_{20} - \frac{R_{ct2}(V_{20} - V_{10})}{R_{ct1} + R_{ct2} + R_t} - V_{b2}\right)}$$

$$\frac{\partial i_c}{\partial i_{a1}} = \frac{-1}{\gamma_{a1}\, i_{a1}}\, \frac{\partial i_c}{\partial V_{a1}}$$

$$\frac{\partial i_c}{\partial i_{b1}} = \frac{1}{\gamma_{b1}\, i_{b1}}\, \frac{\partial i_c}{\partial V_{b1}}$$

$$\frac{\partial i_c}{\partial i_{a2}} = \frac{-1}{\gamma_{a2}\, i_{a2}}\, \frac{\partial i_c}{\partial V_{a2}}$$

$$\frac{\partial i_c}{\partial i_{b2}} = \frac{1}{\gamma_{b2}\, i_{b2}}\, \frac{\partial i_c}{\partial V_{b2}}$$

Aqueous resistance fluctuations comprise a noise source of particular interest in gas evolving systems. As described in chapter two, bubbles on the surface decrease the effective conductivity of the electrolyte. As bubbles grow and detach from the surface, the apparent electrolyte conductivity will fluctuate. Since R_t is equal to the sum of the electrolyte resistance (R_{aq}) and the external resistor (R_1), we can write:

$$\frac{\partial i_c}{\partial R_{aq}} = \frac{\partial i_c}{\partial R_t}\, \frac{\partial R_t}{\partial R_{aq}} = \frac{\partial i_c}{\partial R_t}$$

Solving for the derivative of i_c with respect to R_t yields:

$$\frac{\partial i_c}{\partial R_t} = \frac{-i_c}{R_{ct1} + R_{ct2} + R_t} = \frac{V_{10} - V_{20}}{\left(R_{ct1} + R_{ct2} + R_t\right)^2}$$

Gas bubbles will also have the effect of blocking off part of the electrode area. Thus area fluctuations are another possible noise source. To calculate the consequences of area fluctuations on electrode 1, the equation for i_c through electrode 1 should be modified to read:

$$i_c = \frac{A_1}{A_{10}}\left(i_{a1}e^{\gamma_{a1}(V_1 - V_{a1})} - i_{b1}e^{-\gamma'_{b1}(V_1 - V_{b1})}\right)$$

Here A_{10} is the time average area of the electrode, and A_1 is the actual area. Then the fluctuation relationship can be written:

$$\frac{\partial i_c}{\partial A_1} = \frac{1}{A_{10}} \frac{i_c R_{ct1}}{R_{ct1} + R_{ct2} + R_t} = \frac{1}{A_{10}} \frac{(V_{20} - V_{10}) R_{ct1}}{(R_{ct1} + R_{ct2} + R_t)^2}$$

Two categories of noise sources emerge from the analysis. There are noise sources with a $1/(R_{ct1}+R_{ct2}+R_t)$ dependence, and those with a $1/(R_{ct1}+R_{ct2}+R_t)^2$ dependence. The first are called "active" and the second "passive" noise sources by the author. The active noise sources have their origin in fluctuations in the potentials and rate constants of of the component reactions. The passive noise sources originate from area and resistance fluctuations.

3.2 CIRCUIT MODEL FOR CORROSION CELL

Representation of the electrochemical cell in analog form has the advantage of being more intuitive, and simpler to visualize. While only an approximation for the true electrical behavior of an electrochemical reaction, the approximation is relatively good for small deviations in

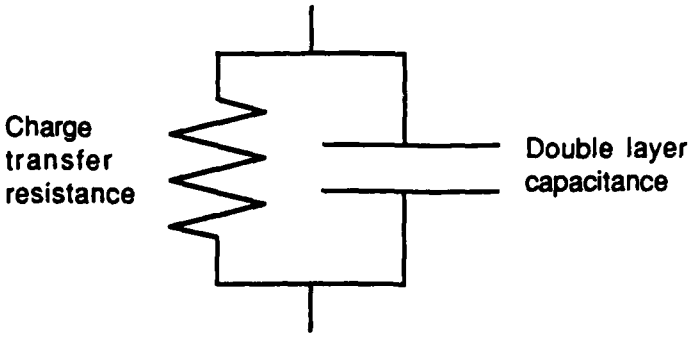

Figure 3.2: Equivalent circuit of an electrochemical interface.

current and voltage. Also, the effects of double layer charging are relatively straightforward to understand in circuit form, and consequently can be incorporated into the model at this point without complicating the problem unnecessarily.

The standard model for the electrochemical interface is a resistor in parallel with a capacitor (see figure 3.2). The resistance is the charge transfer resistance, which has been introduced earlier. Double layer charging effects are represented by the capacitor. The capacitance is referred to as the "double layer" capacitance because its origin is a double layer of charge which accumulates at the interface. One layer of charge is on the metal surface, and the other is distributed through the 10-100 Å of electrolyte immediately adjacent to the electrode. The capacitive term only approximates the effect of double layer charging. Delahay[54,55,56] has presented more rigorous calculations which do not separate charge transfer processes from double layer charging.

The electrolyte acts purely resistive for the frequency range under consideration (0.0001 Hz to 1000 Hz). Similarly, the external metal connection between the electrodes is purely resistive for the experiments described here (although this could be easily changed if desired). Thus, the equivalent circuit of the corrosion cell is simply that of two

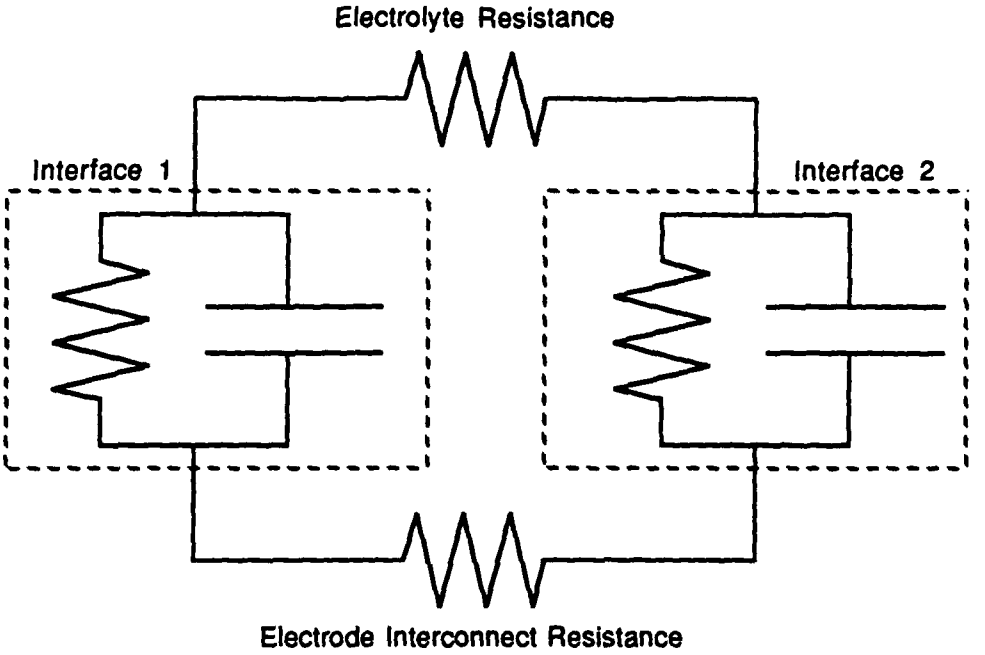

Figure 3.3: Equivalent circuit of electrochemical corrosion cell.

electrochemical interfaces connected by two resistors. Since the electrodes are identical, the charge transfer resistances will be assumed to be approximately equal for the purposes of the subsequent discussion. Figure 3.3 depicts such a circuit.

The circuit model constructed is valid for small signals only. The charge transfer resistance and double layer capacitance are actually linear circuit element approximations for a highly nonlinear process. The approximations are valid only over a small range of potential, typically tens of mV. If the potential exceeds these bounds, the nonlinearity of the electrochemical interface must be taken into account.

Accuracy of the model is tested by measuring the equivalent impedance of an interface as a function of frequency. Such measurements have been made for the electrochemical system used in this thesis (i.e. Zn in HCl). Results indicate that the model for the interface described above are valid for this system.

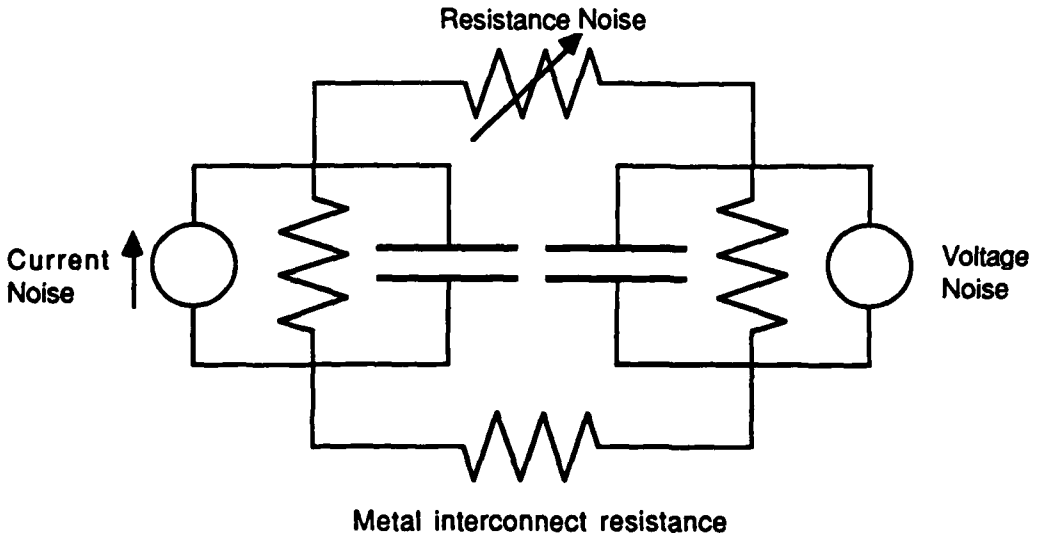

Figure 3.4: Equivalent circuit with three possible noise sources. The possibilities include: a) current source in parallel with interface, b) voltage source in parallel with interface, and c) fluctuating resistance in presence of either current or voltage source.

3.2.1 Electrical Equivalents of Noise Sources

The actual noise detected by the magnetometer depends on how the noise source electrical equivalent fits into the overall equivalent circuit of the corrosion cell. The derivative formulas calculated in the previous section can be used to determine the form of circuit analogs for the various noise sources. Several different electrical equivalents for the noise source are possible. Noise injection could be accomplished by a current source, a voltage source, or a resistance which varies randomly in time. The voltage source does not correspond to any of the noise sources derived in the previous sections, but is included for the sake of completeness. Two fluctuating resistive noise sources are possible. One possibility is fluctuations in resistance of the electrolyte, the other is fluctuations in the charge transfer resistance of the interface. The variable resistance noise source will only generate detectable current

noise if some power source is provided, for example a constant current source. In reality, resistance fluctuations will almost always be accompanied by current or voltage fluctuations. These can be represented as correlated power and resistance fluctuations.

3.2.2 Integration of Noise Source into Corrosion Cell Analog

Sources of noise in the corrosion cell fall into roughly two categories: noise generated by fluctuations in the rate of electrochemical reactions at the interface, and noise generated by changes in the conductivity of the electrolyte. An example of the first are fluctuations in corrosion rate due to emergence of defects from the receeding surface. Hydrogen bubble evolution induced electrolyte resistance noise is an example of the second.

Noise generated due to fluctuations in the rate of electrochemical processes at the interfaces are modeled as either current or voltage sources in parallel with the double layer capacitance and the charge transfer resistance. The equivalent circuit for a corrosion cell with a second electrode. Since the SQUID is sensitive to only to the interaction current which flows between the two electrodes, only current which returns through the second surface will be detected. Thus for a noise source which generates a current $S_i(\omega)$, the detected noise power, $S_m(\omega)$, will be:

$$S_m(\omega) = S_i(\omega)\left|\frac{R_{ct}}{2R_{ct} + R_t(1 + j\omega CR_{ct})}\right|^2$$

Here R_{ct} is the charge transfer resistance, R_t is the sum of the external

resistance and the electrolyte resistance, and C is the capacitance of the double layer.

If the noise generator is a voltage source parallel to R_{ct} and C, then the detected noise power, $S_m(\omega)$, is the following function of $S_v(\omega)$, the voltage noise power:

$$S_m(\omega) = S_v(\omega)\left|\frac{1 + j\omega CR_{ct}}{R_{ct} + R_t(1 + j\omega CR_{ct})}\right|^2$$

The functional dependence of the detected noise power on resistance fluctuations depends on whether the power for the noise process is provided by a current source or a voltage source. Both the current and voltage source are assumed to be in parallel with one or the other of the surfaces. Again, the logic for placing the sources in parallel is that the origin of the voltage or current is the chemical reactions at the surfaces. In the presence of a constant current i_0, $S_m(\omega)$ has the following dependence on the resistance fluctuations, $S_R(\omega)$:

$$S_m(\omega) = S_R(\omega)\left|\frac{i_0R_{ct}(1 + j\omega CR_{ct})}{\left[R_{ct} + R_t(1 + j\omega CR_{ct})\right]^2}\right|^2$$

For a constant voltage (V_0) in parallel with one of the interfaces, the detected noise power becomes:

$$S_m(\omega) = S_R(\omega)\left|\frac{V_0}{\left[R_{ct} + R_t(1 + j\omega CR_{ct})\right]^2}\right|^2$$

Resistance fluctuations are an insufficient explanation for all the noise generated by electrochemical reactions. The postulation of the constant voltage or constant current source is an unsatisfactory since it implies that the two surfaces are not behaving identically. Since the corrosion cell is constructed to have two identical electrodes, the constant current or voltage source must instead be interpreted as either manifestation of either yet another noise source or as evidence of material differences between the two electrodes. If the power source is a second noise source, then certain conditions must be met for it to be modeled as a dc current or voltage. It must contain most of its power at low frequencies compared to the resistance noise source. Such a model appears likely to be correct from measurements on corrosion cells.

A simplification can be made to the above formula for detected power, by specifying that the measurements be made at low frequency. At sufficiently low frequency, the quantity $(1 + j\omega CR_{ct})$ will approach one, and the detected noise power can be simplifed to the forms found in table 3.1. The important features of the simplified forms are as follows. As R_t becomes large compared to R_{ct}, the dependence of measured power on R_t becomes $(R_t)^{-4}$ for resistive fluctuations and $(R_t)^{-2}$ for current or voltage source fluctuations. Second, the turning point at which the measured fluctuations go from no dependence on R_t to an inverse dependence on some power of R_t is at $2R_{ct}$ for a current source and at R_{ct} for a voltage source. The method of analyzing the noise source by determining the dependence of observed noise power on the value of the external

Table 3.1: Power at Low Frequencies

	Current Source	Voltage Source
Power Source Fluctuations	$S_i(\omega)\left[\frac{R_{ct}}{2R_{ct} + R_t}\right]^2$	$S_v(\omega)\left[\frac{1}{R_{ct} + R_t}\right]^2$
Resistance Fluctuations	$S_R(\omega)\left[\frac{i_0 R_{ct}}{\left[2R_{ct} + R_t\right]^2}\right]^2$	$S_R(\omega)\left[\frac{V_0}{\left[R_{ct} + R_t\right]^2}\right]^2$

resistance is referred to as variable load analysis by the author.

The conclusion to be drawn from the preceding discussion is that the distinction between resistive fluctuations and power fluctuations can made simply by observing the functional dependence of observed noise power on R_t. Furthermore, if impedance measurements can be used to determine the value of R_{ct}, then the possibility exists that the "turning point" of the measured power versus R_t curve can be used to distinguish the power source as either a current or voltage source. Or assuming that the power source is a current source (which is physically reasonable) the charge transfer resistance can be extracted directly. Thus, in the most optimistic case, it should be possible to resolve the noise source of a reaction as any one of the four possible noise sources. Plots of the functional dependence of $S_m(\omega)$ for the various noise sources are shown in Figure 3.5.

3.2.3 Experimental Difficulties in Obtaining $S_m(\omega)$ versus R_t

Experimental problems in obtaining the $S_m(\omega)$ versus R_t curve (hereafter referred to as the power-resistance curve) include difficulties introduced by the geometry of the corrosion cell as well as uncertainties

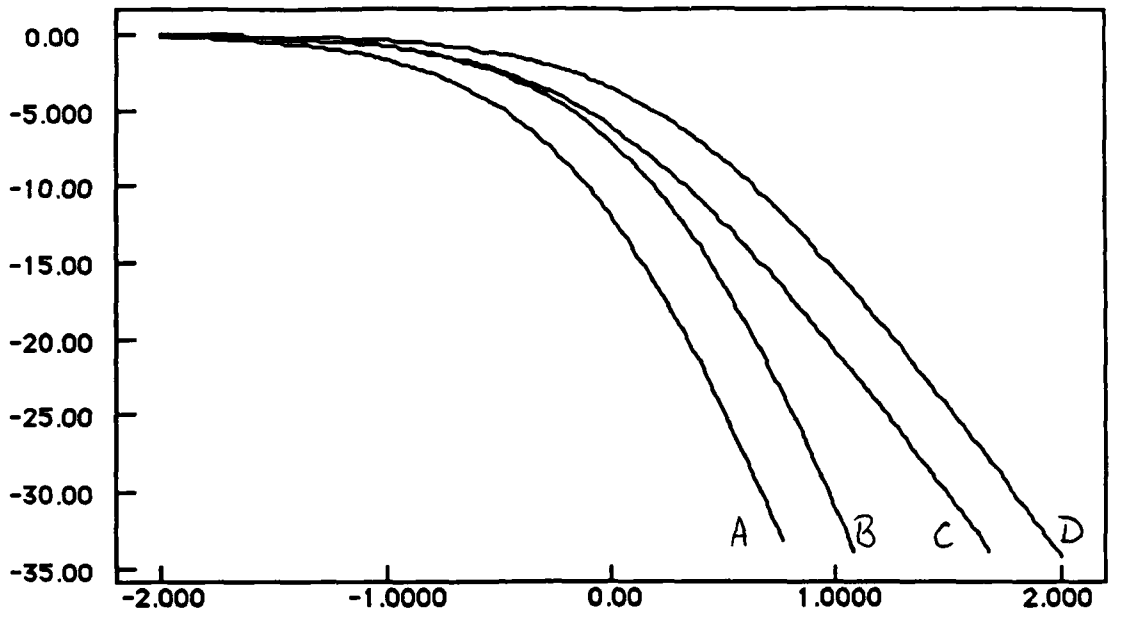

Figure 3.5: Dependence of detected current noise power on R_t. Units of power are dB, ordinate is $\log_{10}$ of (R_t/R_{ct}). All curves are normalized so that noise power at $R_t = 0$ is 0 dB. Curve A: constant voltage, resistance fluctuations. Curve B: constant current, resistance fluctuations. Curve C: voltage fluctuations. Curve D: current fluctuations.

due to the intrinsic difficulty of making noise measurements. One require is that it be possible to decrease R_t to less than R_{ct}. However R_t represents not only the resistance of the external connection between the electrodes, it also includes the resistance of the electrolyte between the two electrodes. Thus R_t cannot be less than the electrolyte resistance, a value which is determined by the geometry of the corrosion cell and by the conductivity of the electrolyte. The geometry of the corrosion cell is dictated by such concerns as keeping sufficient separation between the electrodes that they not interact in any way other than electrically. Thus, the separation between the two electrodes cannot be reduced indefinitely, which puts a lower bound on R_t.

Measurements on systems in which the dominant noise source is

resistance fluctuations provide a special challenge. The power source which drives current through the fluctuating resistor may itself be subject to fluctuations. Then the noise power measurements would change not only with changing R_t, but also with the unpredictably changing power source. One might expect a comparatively large amount of scatter on the power-resistance curves. This in turns makes the accurate extraction of R_{ct} difficult or impossible.

For systems in which the power source generates noise, determining R_{ct} with sufficient accuracy to distinguish between a voltage source and a current source may be difficult. The electrochemical interface undergoes changes which are more accurately described as evolutionary rather than stochastic. Such changes may be transient phenomena which occur immediately after the electrodes are immersed in the electrolyte. For example, as an interface evolves from a state which was stable in atmosphere, to a state which reflects the metal electrolyte interaction, the electrical properties of the surface may change. A passivation layer on the surface may dissolve, or conversely, a passivation layer may form. Such evolutionary changes may occur over a period of seconds or days. The values of R_{ct} and C may therefore change during period during which the power-resistance curve is being measured. The noise mechanism must be assumed to also be subject to the influence of evolutionary processes, and thus the intrinsic noise level may change. If such evolutionary processes are not totally predictable, they introduce an element of uncertainty to the measurement of power-resistance since the measurement takes a finite time.

3.2.4 Extracting $Z(\omega)$ via Noise Measurements

In the previous analysis, the electrochemical interface was assumed to be electrically equivalent to a resistor (the charge transfer resistance) in parallel with a capacitor (the double layer capacitance). A more general treatment of the interface is given below. In particular, no assumptions are made concerning the nature of the electrical equivalent. It is demonstrated that variable load analysis can be used to extract the impedance spectra of the system assuming knowledge of the type of noise source. To best of the author's knowledge this is the only technique which is capable of determining the impedance in a way which requires no application of current or potential to the cell. In effect, the noise generated by the interface is used to probe the interface.

The impedance for the interface can be written as $Z(\omega)$. Here the quantity $Z(\omega)$ *is a complex number which* breaks down into its real and imaginary quanitities as follows:

$$Z(\omega) = Z'(\omega) + i\, Z''(\omega)$$

The variable load technique can be use to measure the impedance of the interface by first extracting $Z(\omega)$ from the noise measurments and then applying the Kramers-Kronig transform to extract $Z'(\omega)$ and $Z''(\omega)$. Determining the value of $Z(\omega)$ can be accomplished by noting that the dependence of observed noise power on the internal noise source and on the total circuit resistance is described by the relationships in Table 3.2. Note that this is just a slight modification of Table 3.1. Thus by taking measurements of observed noise power in a frequency band $\Delta\omega$ centered on a frequency ω range of values of R_t, one can extract the average value of

$Z(\omega)$ for that frequency range. Note that the Taylor expansion of the formulas in Table I around R_t would provide the simplest form for fitting the equations to actual data.

Once $Z(\omega)$ has been determined for a wide range of frequencies, the Kramers-Kronig transform can be used to extract the values of $Z'(\omega)$ and

Table 3.2: Measured Noise Power as a Function of R_t

	Current Source	Voltage Source
Power Source Fluctuations	$S_i(\omega)\left\lvert \frac{Z(\omega)}{2\,Z(\omega) + R_t} \right\rvert^2$	$S_v(\omega)\left\lvert \frac{1}{Z(\omega) + R_t} \right\rvert^2$
Resistance Fluctuations	$S_R(\omega)\left\lvert \frac{i_0\,Z(\omega)}{\left[2\,Z(\omega) + R_t\right]^2} \right\rvert^2$	$S_R(\omega)\left\lvert \frac{V_0}{\left[Z(\omega) + R_t\right]^2} \right\rvert^2$

$Z''(\omega)$. The transformation is accomplished using the following formula:

$$\phi(\omega) = \left(\frac{2\omega}{\pi}\right) \int_0^\infty \frac{\ln\left|Z(\xi)\right|}{\xi^2 + \omega^2}\, d\xi$$

This provides complete knowledge of $Z(\omega)$.

While this techique has been outlined here to point out that it is in principle possible, two problems are encountered in practical application of the technique. First, it is assumes that the form of the noise source is known. Second, the noise levels typically drop as some power of 1/f. Consequently, noise at high frequencies may be difficult to measure with laboratory instrumentation. Finally, the assumption that the impedance of the interfaces satisfy the Kramers-Kronig relation is occasionally unfounded[57,58].

CHAPTER 4: EXPERIMENTAL METHOD

There are five areas pertinent to the experimental characterization of current noise processes which will be described by this chapter:

- Electrochemical system used for noise measurements.
- Design of the electrochemical cell.
- Noise current detection techniques.
- Data acquisition and signal processing of noise data.
- Impedance measurements for determining electrochemical parameters.

Three different techniques have been utilized for observing current fluctuations of two-electrode electrochemical cells. A SQUID magnetometer was used to sense the magnetic field generated by the interaction current in one technique. In another technique, a potentiostat (also called a current clamp), was used as a low input impedance ammeter. Finally, the simplest method was to simply measure the voltage drop induced by the current across a set resistor. Each method had its advantages and disadvantages, as shall be reviewed in this chapter.

Independent of the technique used for sensing the interaction current, data was always acquired on a personal computer. The time series data was transformed via FFT techniques, and the power spectrum determined. Various filtering techniques were used to obtain spectra uncontaminated by aliasing. Aliasing occurs when a frequency component of a signal is sampled less than twice per period. Such data is represented at an artificially low frequency, since at least two samples per period are required to uniquely determine the frequency of a signal.

Another measurement central to this thesis was determining the

impedance of the electrochemical cell. Impedance spectroscopy provided a valuable confirmation of the validity of the model employed for the electrochemical interface. The equipment assembled by the author is capable of measurements from 100 kHz down to 0.1 mHz. For the electrochemical cells used, the lowest frequency measured was typically about 1 Hz.

4.1 Electrochemical System Chosen for Study

The electrochemical system chosen for study is Zn in HCl. There were several features which make this system attractive. First is the relative simplicity of the reaction mechanisms. Second, high corrosion rates are easily obtained. Third, Zn has no stable passive films in highly acidic solutions. Last, Zn in HCl is charge transfer controlled rather than mass transport limited. A substantial drawback to the use of Zn is its high sensitivity to impurities. Also, hydrogen bubble evolution is such a large source of noise in this system that other noise sources are overwhelmed, a point which will be be discussed more fully in the next chapter.

The Pourbaix (potential-pH) diagram for Zn[59] is depicted in figure 4.1. The general conclusion to draw from the diagram is that bulk Zn is thermodynamically unstable in aqueous solutions at all values of pH at potentials more positive than -0.76 V. The stable species in acidic solutions (i.e. pH < 5.5) is Zn^{++}. While the thermodynamic data indicates a tendency to corrode, the actual corrosion properties are influenced by other factors, such as the presence or absence of a passivating film or other adsorbed layer.

Many metals which would normally corrode in a given electrolyte are

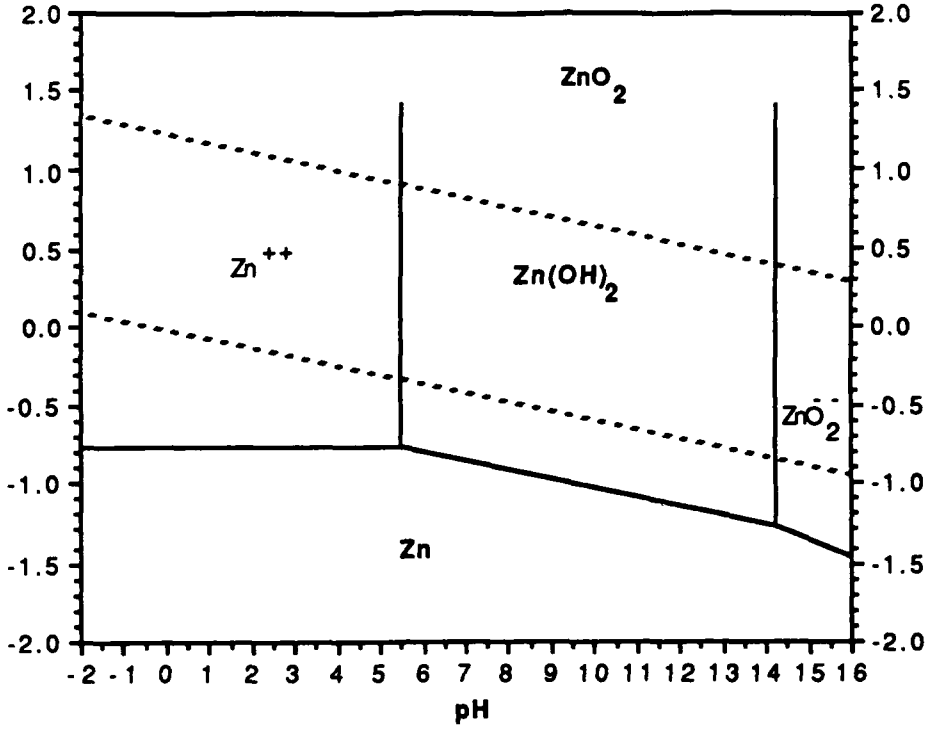

Figure 4.1: Pourbaix diagram for system Zn-water using data from reference (1). Considers ε-$Zn(OH)_2$.

protected by a strong passive layer (e.g. Al protected by an Al_2O_3 film in sea water). Even when a passivated metal does experience corrosion, the process is strongly influenced by the protective film. The film may break down only in small regions in which the exposed metal reacts rapidly, generating local current densities as high as amps/cm^2. This form of corrosion is referred to as localized corrosion. The two forms of localized corrosion typically encountered are pitting and crevice corrosion, named for the shape of the anodically reacting sites. The author chose not to study localized corrosion reactions since the dynamics of the passivation layer make noise analysis more complex. Thus, a corrosion system with no stable passive films on the electrode is preferable.

Of the passive films which are possible on Zn surfaces, $Zn(OH)_2$ is the most influential. The most stable form of zinc hydroxide is ε-$Zn(OH)_2$, one of the six crystalline forms of the substance. An amorphous form of $Zn(OH)_2$ also occurs, but it is the least stable and therefore the most soluble of the zinc hydroxides. The Pourbaix diagram (figure 4.1) shows $Zn(OH)_2$ is stable at neutral pH. Since the zinc oxides are amphoteric, they are unstable in both acid and alkaline solutions[60].

The Pourbaix diagram of figure 4.1 does not consider carbonate passive films. Such films are important in electrolytes exposed to atmosphere (which can absorb atmospheric CO_2) as well as in carbonate solutions. The Pourbaix diagram for Zn has been expanded to include the possibilities of carbonate passive films by Kannangara and Conway[44] using data from several sources[59,61,62]. Their modified diagram shows that carbonate films are not stable in the low pH regime.

To summarize the above discussion, the dissolution of Zn to Zn^{++} occurs unimpeded by a passivation layer in sufficiently concentrated acid electrolytes. Figure 4.2 shows corrosion rate as a function of pH as determined by Roetheli et al.[63]. The region of reduced corrosion rate is interpreted as evidence of a passivation layer, most likely of $Zn(OH)_2$. Consequently the corrosion of Zn in HCl is generalized in nature, rather than localized, for concentrations of HCl greater than 1×10^{-5} M (i.e. a ph of 5).

4.1.1 Reaction Scheme of Zn in HCl

The overall reaction scheme for the dissolution of Zn in HCl is given

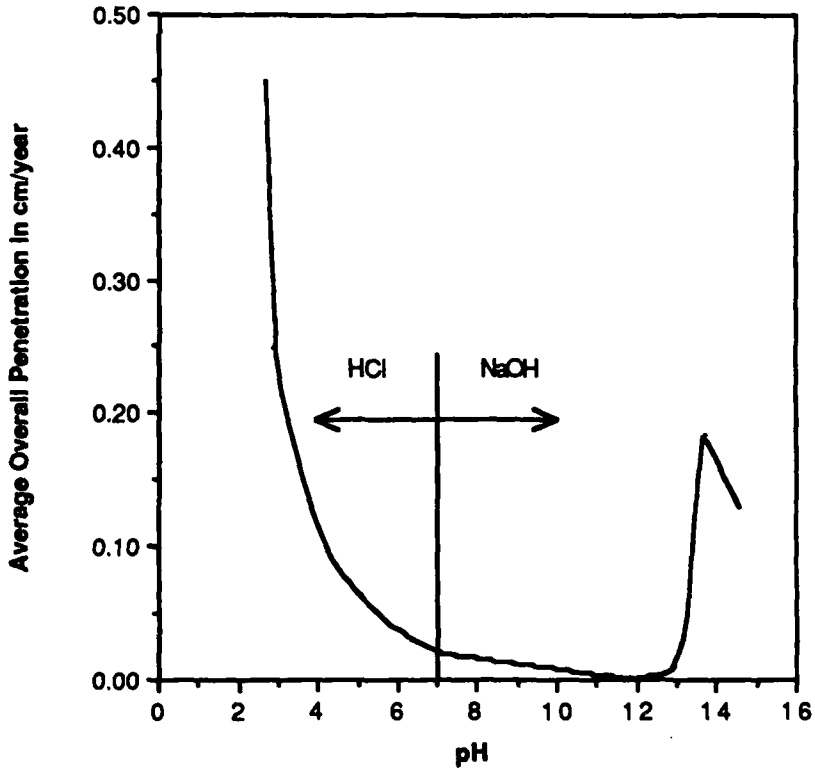

Figure 4.2: Corrosion rate of Zn versus pH[63]. *A stable film is suspected to impede corrosion in the region between pH 6 and 12.25.*

below:

$$Zn(s) + 2\ H^{+}(aq) \rightleftharpoons Zn^{++}(aq) + H_2(aq)$$

The notation (s) and (aq) indicate the presence of the species in the solid or the electrolyte, respectively. The reaction mechanism can be separated into its anodic and cathodic components, each of which progresses separately. The oxidation step is written:

$$Zn(s) \rightleftharpoons Zn^{++}(aq) + 2\ e^{-}(s)$$

The cathodic reaction is:

$$2\ H^+(aq) + 2\ e^-(s) \rightleftharpoons H_2(aq)$$

Both the anodic and the cathodic reactions likely require multiple steps for completion. For proton reduction this seems especially obvious, as a single step would require a three-way interaction between two protons and the surface. The consequences of multiple reaction steps for noise generation is discussed in the second chapter of this thesis.

4.1.2 Zn Dissolution

Several models for the actual mechanism of divalent Zn dissolution exist. The simplest involves two steps: first the transition of a neutral surface zinc atom to a singly charged adsorbed zinc atom, then the dissolution of the adsorbed ion into solution as Zn^{++}[64]. The steps can be written:

$$Zn(s) \rightleftharpoons Zn^+(ads) + e^-(s)$$
$$Zn^+(ads) \rightleftharpoons Zn^{++}(aq) + e^-(s)$$

Here (ads) identifies species adsorbed on the solid surface. An elaboration of this process, developed for Zn electrocrystallization, involves the participation of adsorbed hydrogen on the surface catalyzing the transition of adsorbed neutral zinc to zinc growth site reaction step[65-69]. The reaction pathway for dissolution is often different than that for dissolution. However, alternative pathways for dissolution have not been proposed for Zn.

A complication to understanding the anodic reaction scheme is that the apparent valence of Zn going into solution is sometimes less than two,

depending on the electrolyte[70,71,72,73]. The apparent valence is measured by driving metal into solution by application of a current. It is assumed that the dominant charge transfer mechanism at the interface is the reaction $M(s) \leftrightarrow M^{+n}(aq) + n\ e^{-}(s)$, where n is the valence of the reaction. Integration of the current over time should therefore yield the total material loss. The material lost can also be determined by weight loss measurements. Consequently, the apparent valency of the reaction can be determined from the expression:

$$n = \frac{Q A}{F \Delta m}$$

The apparent valence, n, is determined by the time integral of the applied current, Q, and the mass loss as determined by weight measurement, Δm. The constant A is simply the atomic mass of the metal.

The apparent valency of less than two for Zn is suspected to result from either disintegration of the surface[71,72] or from participation of the univalent dissolution of Zn[70,73]. Univalent zinc has not been observed in solution, consequently any entering solution must subsequently react with an oxidizer[73]. Univalent zinc dissolution is contradicted by experiments with zinc amalgam electrodes, which show no evidence of apparent valences less than two[74]. Zinc amalgam electrodes are used to prevent disintegration of zinc. Thus the lack of reduced apparent valence argues that the cause is disintegration. Typically the reduced apparent valence occurs under higher current densities (e.g. 140-250 mA/cm^2 [16]) or higher temperatures (e.g. 50°C[70,73]). At lower current densities and at room temperature, the apparent valence approaches two in aqueous salt solutions[73]. Measurements of the apparent valence in acidic $ZnCl_2$ have

determined a value of 1.98 at 30°C and unspecified current density[75].

The corrosion rates of Zn in HCl observed by the author seldom generate current densities in exceess of 10 mA/cm^2. Experiments are carried out at room temperature (i.e. ≈ 22°C). Consequently, the apparent valency is assumed to be two. This is equivalent to assuming that disintegration of the surface and any possible univalent dissolution are not important anodic processes. The apparent valence is difficult to measure in concentrated acid solutions since hydrogen evolution becomes increasingly vigorous at low pH. The additional charge transfer process at the interface invalidates the assumption that the time integral of impressed current yields faradaic metal loss. Consequently apparent valence measurements were not made by the author for the Zn in HCl system.

Crystalline orientation of the Zn electrode is known to be a factor in determining the equilibrium potential. The standard reduction potential generally used for Zn is -0.763 V at Zn^{++} concentrations of 10^{-6} mol/l[76]. The potential versus exposed crystalline orientation has been measured using a polycrystalline amalgamated Zn electrode[33] as reference, and is listed in the table below:

Table 4.1

Crystal Orientation	Potential(mV)	Anodic Current
(1011)	8	1.37
(1211)	4	1.17
(0001)	1	1.04
(1010)	0	1.00
(1120)	-2	0.93

In the last column, the factor by which the anodic current should be modified as compared to a surface with (1010) held at the same potential, is listed. The calculation assumes a transfer coefficient of 0.5 and

identical Tafel kinetics. Thus, for a polycrystalline sample of Zn undergoing dissolution, the corrosion rate on a (1011) surface should be 1.5 times that of a (1120) surface, assuming identical interface conditions. Experimentally, the effect of crystalline orientation on corrosion properties of Zn can be readily discerned since etching in HCl can be used to expose crystallite boundaries.

The effect of defects on corrosion rate of Zn in HCl have not been examined to the best of the author's knowledge. However, Abdou[77] found preferential attack along slip lines of single crystal Zn in 20% chromeric acid. The slip lines were generated by deforming the crystal under tension. Since the accelerated corrosion appeared as pitting, it is not clear whether a different local equilibrium potential or whether a weaker protective passivation layer along a slip line is responsible. Evidence that screw dislocations have substantially higher growth rates during electrocrystallization of Zn[78] argues that defects can have a substantial effect on the local equilibrium potential. Furthermore, Horn[79] has observed that screw dislocations are replaced by an etchpit under vigorous electrochemical attack.

4.1.3 Cathodic Process

The proton reduction process considered most likely for Zn surfaces is the Volmer-Heyrovsky mechanism[80,78]:

$$H^+(aq) + e^-(s) \rightleftharpoons H(ads)$$

$$H(ads) + H^+(aq) + e^-(s) \rightleftharpoons H_2(aq)$$

This mechanism involves the adsorption of a hydrogen proton onto the

surface of the electrode as the first step. The second step is the reaction of the adsorbed hydrogen atom with a proton. Desorption of the resulting hydrogen molecule occurs simultaneously with its formation. The second step is typically considered to be rate controlling.

That the cathodic reaction is dominated by hydrogen evolution is relatively simple to confirm. The reaction scheme predicts that for every mole of Zn lost, a mole of H_2 should be produced. An experiment by the author which measured the volume of gas evolved for the dissolution of a known amount of Zn found that the gas volume was within 2% of the predicted value. Since the likely alternative cathodic reactions (e.g. $2\,H_2O + O_2 + 4\,e^- \rightarrow 4\,OH^-$) do not generate gas, this indicates the hydrogen evolution reaction is the dominant cathodic process.

The hydrogen evolution reaction is sensitive to roughness of the electrode. Very large scale roughness (i.e. morphology larger than the bubble size) has the effect of increasing the surface area and therefore increasing the reaction rate, a fact which has been utilized for industrial processes. Kuhm et al.[81] examined the effect of electrode roughness and found that smoother surfaces actually raised the hydrogen reduction overpotential of the electrochemical cell. They attributed this effect to small bubbles becoming lodged in surface topography on the rough electrodes.

An outstanding feature in the corrosion of Zn is its sensitivity to impurities. That the corrosion resistance of Zn decreases with increasing impurity concentration has been understood for decades[82]. The cause of this great sensitivity to impurities is zinc's high overpotential to proton reduction. Impurities on the surface apparently lower the overall

hydrogen reduction overpotential. The suggested mechanism[82] is that cathodic impurities act as centers for proton reduction. Studies of the inhibition of Zn corrosion in HCl have confirmed the importance of the cathodic reaction in determining the corrosion rate[83,84,85].

The kinetic parameters for hydrogen reduction on Zn have not been determined with any degree of precision. This is probably because of the substantial role of impurities in influencing the cathodic reaction.

4.1.4 Experimental Parameters of Corrosion System

While experiments have been conducted for a range of Zn purities, the results described in this thesis primarily used 6N purity Zn from Johnson Matthey Inc.. All 6N purity electrodes were made using 1 mm diameter wire from the same batch. All of the results discussed in this thesis are from one electrode pair, sample LC-9.

Electrode surface preparation consisted of sanding the electrode surfaces then rinsing with methanol and distilled water. The final stage of sanding was with 600 grit silicon carbide paper. Other experiments investigating the corrosion of Zn in HCl have also used this preparation technique[85,86,87]. Further polishing of the surface is not particularly useful. The corrosion reaction removes on the order of several monolayers per second, so initial surface conditions are erased relatively rapidly.

The HCl concentrations used for this thesis were 0.33 M, 1.0 M, and 3.0 M HCl, having pH values of 0.60, 0.09, and -0.60 respectively. Solutions were mixed with reagent grade HCl and 18 MΩ water.

4.2 Corrosion Cell Design

The corrosion cells used for the experiments described in this thesis

were designed to meet several objectives: simplicity, minimal impurity contamination, small electrode size, horizontal electrode orientation, minimal convectional "cross talk" between electrodes, and low electrolyte impedance. Since a large number of experiments were done with the SQUID magnetometer, the cell was constructed with nonmagnetic materials and without extra electrical elements. These construction constraints were intended to minimize interfering sources of magnetic field.

Not all of the parameters of the cell were strictly controlled. In particular, temperature and the pressure of dissolved gas in the electrolyte were determined by ambient laboratory conditions. The judgement was made that attempting to control these two parameters would in effect introduce more complications than would be removed. Temperature control could have been achieved by a heater. However, temperature gradients and thermally-driven electrolyte circulation would have been sources of noise introduced by the "fix." Gas concentration is usually controlled by bubbling an inert gas through the cell, which would also generate a turbulent electrolyte environment. Since convection is a large potential source of noise, experimental techniques which would have generated any convective currents were avoided.

4.2.1 Constraints Imposed by Noise Measurements

For variable load analysis to be used, the turning point of the current noise power versus total load resistance (R_t) must be observable (see Figure 3.5). This in turn means it must be possible to reduce R_t to less than the electrode interface impedance. R_t is the sum of the electrolyte impedance, the external impedance, and the ammeter impedance.

Consequently, the minimum R_t possible will never be less than the electrolyte impedance. Thus, the electrolyte impedance must be less than the interface impedance for variable load analysis to be used, suggesting that the separation between the electrodes be minimized.

The techniques used for measuring the interaction current are sensitive to the impedance of the electrochemical cell plus the external circuit. Basically, the instrumentation noise is lower when the impedance of the entire system is higher (the reasons underlying this will be discussed in the instrumentation sections). The consequence for the corrosion cell design is that the electrode impedance should be as large as possible.

4.2.2 Constraints Imposed by Electrochemical Processes

Two aspects of the electrochemical process which affect the design of the corrosion cell are concentration gradients in the electrode vicinity and the evolution of H_2. Detatchment of hydrogen bubbles from the electrode surface is a source of significant convection. Since concentration gradients stemming from diffusion of reactants to and from the surface also exist near the surface, the convection also leads to changes of concentration (see chapter two). To properly investigate this source of fluctuations, factors such as orientation of the cell relative to the direction of gravity must be controlled.

Evolution and separation of hydrogen bubbles have generally been studied with horizontal electrodes (i.e. electrodes oriented face up, with gravity normal to the surface). In this orientation bubbles which detach rise away from the electrode. If the electrode is mounted vertically,

bubbles detaching from the lowest part of the electrode pass along the entire length of the interface as they rise upwards. Bubble-induced convection for vertically mounted electrodes is therefore different from that of horizontally-mounted electrodes. The electrodes were mounted face up (i.e. horizontally) for the experiments discussed in this thesis.

To prevent the overall concentration of species in the electrolyte from changing as the reaction progresses, the volume of electrolyte must be large. The significance of the Zn^{++} concentration comes from its relation to the reduction potential of Zn^{++} which shifts downwards by 0.029 mV for every factor of ten increase in concentration. The concentration of concern is that immediately adjacent to the electrode. Assuming steady state diffusion of reactants through a diffusion layer of thickness δ, one has for the concentrations change from bulk to interface:

$$\Delta C = \frac{\delta J}{2 e D_{Zn^{++}}}$$

Taking a values $J = 10$ mA/cm^2 (typical of the author's experiments with 3.0 M HCl), $D_{Zn^{++}} = 7 \times 10^{-6}$ cm^2/s[87], and $\delta = 0.01$ cm (a fairly typical value for electrochemical reactions) yields a concentration change of 0.07 M across the interface. The fastest reactions examined by the author resulted in material loss on the order of 10 mg of Zn during a single experiment. This corresponds to roughly 1.5×10^{-4} moles of material, and with the 7 ml volume used results in a shift of the bulk concentration of about 0.02 M. The concentration increase at the interface is 29%, resulting in a change of the reduction potential of 3 mV. This was considered acceptable since it represent a change in potential on the order of the potential differences between different Zn crystalline

orientations. Note that under the same conditions the concentration of H^+ changes by only 1%.

4.2.3 The Corrosion Cell

A summary of the criteria outlined in the previous two sections for the design of the corrosion cell are as follows:

1) Separation between electrodes should be small to minimize ohmic drop of electrolyte.
2) Areas of electrodes should be minimized to increase electrode impedance.
3) Electrodes should be mounted face-up for minimizing bubble-induced convection.
4) Separation of electrodes should be sufficient that ohmic drop along electrode surfaces is uniform.
5) Volume of the electrolyte should exceed 7 ml for 1 mm dia electrodes.

Well-defined electrode surfaces were required for reproducible and controllable experiments. This was achieved by embedding two parallel Zn wires in epoxy (see figure 4.3). The epoxy surface was abraided with sandpaper to expose the ends of the wires, forming two circular Zn electrodes, both coplanar with a flat epoxy surface. The Zn wires stuck out the opposite side of the epoxy cast, so that electrical connection could be made to them. Miller-Stephenson Epon epoxy, cured at 80°C for two hours, was employed as a mounting material (it is frequently used as a potting material for corrosion cells, and did not react with HCl at

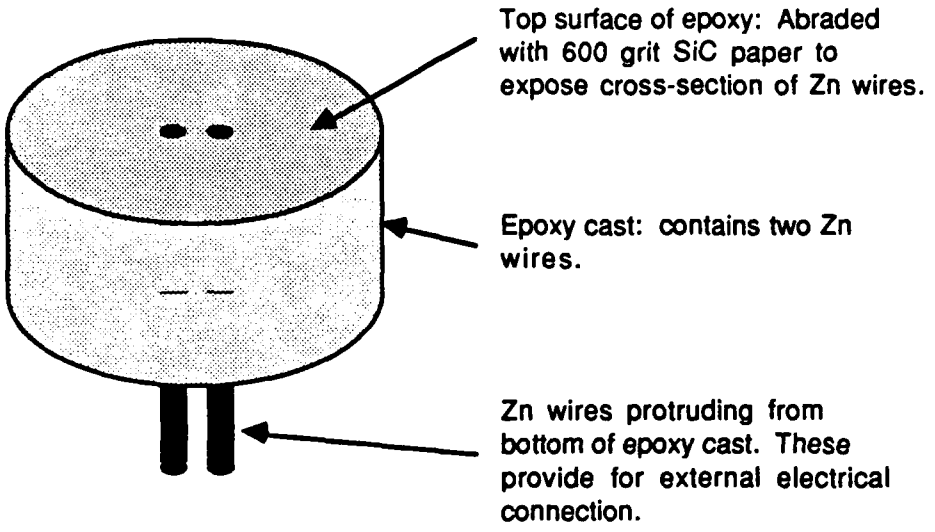

Figure 4.3: Epoxy cast containing Zn electrodes. Top surface is exposed to electrolyte. Diameter of cast is 1 inch, while electrode diameter is 1 mm.

concentrations as high as 10 M).

The corrosion cell was made from a two inch diameter teflon rod. Teflon was chosen because it is relatively inert chemically and is easy to machine. Figure 4.4 is a schematic of the corrosion cell. The electrolyte volume was a 11/16 inch diameter hole, penetrating the teflon rod from the bottom. A smaller 1/4 inch hole created an access to the electrolyte chamber from the top. A lip around the opening of the larger bottom hole provided a seal against which the epoxy sample could be pressed. Because teflon flows under pressure, the teflon-epoxy seal was both air-tight and water-tight. A plexiglass frame, secured by nylon screws to the electrolyte volume, held the epoxy firmly against the teflon seal.

4.2.4 Variable External Resistor

A requirement of the variable load experiments was that the corrosion cell circuit include a resistance element of which the value could be

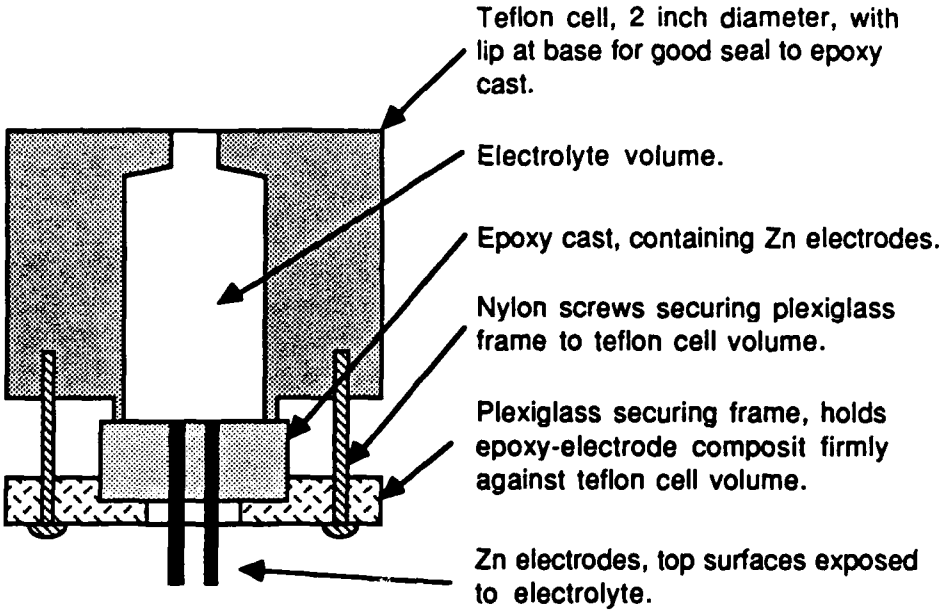

Figure 4.4: Corrosion cell schematic. Cross section of a cylindrical teflon corrosion cell, with a cylindrical inner volume. A plexiglass securing frame holds the sample firmly against the base of the teflon volume. Nylon screws are used to clamp the securing frame in place. A hole at the top of the teflon chamber prevents the pressure from building due to the evolution of hydrogen gas and provides easy access to the electrolyte volume. The cell was oriented so that the electrode surfaces were at the bottom of the chamber.

changed. A combination of switches and resistors were used to supply a range of discrete resistance values. Metal thin film resistors were used because of their low noise characteristics (e.g. granular carbon resistors exhibit high levels of 1/f noise). Switches with gold plated contacts were used because gold does not form strong passive films, and therefore gives more reliable, low noise contacts.

Ideally a method which would have allowed the continuous variation of the resistance from very low values to very high values would have been preferable. However resistance elements which can be varied continuously are either noisy (e.g. potentiometers) or are not capable of supplying very low resistances (e.g. FET based switches).

Table 4.2:

Resistance of External Circuit in Ohms vs. Switch Positions

	Switch(1): 1	Switch(1): 2	Switch(1): 3
Switch(2): 1	0.0	49.6	8.3
Switch(2): 2	2320	10,010	5010
Switch(2): 3	87.6	910	221

Note: Switch(n): m notation means switch number n at position m.

4.3 Noise Current Detection Techniques

The initial measurements by the author of current noise in electrochemical systems used a SQUID magnetometer to detect the magnetic field generated by corrosion currents. Magnetic detection of current noise has the advantage of being totally non-invasive. Also, magnetic field measurment has the potential for spatial resolution[10] of noise currents over extended electrodes, although these capabilities are not utilized for this thesis.

Other techniques for detecting current noise include the use of a potentiostat, and the measurement of the ohmic drop across a resistor. Descriptions of each of the above techniques provides the content of the following section. The regime of measurement for which each measurement is useful is also discussed.

4.3.1 Magnetic Coupling to Currents

Magnetic detection of corrosion was proven possible for a variety of corrosion systems in experiments by Bellingham, MacVicar, Nisenoff, and

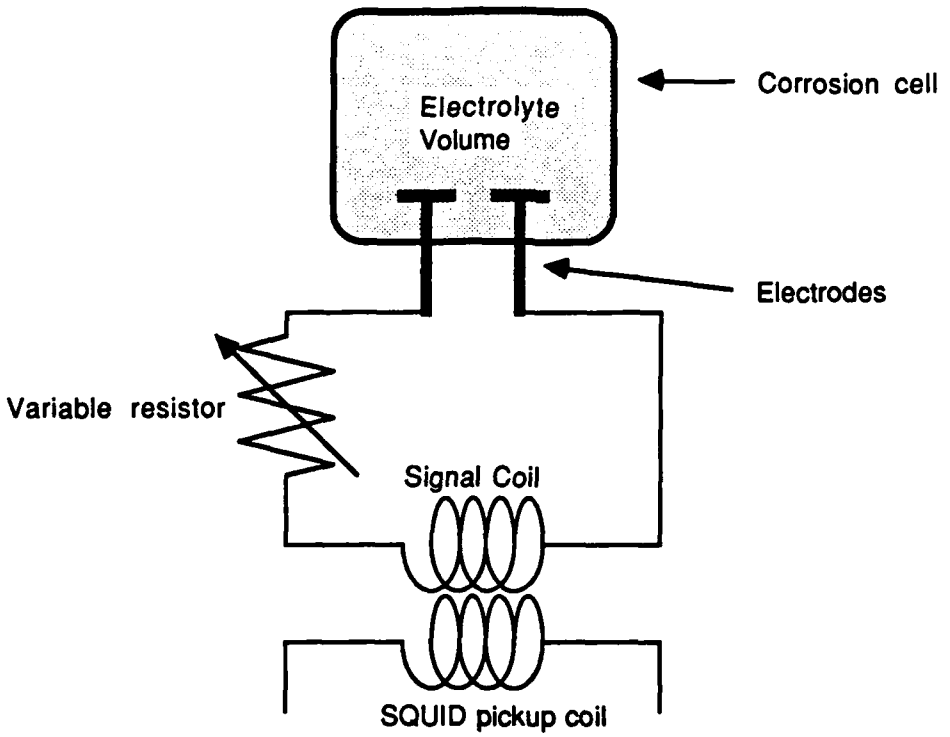

Figure 4.5 Illustration of set-up used to detect current in corrosion cell. Interaction current flowing between electrodes must complete circuit through external circuit elements. The variable resistor is used for the variable load measurements and is described in the previous section. The signal coil is used to efficiently inductively couple the interaction current into the SQUID pickup coils.

Searson[4]. The measurements are noninvasive since no electrical connection to the system under study is necessary. The measurements suggest two possible applications for magnetometers as corrosion sensors: use of magnetometers as remote detectors of corrosion processes, and use of magnetometers to understand electrochemical noise processes on a single electrode.

Figure 4.5 illustrates the general scheme used to measure interaction currents with the SQUID. Since one of the underlying motivations of this thesis is the utilization of SQUID magnetometers to detect and characterize corrosion reactions, a brief review of SQUID instrumentation is included.

4.3.1.1 SQUID Magnetometer

A SQUID magnetometer uses a Superconducting QUantum Interference Device (SQUID) to obtain extremely high sensitivity to magnetic field[88,89]. The SQUID itself is a cryogenic electronic device which uses the Josephson effect to obtain its extreme sensitivity. Metallic (i.e. low T_c) superconductors are required for high quality SQUIDs. Ceramic high T_c SQUIDs, which could be operated in liquid nitrogen, are still in the developmental stage at this time[90,91], and at any rate, better noise performance is generally obtained at lower temperatures. A commercial biomagnetic SQUID magnetometer with a noise level of 2×10^{-10} gauss was used for the experiments described in this thesis[92].

A typical SQUID magnetometer consists of four elements (see figure 4.6). There is the SQUID itself, usually a thin film device a fraction of an inch in size. The control electronics extract the magnetic field measurements. A pickup coil traneports flux from the sensor region into the SQUID. Finally, a dewar maintains the superconducting elements at cryogenic temperature.

Two classes of SQUIDs exist, rf SQUIDs and dc SQUIDs. An rf SQUID consists of a superconducting loop with one Josephson junction, while a dc SQUID is a superconducting loop with two (ideally identical) junctions.

Suitable external control electronics enables one to construct a highly linear magnetometer despite the highly nonlinear variation of SQUID inductance in magnetic field. The control electronics monitor the inductance of the SQUID, and apply a magnetic field to the device to keep

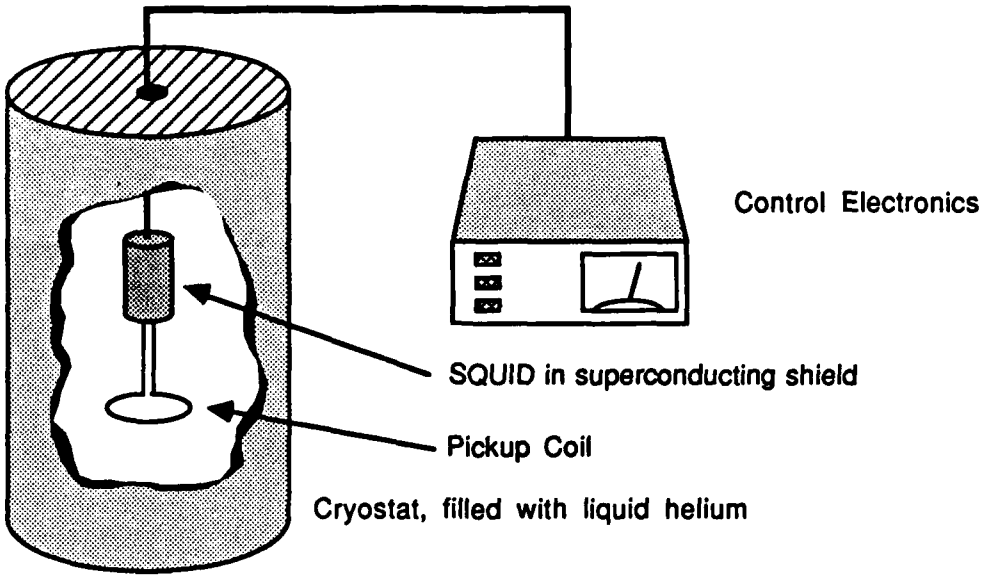

Figure 4.6: Elements of a SQUID magnetometer. The function of each element is described in the text.

the inductance constant. Thus the amount of negative feedback applied by the control electronics represents the field measurement of the magnetometer. One of the great advantages of SQUID magnetometers is their extremely high dynamic range. A SQUID can be operated in fields of hundreds of gauss.

Rather than placing a SQUID directly in the magnetic field environment to be measured, superconducting pickup coils are employed to transport flux to the SQUID from the sensor area. A closed superconducting loop has the property that it will maintain the total magnetic flux contained by the loop to be constant. Consider a loop containing two coils, as in figure 4.7. When the magnetic field applied to one ring changes, a net current through the loop will be induced, causing the total magnetic flux through the second coil to change. Quantitatively, if the two coils have inductance L_1 and L_2, then a change

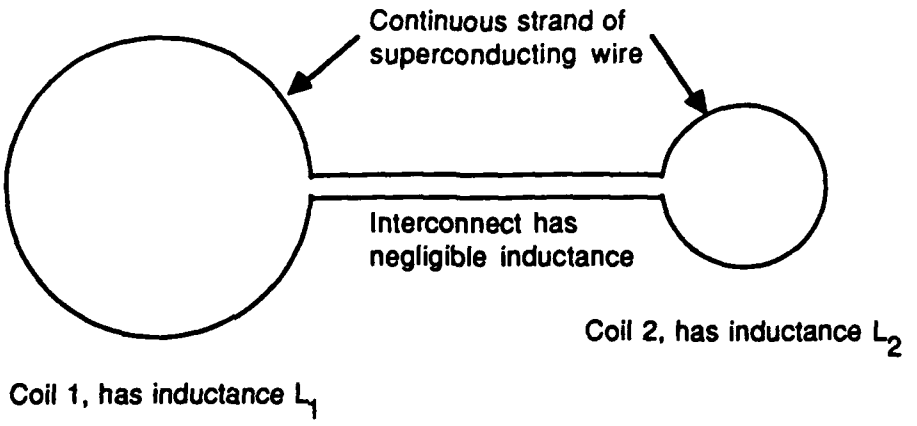

Figure 4.7: A closed superconducting loop consisting of two coils.

of applied flux $\Delta\Phi_a$ to loop 1 will result in change of flux in in loop 2 of:

$$\Delta\Phi_2 = \frac{L_2\Delta\Phi_a}{L_1 + L_2}$$

This is analogous to a transformer, except that the superconducting flux transformer operates to zero frequency.

SQUIDs require cryogenic temperatures to operate because of their superconducting nature. Commercial SQUIDs typically operate in a liquid helium bath. The biomagnetic system has a superinsulated fiberglass dewar. The primary advantage of using superinsulation, as opposed to a liquid nitrogen jacket, is that the separation between the helium space and the outside of the dewar can be minimized. The BTi dewar had a minimum separation of 11mm, which is significant since it imposes limitations on the efficiency of inductive coupling.

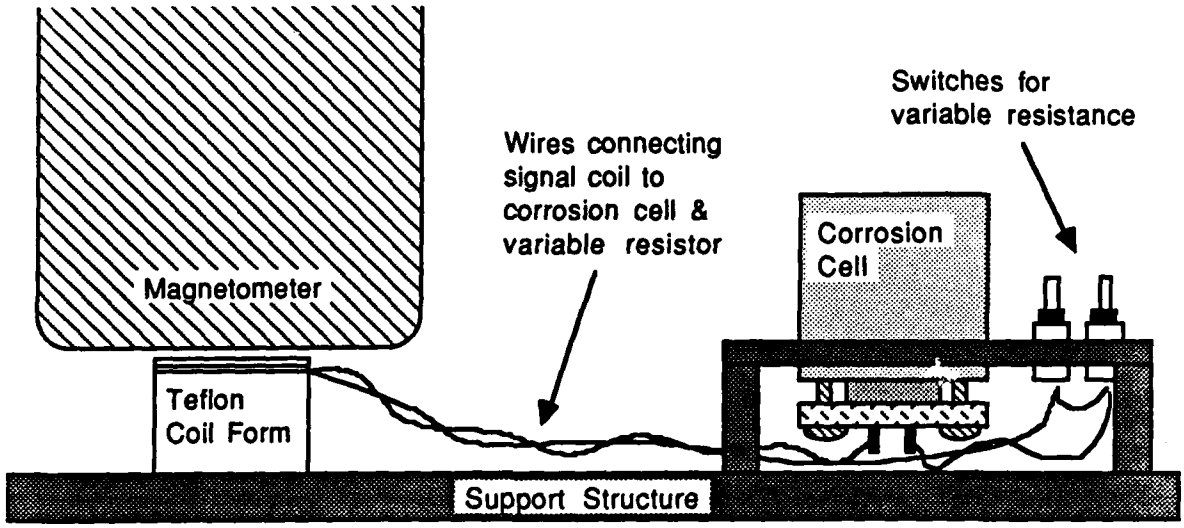

Figure 4.8: Apparatus used for measuring corrosion currents with SQUID magnetometer. Interaction current flows through wires connected to variable resistors and signal coil. The signal coil is wrapped on a teflon coil form, and is positioned directly under the magnetometer.

4.3.1.2 Coupling to Cell

One particular problem with the biomagnetic SQUID magnetometer was that the coupling of the corrosion current into the SQUID input coils was not particularly efficient. While initial measurements coupled to currents flowing in the electrolyte, more efficient coupling was achieved by wrapping a coil directly under the magnetometer tail (referred to as the signal coil). Figure 4.8 shows the entire experimental arrangement under the SQUID. The signal coil, which carries the interaction current generated by the corrosion cell, is wrapped around a teflon coil form and positioned under the SQUID magnetometer. The geometry of the pickup coils relative to the signal coil is illustrated in figure 4.9.

To determine the optimum size and position of the signal coils, the detected field was calculated as a function of coil radius, R, and vertical separation, z. The vertical separation was measured between the

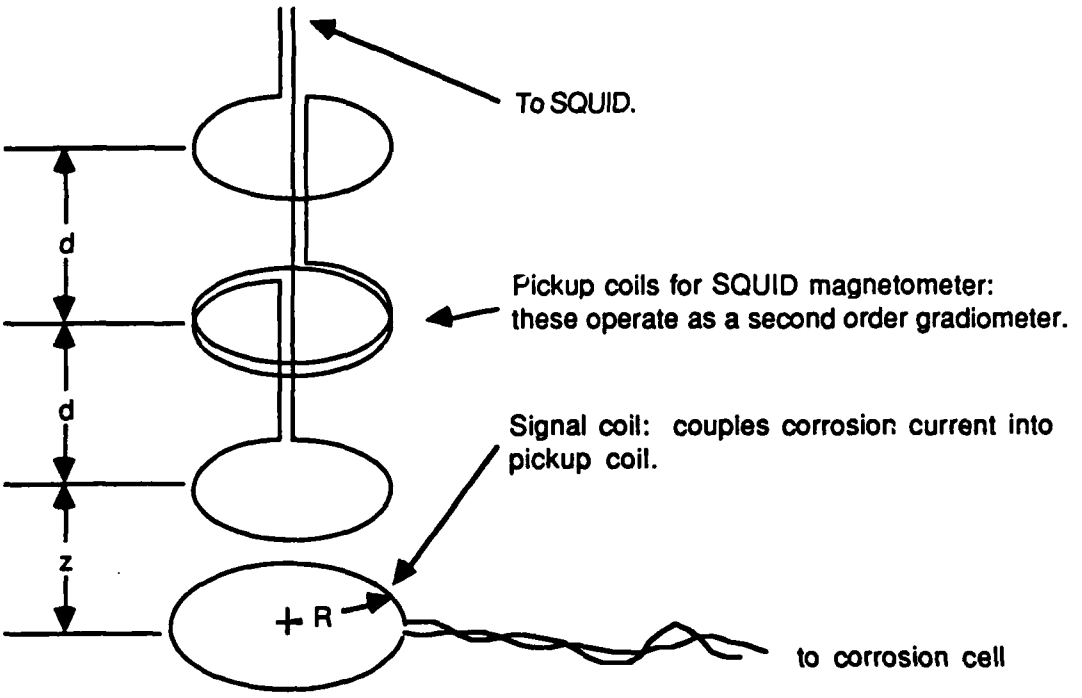

Figure 4.9: Schematic of SQUID pickup coils and corrosion cell signal coil. For simplicity, the cryostat, which would enclose the the pickup coils, is not shown. SQUID pickup coils are depicted in second order gradiometer configuration. Actual pickup coils have twice as many turns as is depicted in this figure. Thus the top coil would have two loops instead of just one. The signal coil used has 45 turns.

signal coil and the bottom pickup coil. A downward displacement is positive. The second derivative pickup coil was assumed to be coaxial with the signal coil. The pickup coil had three coaxial loops with a separation of d between adjacent elements (this configuration operates as a second order gradiometer[93]). The centermost loop of the pickup coil had twice the sensitivity and the opposite polarity of the end loops. The magnetic field coupling, in gauss detected per signal coil statamp, is:

$$\frac{B}{I} = \frac{4\pi R^2}{c}\left\{\left(z^2 + R^2\right)^{-3/2} - 2\left[(z-d)^2 + R^2\right]^{-3/2} + \left[(z-2d)^2 + R^2\right]^{-3/2}\right\}$$

To arrive at this expression, it is assumed that the field detected by

each of the loops of the pickup coil is the field on the axis. The loops have a diameter of about one inch, so the actual detected field is somewhat less than the axial field. This is because the magnetic field off axis is less than the on axis field. Since the error incurred by neglecting the diameter of the pickup loops is greatest for the bottom coil (i.e. the coil closest to the signal coil) the coupling is slightly overestimated.

The optimum vertical separation as defined by the above formula is less than the separation between the bottom coil and the exterior of the dewar. Thus the experimental coils were located immediately adjacent to the dewar, the actual separation being about 1.3 cm. The radius of the signal coil was 2.5 cm, and the resulting coupling was 3.31 A/G.

4.3.1.3 Environmental Noise

The presence of environmental electromagnetic noise prevents realization of the full potential of a SQUID magnetometer. At high frequencies (i.e. at radio frequencies) electromagnetic signals interfere with SQUID operation. This occurs both because the SQUID itself is extremely sensitive to rf, and because rf radiation interferes with the 20 MHz signal applied to the SQUID by the control electronics. At low frequencies (i.e. kHz and below) the magnetic component of electromagnetic radiation is picked up directly by the magnetometer. In a laboratory, environmental magnetic noise is primarily man made. Contributions at 60 Hz and 180 Hz are particularly strong.

The 60 Hz and 180 Hz interference posed a problem for experiments with the SQUID, even after using Fourier transform techniques to isolate their contribution. Amplitudes were so high that the sidebands of the

peaks contaminated the entire spectrum. Further discussion of this phenomena is found in the signal processing section. Use of analog notch filters to remove the peaks was not a good solution since they distort the rest of the spectrum.

Radio frequency interference is a substantial problem for SQUID magnetometers, primarily because the SQUID itself is extremely sensitive to rf radiation. Most locations around the institute have sufficiently high rf levels that SQUID operation is prevented altogether, or substantially degraded in performance.

4.3.1.4 Shielding

The magnetometer was shielded against both high and low frequency electromagnetic noise. High frequency shielding was used to eliminate rf radiation. Low frequency shielding was used to eliminate 60 Hz and 180 Hz pickup.

Low frequency shielding was obtained by using two nested mu-metal cans into which the SQUID could be inserted. Mu-metal has an extremely high permeability and shields against low frequency electromagnetic radiation by reflection of its magnetic component[94]. However two large problems are created by placing the SQUID in a mu-metal shield. The first is that the field gradients are fairly high inside a shielded enclosure, despite their low absolute level (on the order of μG). Very slight movements of the SQUID pickup coils generated large low frequency magnetic signals. Also, a low frequency drift in the measured magnetic field was sometimes observed, which was interpreted as flux creep in the mu-metal shielding (i.e. realinement of magnetic domains, as the magnetization slowly changes in the earth's field).

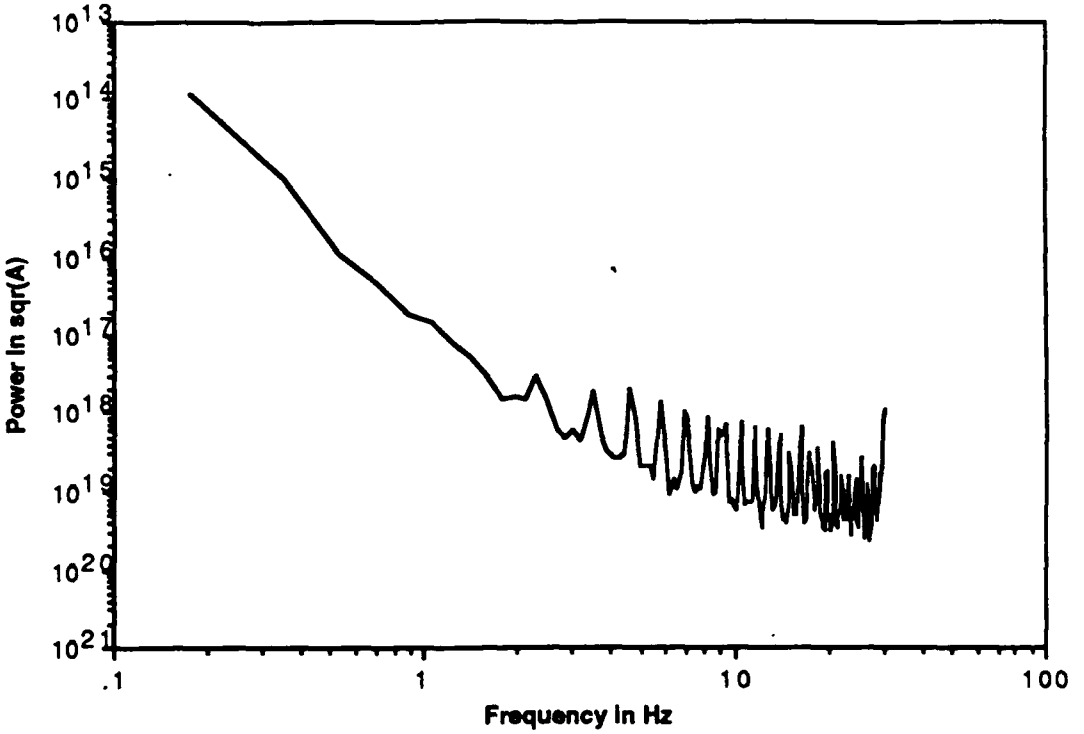

Figure 4.10: Equivalent current noise of SQUID inside mu-metal shields. Calculated using a sensitivity of 3.31 A/G. Note the high noise levels at low frequency, and the 60 Hz pickup, which appears at 30 Hz.

Radio frequency noise proved to be the greatest problem for routine SQUID operation, as described in the previous section. However by building a copper screen "hat" which could be used to enclose the SQUID in the mu-metal shields, the rf levels were reduced sufficiently for SQUID operation. A copper screen booth was also built so that the SQUID can be operated in rf shielding outside the mu-metal cans. However for all of the experiments presented in this thesis, the mu-metal shields were used. The background noise level with the SQUID in the mu-metal shields is shown in figure 4.10.

4.3.2 Potentiostat

A potentiostat can be used as an active low input impedance ammeter.

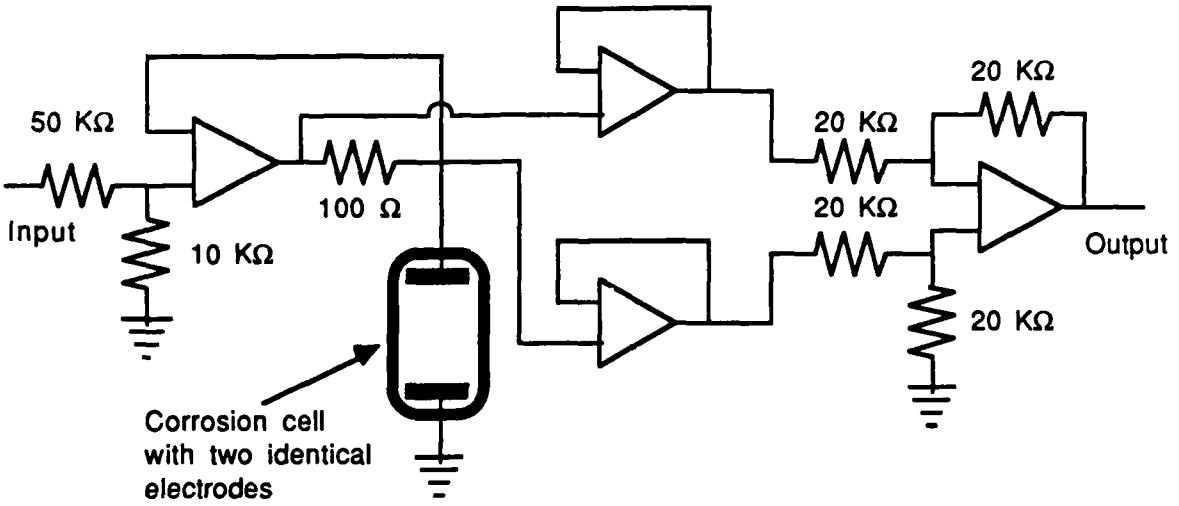

Figure 4.11: Potentiostat used for measurements on corrosion cell. Voltage applied at input is divided by six, and applied to the corrosion cell. The current required to maintain voltage is determined by measuring the voltage drop across 100Ω resistor on output of first op-amp. To use the potentiostat as a low input impedance ammeter, the input voltage need only be set to ground (i.e zero volts). The output is thus proportional to the current required to hold the electrodes at the same potential.

A potentiostat applies some programmed voltage to a external device, and monitors the current required to maintain that voltage. A voltage proportional to the applied current is output by the device. By setting the programmed voltage to zero volts, and measuring the current required to hold the voltage at zero, one can use the potentiostat as an ammeter.

The potentiostat used as an ammeter was originally designed by the author for impedance measurements. Noise levels on the order of 1 nA/$\sqrt{Hz}$ were considered acceptable. The current noise generated by the corrosion cells is of sufficiently high amplitude that instrumentation noise was not a problem. However it is important to note that the performance of this potentiostat is comparable with other low noise potentiostats reported in the literature[95].

The primary source of noise in the potentiostat used by the author (see figure 4.11) is the input voltage noise of the first stage op-amp.

Any input noise on this op-amp, $S_v(\omega)$, is translated into current noise through the corrosion cell. If the impedance of the cell is $Z(\omega)$, then the current noise due to the potentiostat will be:

$$S_i(\omega) = \frac{S_v(\omega)}{|Z(\omega)|^2}$$

This noise is actually injected by the potentiostat into the corrosion cell, since op-amp will attempt to correct the perceived voltage signal by injecting current into the circuit of the magnitude given above.

The second two stages of op-amps will also contribute noise, although only on the output signal. The apparent current noise level as measured from the output signal, assuming all four op-amps have the same input voltage noise, will be:

$$S_i(\omega) = S_v(\omega)\left(\frac{1}{|Z(\omega)|^2} + \frac{3}{R_c^2}\right)$$

Here R_c is the size of the resistor on the output of op-amp 1, which is 100Ω in the circuit shown above.

The effective input impedance of this circuit, as seen by the corrosion cell, is effectively zero for low frequencies (i.e. f < 100 kHz). Figure 4.12 shows the measured instrumentation noise for a 466 Ω load.

4.3.3 Direct Voltage Measurement

A simple method for detecting current noise is to simply measure the voltage drop across a resistor. This method also provides fairly low instrumentation noise. Sources of instrumentation noise are: the noise inherent in the voltage measurement, and Nyquist noise of the resistor

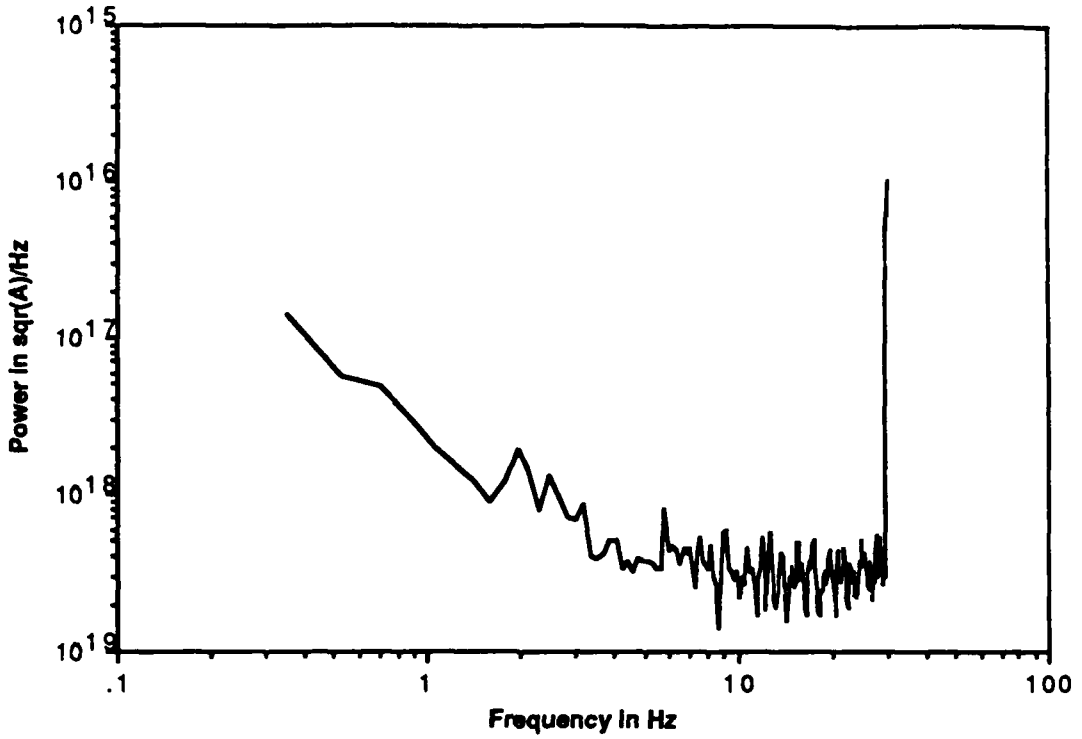

Figure 4.12 Instrumentation noise of potentiostat with OP-27 operational amplifiers. Noise power has been measured with a 466Ω load. The large spike at 30 Hz is due to aliasing of 60 Hz power-line pickup.

across which the ohmic drop is measured. The resulting current noise, $S_i(f)$, due to instrumentation is:

$$S_i(f) = \frac{4\,k\,T}{R} + \frac{S_v(f)}{R^2}$$

Here $S_v(f)$ is effective input noise power of the voltage sensor.

For the experiments on the corrosion cells, the voltage measurement is made across the external load of the corrosion cell. A 1201 Ithaco preamplifier with an input noise level of 15 nV/√Hz at 1 kHz is used. The instrumentation noise across a 10 kΩ resistor is illustrated in figure 4.13.

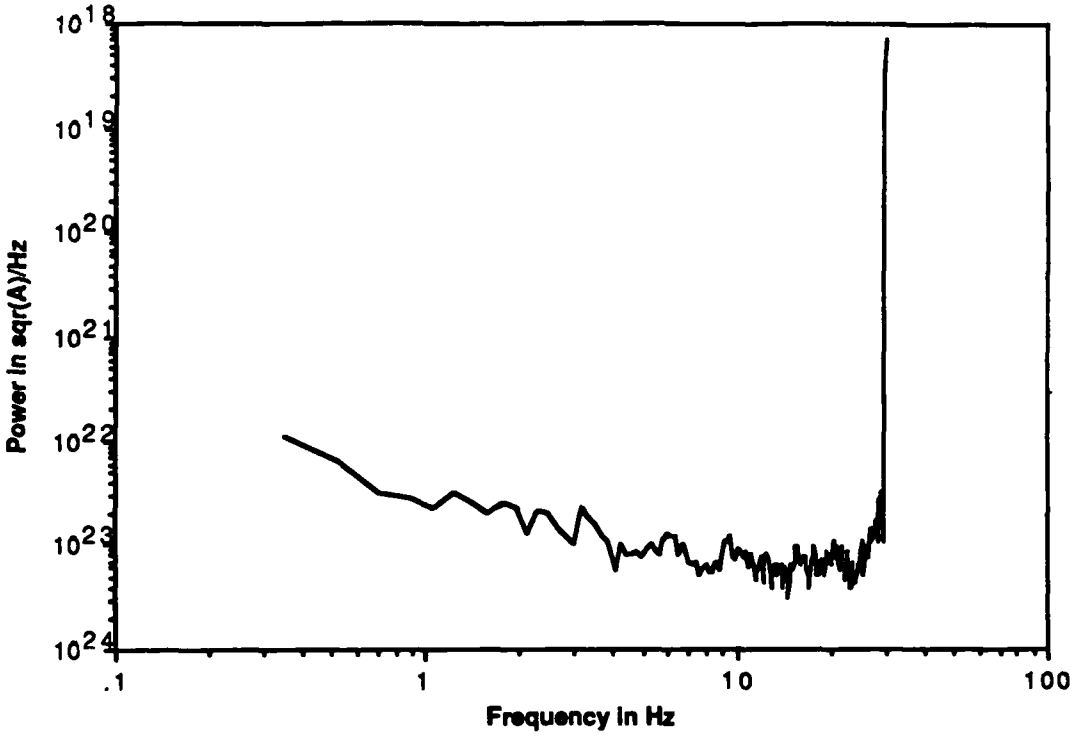

Figure 4.13: Instrumentation noise level of current measurement by voltage detection of ohmic drop across a 10 kΩ resistor.

This technique is capable of obtaining the best noise performance when high load resistances can be used in the circuit. At higher load levels the Nyquist contribution is dominant, posing a fundamental limitation. When the load resistor must be kept below 10 Ω, either the SQUID or the potentiostat are capable of more sensitive measurements. At low load, voltage sensor noise becomes important and the potential for improvement exists. Preamplifiers with background noise of 2 nV/√Hz at 1 Hz have been used for electromigration experiments in this laboratory, and could be incorporated into the electrochemical measurements.

4.4 Data Acquisition and Signal Processing of Noise Data

Digital data acquisition techniques are used because of the

versatility of digital signal processing. Both data acquisition and data analysis was done with personal computers.

A Leading Edge model D with a 30 MB hard disk is used to control a 12 bit A/D board (a Techmar Labmaster). The A/D board is configured for an input range of ±10 V, yielding a maximum resolution of 5 mV. A 1201 Ithaco instrumentation amplifier provided an amplification and analog filtering stage before A/D conversion. For most of the experiments, a conversion rate of 90 Hz is used. Data was stored in sets of 4608 points. Software for data acquisistion and signal processing was written by the author in Pascal.

4.4.1 Data Acquisition

The primary concern for the actual acquisition of digital data is the prevention of contamination of the data by aliasing. The author's arrangment consisted of two successive stages of filtering. The object the filtering is to remove frequency components above the Nyquist frequency, while leaving the bandwidth below the Nyquist frequency undistorted. Analog filtering prior to data acquisition provides the first filter, and post acquisition digital averaging provides the second.

Analog filtering is accomplished with a 1201 Ithaco Preamplifier. The Ithaco has a selectable low pass filter with a roll-off of 20 dB per decade. For sampling at 90 Hz, the low pass filter's 3 dB point is set to 30 Hz. Thus the onset of the analog filter was below the Nyquist frequency, so some distortion of the data was expected. The preamplifier also has a high pass filter and an option of AC coupling on the input. AC coupling (0.008 Hz high pass) was used with the SQUID experiments because of the large amount of drift induced by the mu-metal shields, otherwise no

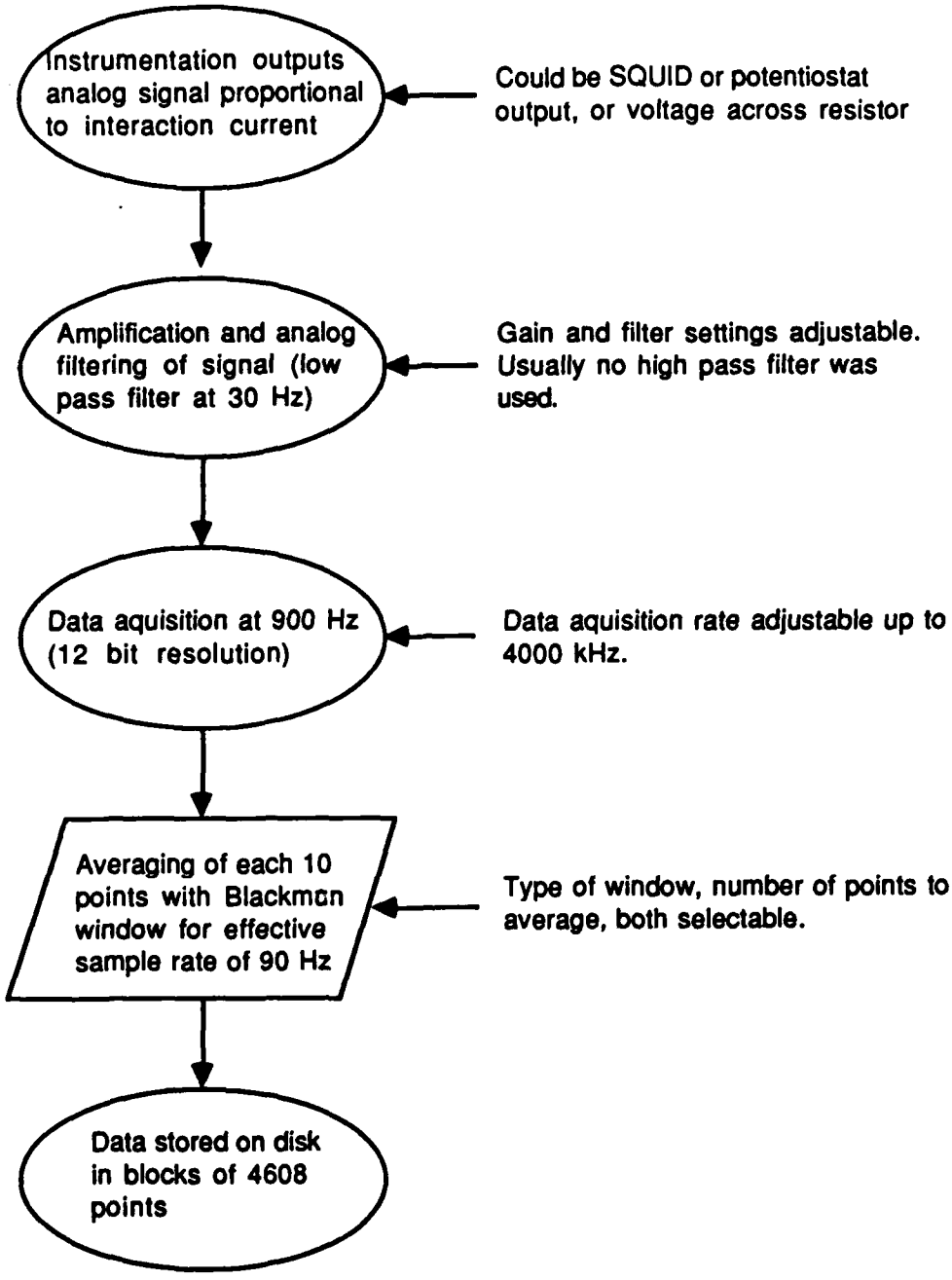

Figure 4.14 Flow diagram for data acquisition. The primary objective of the acquisition process was to prevent contamination by aliasing.

high pass filtering was used.

Digital averaging provides a powerful second filter. The specific digital filtering method used is to take a weighted average of the input

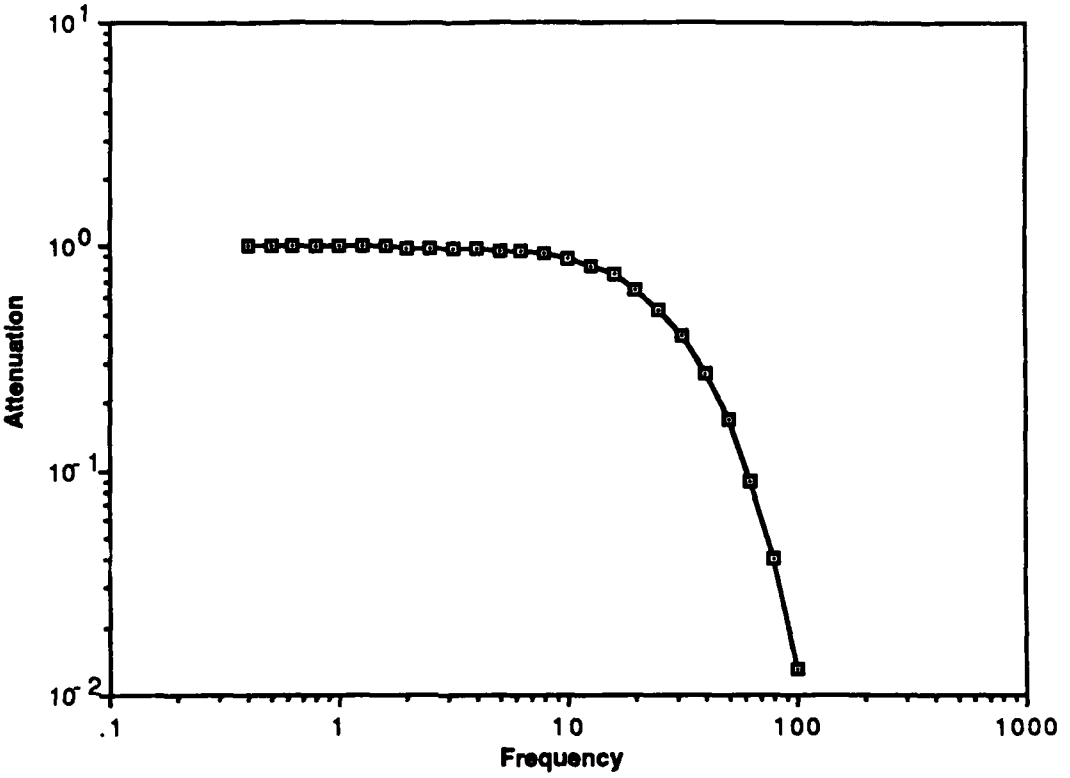

Figure 4.15: Attenuation resulting from analog and digital filtering for data acquisition rate of 90 Hz. Attenuation is given as fraction of signal power detected after filtering. Thus an attenuation of 0.01 means the signal power is reduced by a factor of 100, while the peak-to-peak amplitude is reduced by a factor of 10. The graph is of the measured response of the filtering.

signal. For a acquisition rate of 90 Hz, ten data samples are taken for each data point. The ten data samples, spanning 11 ms in time, are weighted by a Blackman window and then averaged. A Blackman window was used because of its low sidelobe level in the frequency domain[96].

A block diagram of the signal path is illustrated in figure 4.14. The resulting attenuation is plotted as a function of frequency in figure 4.15. The data for figure 4.15 was determined by sampling a sinewave at a given frequency from a function generator, and determining the total power in the signal after filtering.

4.4.2 Signal Processing

Fourier transform based signal processing was used extensively for this thesis. Fourier transformation of the data was accomplished by using the Cooley-Tukey Fast Fourier Transform (FFT) algorithm[98]. The Fourier transform was used to obtain the power spectrum of a given data set or to determine the coherence function between two data sets. Data was processed in blocks of 512 data points (the Cooley-Tukey algorithm requires the data set length to be a factor of two).

A single data run consisted of 4608 data points (see preceeding section). The entire run was subdivided into 512 point segments, each overlapping its neighboring segments by 50%. Thus a data run yielded 17 blocks of data. Power spectra of each of the individual blocks were averaged to obtain a power spectrum estimate for the entire set. This method of power spectra estimation was proposed by Welch[97]. Each of the blocks of data was processed individually using the techniques described below.

4.4.2.1 Pre-FFT Data Conditioning

Prior to Fourier transforming a data block, any or all of three operations are used on the data. These operations are: removal of the dc component, removal of any trends, and application of a window to the data.

The removal of the dc component of the data consists of simply removing the average of the data set from each point in the data set. The removal of trends is accomplished by determining the best fit line to the data, then substracting that line from the data set. In practice, removal of data trends automatically also accomplishes removal of the dc component. These operations prevent extreme low frequency artifacts from

contaminating the entire bandwidth[99]. Power contribution from frequencies below f_s/N are diminished while higher frequencies remain relatively unaffected. Here f_s is the sample rate, and N is the number of points in the data set. The lowest data point in an FFT transform of a data set is f_s/N. If trends are not removed, they can add a $1/f^2$ contribution to the data.

After trend removal, a Hamming window was applied. The Hamming window was choosen for the low level of its sidelobes (-43 dB)[96]. Low sidelobe level was crucial because signals were often contaminated by power-line pickup. The 60 Hz line frequency was aliased, even through the preventive filtering, and appeared as a 30 Hz signal in the acquired data. Without the low sidelobe levels, the large power-line spike "leaks" power into the entire spectrum. For example, a rectangular window (i.e. no window) has a sidelobe level of only -6 dB, and will therefore allow a signal 50 times smaller to contaminate adjacent frequencies[96].

The cost of using a Hamming window is loss of spectral resolution (degradation is by roughly a factor of 1.4 compared to a rectangular window). Since the object of the analysis is not to resolve closely spaced signals, but to measure the frequency dependence of a fairly featureless spectrum, the loss of resolution is not important.

After application of the Hamming window, the coherence between adjacent data sets overlapping by 50% is only 24%[96]. This is an important consideration, since processing of the data for given experiment could take up to eight hours. Since the coherence between data sets is relatively low, additional information is obtained with the extra processing. The flow chart for pre-FFT conditioning is illustrated in

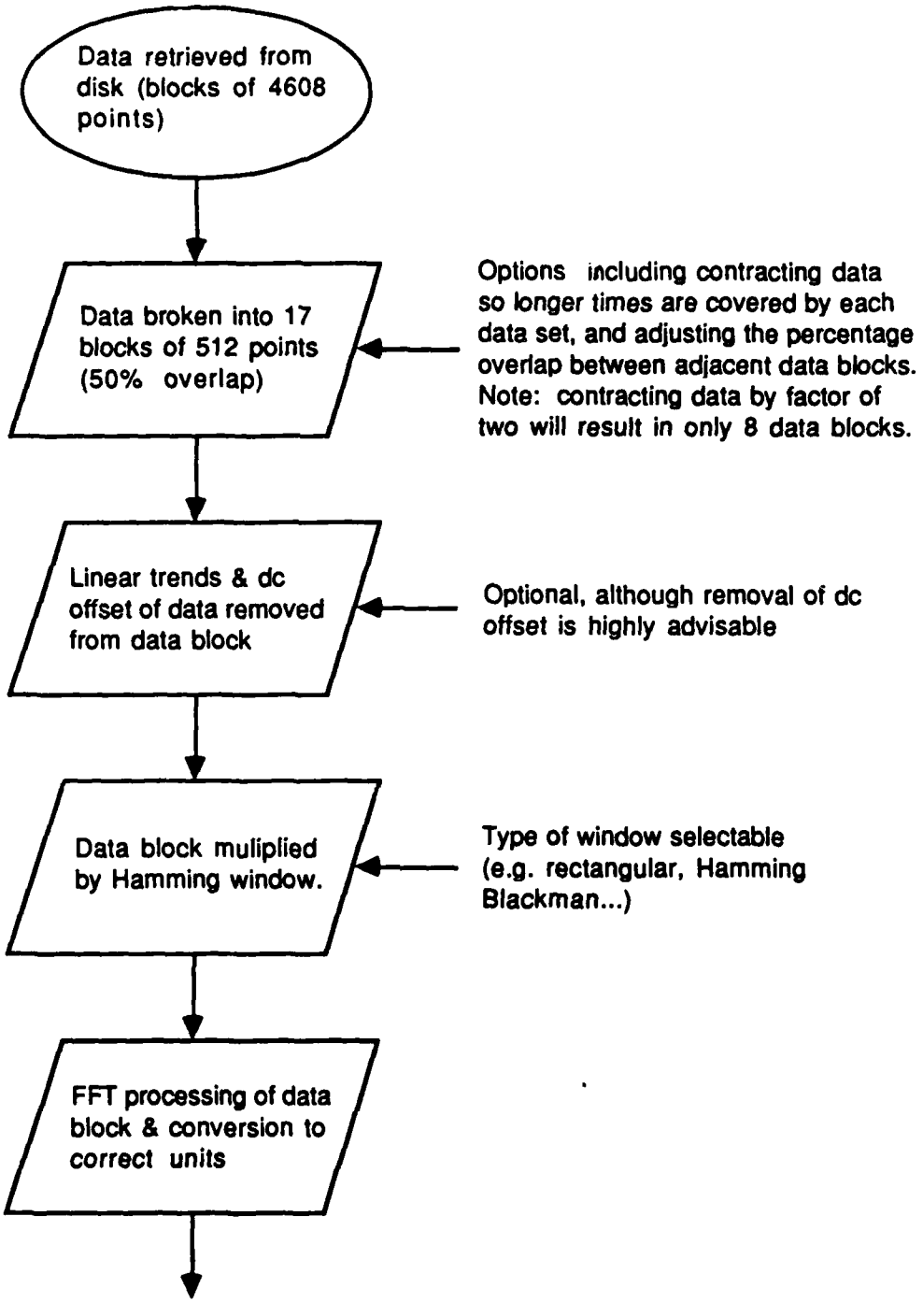

Figure 4.16: Flow chart for pre-FFT data conditioning.

figure 4.16.

4.4.2.2 FFT Processing

As mentioned above, the Fourier transform of x(t) into X(f) is accomplished using the Cooley-Tukey algorithm. The FFT algorithm calculates the discrete Fourier transformation:

$$X_k = \sum_{n=1}^{N} x_n \exp\left(-i \frac{2\pi n k}{N}\right)$$

Here x_n is the time series (i.e. $x_n = x(n\Delta t)$, where Δt is the interval between samples), and X_k is the transformation of the data. The X_k yields the Fourier transform by the mapping:

$$X(f) = X\left(\frac{k}{N\Delta t}\right) \approx \frac{X_k}{\Delta t\sqrt{N}}$$

Note that X(f) is a complex quantity.

The power spectrum is obtained by multiplying the Fourier transform by its complex conjugate. The resulting power spectrum is "two-sided", i.e. the entire power in the spectrum is obtained by integrating over both positive and negative frequency. To obtain the single-sided power spectrum, the two-sided spectrum is multiplied by two, and the negative frequency half is discarded. If the time series is x(t), and its Fourier transform is X(t), then the (single-sided) power spectrum is:

$$S_x(f) = 2\,X(f)\,X^{*}(f)$$

The FFT techniques were also used to determine the coherence function of two data sets[99]. The coherence function, $\gamma^2(f)$, tells the degree to

which one signal can be predicted from the other. The coherence function ranges from zero to one, with zero corresponding to no correlation between data sets, and one corresponding to complete correlation.

The following procedure can be used to determine $\gamma^2(f)$. Start with two data sets, $x(t)$ and $y(t)$, spanning the same period of time. Break the data sets into blocks, $x_i(t)$ and $y_j(t)$, with Fourier transforms $X_i(f)$ and $Y_j(f)$. Blocks with the same index (i.e. $i = j$) span the same time. Then the coherence function between the two data sets is:

$$\gamma^2(f) = \frac{\left| \sum_{i=1}^{N} X_i(f)\, Y^*_i(f) \right|^2}{\left(\sum_{i=1}^{N} X_i(f)\, X^*_i(f) \right) \left(\sum_{i=1}^{N} Y_i(f)\, Y^*_i(f) \right)}$$

4.4.2.3 Post FFT Power Spectra Conditioning

In practice, not all of the noise power above the Nyquist frequency was removed by filtering during data acquisition. Furthermore, some distortion in the Nyquist interval is observed (see figure 4.15). The data most susceptable to contamination is therefore discarded, i.e. the frequency range above 30 Hz. The distortion of the remaining data is removed by dividing the observed power by the attenuation factor to get the undistorted power. These two operations are extremely important, as without them the frequency dependence observed at higher frequencies does not correspond to the actual frequency dependence. All of the spectra presented in this thesis have been processed in this fashion.

Two electrode cell

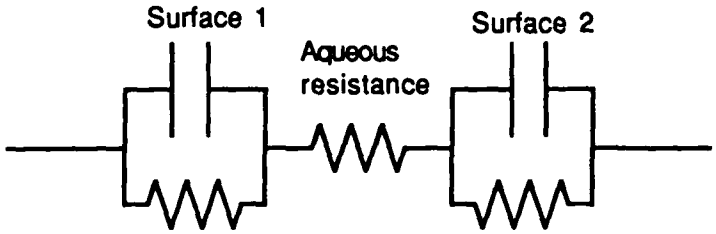

Equivalent circuit

Figure 4.17: Corrosion cell configuration for impedance measurement and equivalent circuit. The identical electrodes are used as the terminals across which the impedance of the electrochemical cell is determined.

4.5 Impedance Measurement

Impedance measurements of the electrochemical cell were used to extract the values of the charge transfer resistance, the aqueous resistance and the double layer capacitance. The experimental apparatus assembled by the author was capable of measuring impedance from 100 kHz down to 0.001 Hz. Rather than introducing additional electrodes to impress current and measure potential, as is conventional, the impedance of the cell was measured across the two identical electrodes.

Figure 4.17 shows the electrochemical cell and its analog circuit model, as it is connected to the impedance measurement apparatus. The path of the current impressed to measure the cell impedance follows the same path as does the interaction current. The aqueous resistance, as seen by the interaction current is measured. The cumulative electrode

impedance is measured. If the standard counter electrode, reference electrode arrangement were used, the cell impedance measured would either be of only one surface, or of the the two surfaces in parallel, rather than the two surfaces in series.

4.5.1 Impedance Apparatus

Measurement of impedance spectra is accomplished by applying a voltage sine wave of known amplitude and frequency, and measuring the resulting amplitude and phase of the current required to mantain the voltage signal. Writing the relationships between current, voltage, and impedance:

$$V = V_o \exp\left[i(\omega t - \phi_v)\right]$$

$$I = I_o \exp\left[i(\omega t - \phi_i)\right]$$

$$Z = \frac{V}{I} = \frac{V_o}{I_o} \exp\left[i(\phi_v - \phi_i)\right]$$

The impedance measurement apparatus measured the phase of the current relative to the voltage phase, i.e. $\phi_i - \phi_v$, and the amplitude of the current. Given knowledge of the applied voltage, this yields the impedance.

All elements of the impedance measurement system were under computer control. A Leading Edge model D with a National Instruments IEEE-488 interface board and the previously mentioned Techmar Labmaster A/D board were used.

The amplitude and frequency of the applied sine wave are determined by the computer and generated by an HP3125A (Hewlett-Packard) function

generator (which is under IEEE-488 control). A potentiostat applies the voltage signal to the cell, and outputs a voltage signal proportional to the required current signal.

For frequencies above 100 Hz, a SR530 (Stanford Research) dual phase lockin amplifier is used to measure the phase difference between the voltage signal and the resulting current. The trigger output of the function generator is used as the reference signal for the lockin amplifier. The lockin, under IEEE-488 control, outputs the phase and amplitude of the current.

An A/D board is used in a different fashion to obtain impedance measurements below 100 Hz. The applied voltage and resulting current are sampled simultaneously by the computer over an integral number of periods. By fourier decomposing each signal, the phase and amplitude of the voltage and current signal are determined.

Some error is expected in the phase measurements as described above. The lockin reference signal will typically not be completely in phase with the voltage signal, introducing a small error in phase (although this error becomes larger at 100 kHz, when the capacitance of the coaxial cables introduces significant phase lag). The A/D board also introduces an artificial phase difference between the voltage and current signals since conversions on the two channels occur sequentially rather than simultaneously.

To remove such systematic errors, the impedance apparatus was calibrated prior to each run by obtaining the impedance of a known resistor, R_c. The calibration could then be used to correct subsequent impedance measurements by the following operation:

$$Z_c = \frac{Z_m}{Z_c} R_c$$

Here Z_m is the measured impedance, Z_C is the measured impedance of the calibration resistor, and Z_c is the corrected impedance measurement.

4.5.2 Interpretation of Impedance Spectra

The impedance of the circuit in figure 4.17 can be written:

$$Z(\omega) = R_{aq} + \frac{R_{ct1}}{1 + i\omega C_1 R_{ct1}} + \frac{R_{ct2}}{1 + i\omega C_2 R_{ct2}}$$

If the time constants of the two surfaces are equal (i.e. $\tau = C_1 R_{ct1} = C_2 R_{ct2}$) then the impedance becomes:

$$Z(\omega) = R_{aq} + \frac{R_{ct1} + R_{ct2}}{1 + i\omega\tau}$$

Experimental evidence that the $R_{ct}C$ product is relatively constant as function of time is given in the next chapter.

Plotting the impedance spectrum in the complex plane offers a straightforward method to determine the electrical analogs. The spectrum describes a semicircle (see figure 4.18). Methods of extracting the values of the parameters in the model have been discussed by a number of authors[100,101,102,103]. For simple system, e.g. Zn in HCl, extraction of R_{ct}, C, and R_{aq} is straightforward. For the high frequency limit, i.e. $\omega \rightarrow \infty$, one finds $Z(\omega) \rightarrow R_{aq}$. For the low frequency limit, as $\omega \rightarrow 0$ one finds $Z(\omega) \rightarrow (R_{aq} + R_{ct1} + R_{ct2})$. The double layer capacitance can be

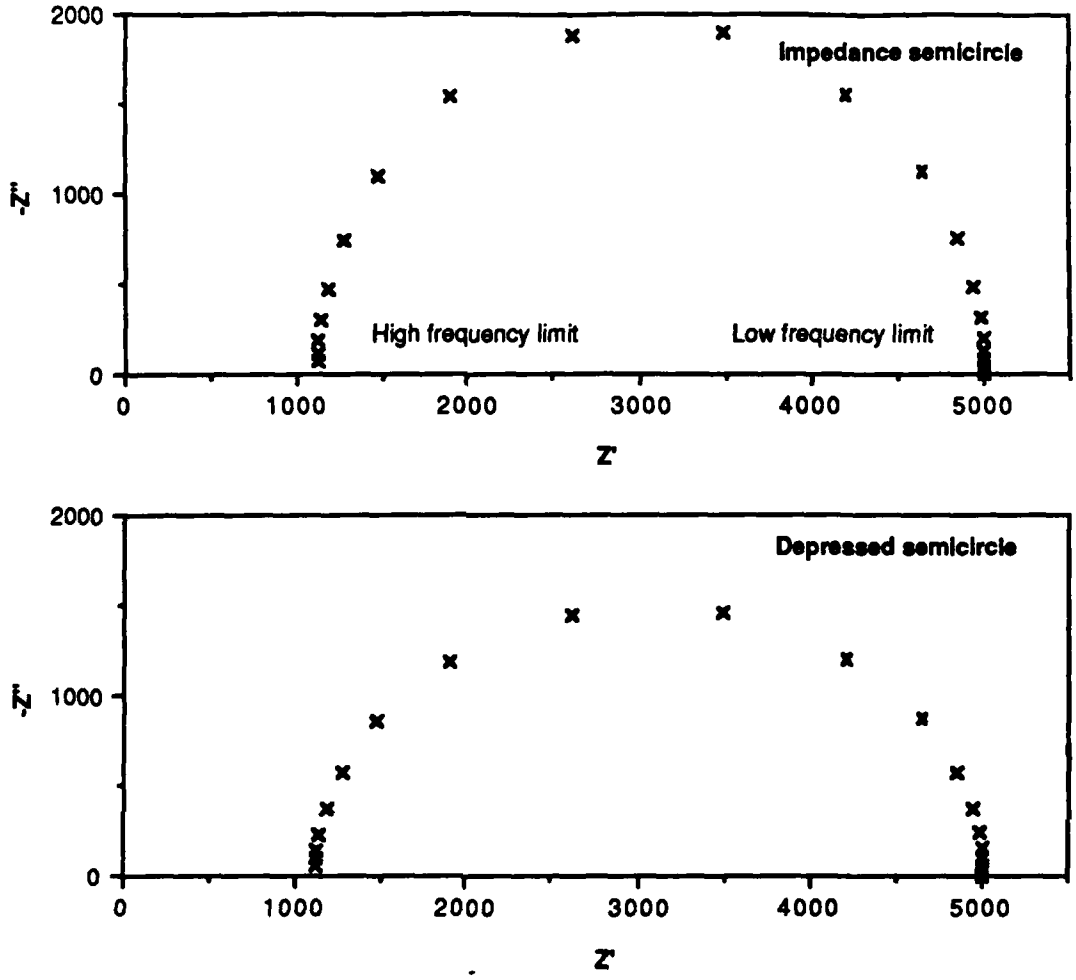

Figure 4.18: Illustrations of impedance plots (not real data).

found by determining the frequency, ω_{max}, at which the maximum excursion of impedance occurs from the real axis and using the relationship $C = 1/R_{ct}\omega_{max}$.

To overcome distortions of the data, this thesis uses an algorithm proposed by Kendig et al.[100] which fits a circle to the impedance spectrum in the complex plane. They call this algorithm CIRFIT. The algorithm does not constrain the center of the circle to the real axis. Thus a better fit can be obtained to "depressed semicircle" data. Depression of the complex plane semicircle (see figure 4.18) is often

observed in impedance data on corrosion systems. It is usually attributed to absorption processes on the electrode. The CIRFIT algorithm yields the best values for the high frequency and low frequency intercept of the impedance data with the real axis. Thus one can obtain $(R_{ct1} + R_{ct2})$ and R_{aq} but not C. The algorithm also yields the error bars for the circle radius fit. This is used to determine the the error in the fit parameter according to the following relations:

$$\Delta R_{aq} = \frac{\Delta(R_{ct1} + R_{ct2})}{2} = \frac{\sqrt{R^2 - y^2}}{R} \Delta R$$

Here R is the circle radius, y is the displacement of the center of the circle from the real axis, and ΔR is the error inherent in the determination of R.

The double layer capacitance is obtained by using the values for R_{aq} and $(R_{ct1} + R_{ct2})$ and determining the least squares fit to the data using τ as the adjustable parameter. The "average" capacitance can be found from: $C = 2\tau / (R_{ct1} + R_{ct2})$.

The charge transfer resistance quoted in this thesis for the double electrode system is always the average charge transfer resistance of the two interfaces, i.e. $(R_{ct1} + R_{ct2})/2$. The value $(R_{ct1} + R_{ct2})$ is referred to as the cumulative charge transfer resistance.

CHAPTER 5: RESULTS AND DISCUSSION

The experiments conducted for this thesis fall in two categories. The first class of experiments examines the validity of the series of approximations made in chapter three for analyzing corrosion reactions. The second class measures the actual electrochemical noise generated by the cell. This chapter is accordingly divided into two sections, the first on general electrochemical measurements made on the system (primarily impedance measurements) and the second on noise measurements.

Information such as the corrosion rate, the charge transfer resistance, and the double layer capacitance are critical to analysis of the noise data. For the theory developed in chapter three to apply, the reaction must be activation controlled, not diffusion limited. Under diffusion control, the Bulter-Volmer relation does not describe the kinetics of the interface. Another key assumption is that the effect of double layer charging can be modelled as a capacitance. Experiments to obtain the above data have been run by the author, and are reviewed in the following section.

All experiments use the same pair 6N purity Zn electrodes (sample LC-9) unless explicitly stated otherwise. This minimized variations in microstructure of the Zn surface from run to run. Both electrodes were cut from the same piece of Zn wire. The electrode diameter is 1 mm, with a separation of 2.6 mm from electrode center to electrode center.

Experiments by the author with different purity Zn wires confirmed the extreme sensitivity of Zn to impurities. The noise characteristics appeared to be far more sensitive than the corrosion rate. Consistent data was obtained only by using the same set of electrodes and identical

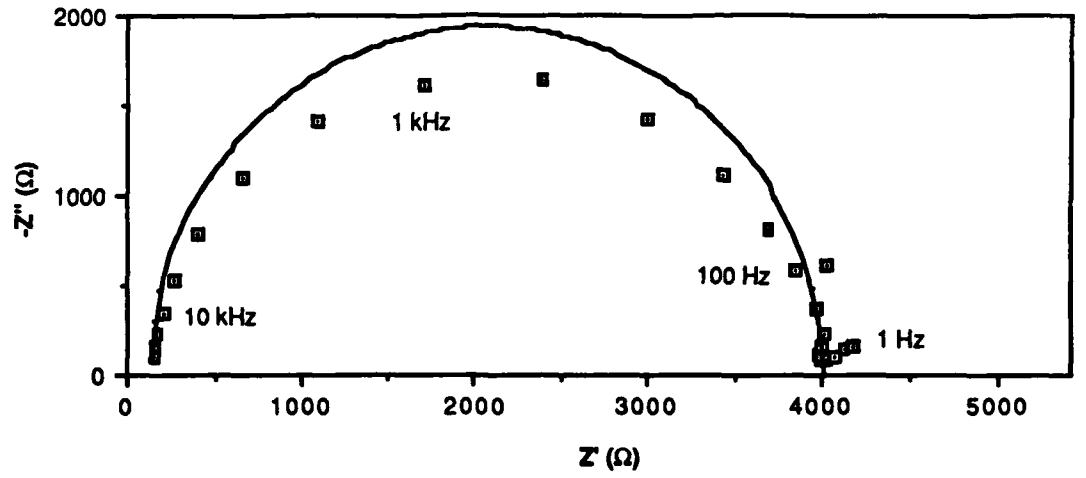

Figure 5.1: Real versus imaginary component of impedance for 6N purity Zn in 0.33 M HCl. The electrochemical cell consisted of two identical 1.0 mm diameter Zn electrodes. The solid curve represents the best fit to the experimental data with values: R_{ct} = 1940 Ω, R_{aq} = 125 Ω, and C = 0.1 μF.

preparation procedures. The experimental precautions are described more fully in the preceding chapter.

5.1 IMPEDANCE MEASUREMENTS

The impedance spectra in this section were obtained for a frequency range of 1 Hz to 100 kHz. R_{ct} and R_{aq} were obtained from the spectra using the CIRFIT algorithm. The double layer capacitance was determined via a least squares fit to impedance data in the real-imaginary plane, using the previously determined R_{ct} and R_{aq} as constants. A more complete description of the experimental technique is found in chapter four.

An impedance spectrum for Zn in 0.33 M HCl is shown in figure 5.1. The imaginary component of impedance is plotted against the real component. The impedance spectrum calculated using the best fit to R_{ct}, R_{aq}, and C_d is also shown. A slight depression of the observed spectrum is visible, and was always observed. Figure 5.2 shows Bode plots for the

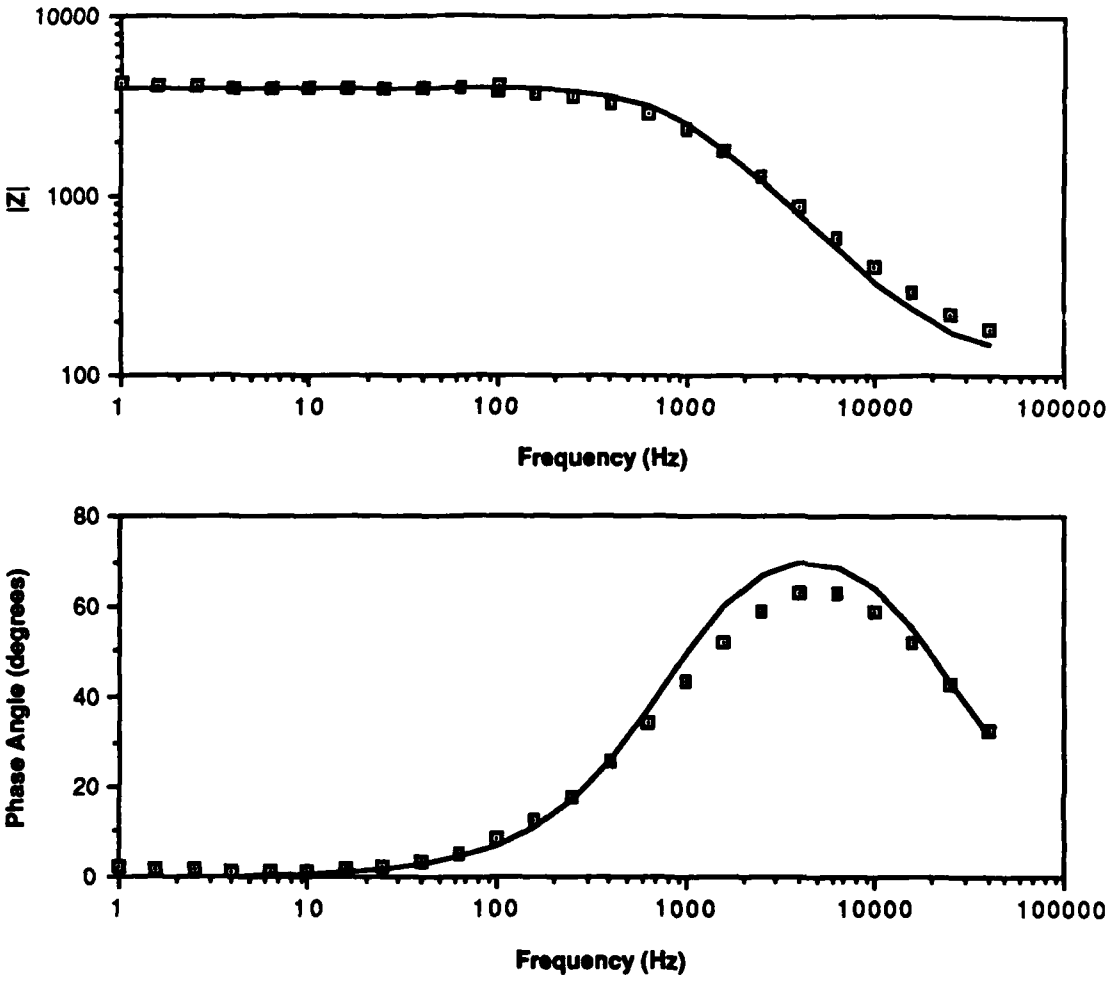

Figure 5.2: Bode plots of impedance of a two-surface Zn cell with 0.33 M HCl. This is the same data as that represented in figure 5.1. The solid line is the best fit using the parameters: R_{ct} = 1940 Ω, R_{aq} = 125 Ω, and C = 0.1 μF. Electrodes are 1 mm in radius.

impedance data depicted in figure 5.1. The proposed electrical analog appears to give a reasonable fit.

Diffusion control of reaction rate, when it occurs, is readily apparent in impedance spectra as the "Warburg" impedance[104]. Neglecting double layer charging but accounting for diffusion of reduced and oxidized species through an infinite diffusion layer, the impedance for an electrochemical interface is written:

$$Z(\omega) = R_{ct}\left[1 + \sqrt{\frac{i}{\omega}}\left(\frac{k_f}{\sqrt{D_O}} + \frac{k_b}{\sqrt{D_R}}\right)\right]$$

The first term is the charge transfer resistance. The second term, with the frequency dependence, is the Warburg impedance[105]. The constants k_f and k_b are the forward and reverse reactions rates, and D_O and D_R are diffusion constants for the oxidized and reduced species.

The Warburg impedance forms a straight line in the real-imaginary plane, at a 45° angle to the real axis. It becomes significant at low frequencies. The slight increase in impedance between 10 Hz and 1 Hz in figure 5.1 might be due to diffusion control. However the perturbation is small compared to the charge transfer resistance. In general, impedance spectra for Zn in 0.33 M, 1.0 M and 3.0 M HCl show no evidence of a Warburg impedance.

Impedance spectra were taken for identical zinc electrodes in HCl concentrations of 0.33 M, 1.0 M, and 3.0 M. Average values of the electrical analogs for the cells are listed below. These values were determined from a typical run at each concentration level. Data was taken for at least four hours for each data set listed in table 5.1.

Table 5.1: Average Electrical Analog Values

Concentration	R_{ct} (Ω-cm^2)	C (μF/cm^2)	R_{aq} (Ω)	$R_{ct}C$ (ms)
0.33 M	9.0±0.7	21±1	187±4	0.173±0.003
1.0 M	4.66±0.15	56±4	41.4±1.4	0.250±0.024
3.0 M	0.76±0.02	101±3	20.4±0.7	0.077±0.002

The trends are as one would expect. The higher corrosion rate at greater concentrations leads to lower charge transfer resistance values. On the

other hand, the capacitance should decrease roughly as the square root of the electrolyte concentration, according to Gouy-Chapman theory[107]. This is approximately observed. The electrolyte resistance decreases with increasing concentration, which is also expected since electrolyte conductivity is roughly proportional to concentration.

5.1.1 Corrosion Rates

Average corrosion rates were determined by measuring the amount of material which was removed from the electrode during exposure to the electrolyte. Since the electrode is abraded prior to immersion in the electrolyte, the electrode and epoxy surfaces are coplanar at the initiation of a run. An optical microscope was used to measure the electrode-epoxy relief after corrosion of the metal surface. The microscope, with a focus mechanism calibrated in μm, was alternately focused on the epoxy and the electrode. Measurements of the relief were made for both electrodes, and the standard error of the readings used as the error.

Average corrosion rates were determined for the runs described in table 5.1. The corrosion rate is used to establish the corrosion current, using Faraday's law and a valence of two for the zinc dissolution reaction. The resulting values are listed in table 5.2.

Table 5.2: Average Corrosion Rates

Concentration HCl Acid	Corrosion Rate (μm/hr)	Corrosion Current (μA)
0.33 M	1.16±0.08	5.3±0.3
1.0 M	1.9±0.6	7.6±2.8
3.0 M	11.1±0.9	51±4

5.1.2 Temporal Dependence of Interface Parameters

The characteristics of the electrochemical interfaces did not remain constant in time. Rather, changes in all the electrical parameters of the interface were observed. The primary cause appears to be roughening of the surface as the reaction progresses. Roughening leads to an increase in the effective surface area of the electrode. The area expansion, in turn, increases the double layer capacitance and decreases the charge transfer resistance. The increase in the aqueous resistance is consistent with results of Kuhm et al.[81] which demonstrate a higher hydrogen reduction overpotential on rough surfaces. Figure 5.3, 5.4 and 5.5 show the evolution of the interfacial electrical analogs for the data listed in table 5.1.

5.1.3 Consistency of $R_{ct}C_d$ Product

Area fluctuation as an explanation for the fluctuation of interface capacitance and resistance is subject to a relatively simple test. Assuming the charge transfer processes are not modified substantially as the roughness of the electrode changes, or as the reaction progresses, the product $R_{ct}C_d$ should remain constant. Writing the capacitance of a unit area of electrode as C_o, and the resistance as R_o, the capacitance of an electrode with area A is C_oA and the resistance is R_o/A. The product of the interfacial resistance and capacitance (the "RC product") is R_oC_o, which is independent of area. The product $R_{ct}C_d$ for the three different electrolyte concentrations is approximately constant as a function of time, and is depicted in figure 5.6.

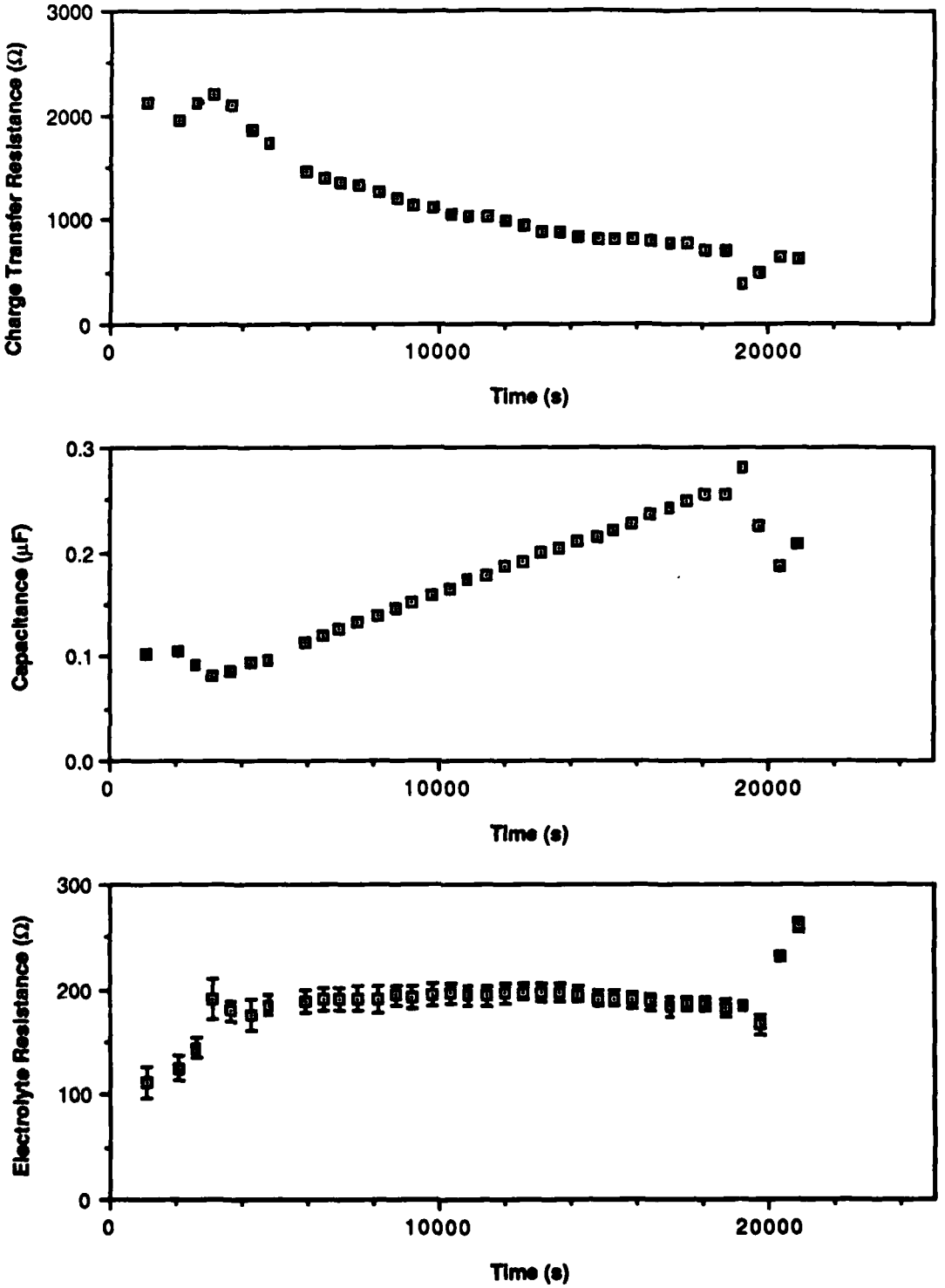

Figure 5.3: Electrical analog values representing best fit to impedance data. Electrolyte was added to the corrosion cell at t = 0. The above data is for 6N purity Zn in 0.33 M HCl. No error bars were calculated for the capacitance.

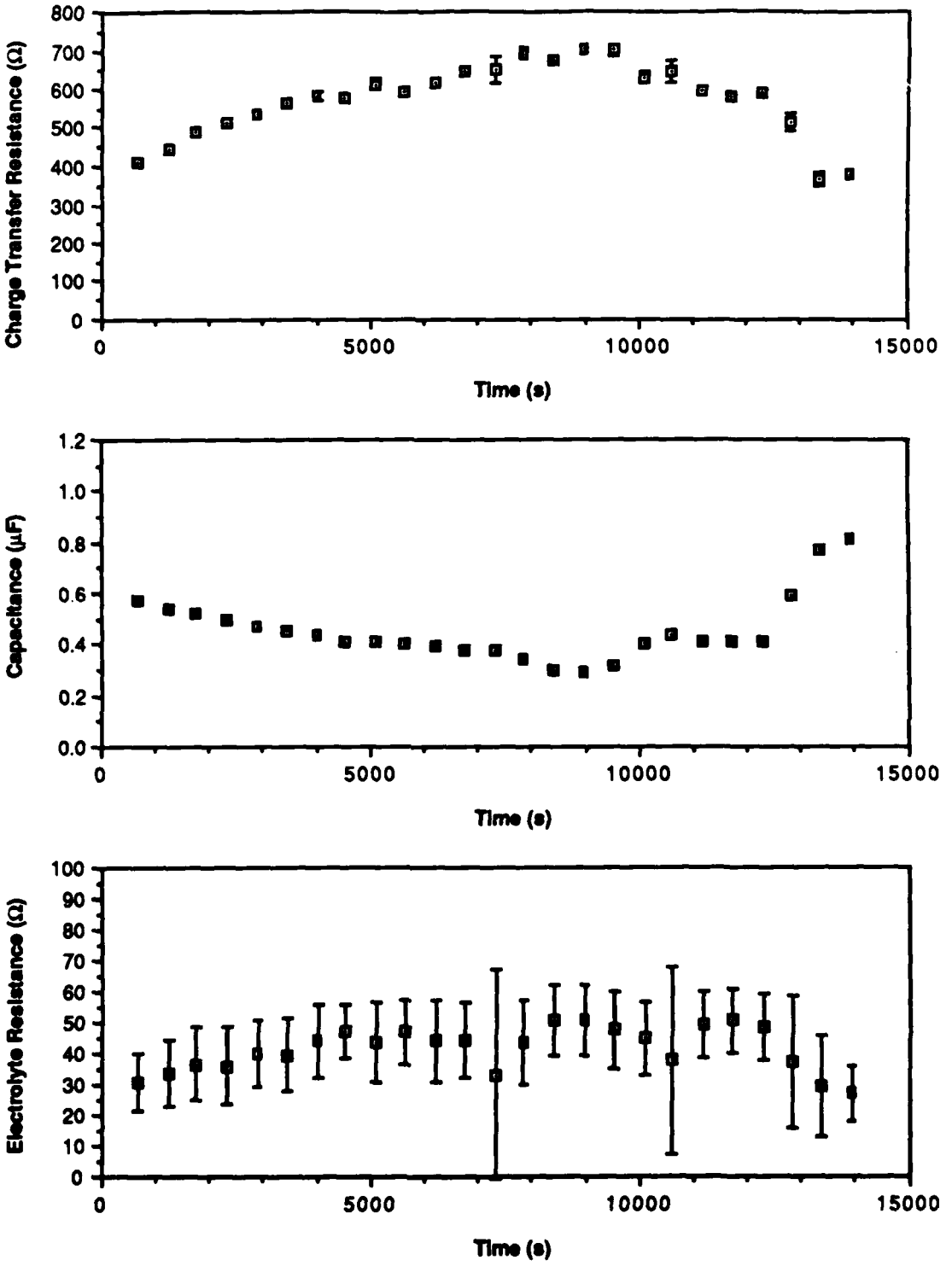

Figure 5.4: Electrical analog values representing best fit to impedance data as a function of time. Electrolyte was added to the corrosion cell at t = 0. The above data is for 6N purity Zn in 1.0 M HCl. The same electrodes were used for this data as for the data of figure 5.3. No error bars were calculated for the capacitance.

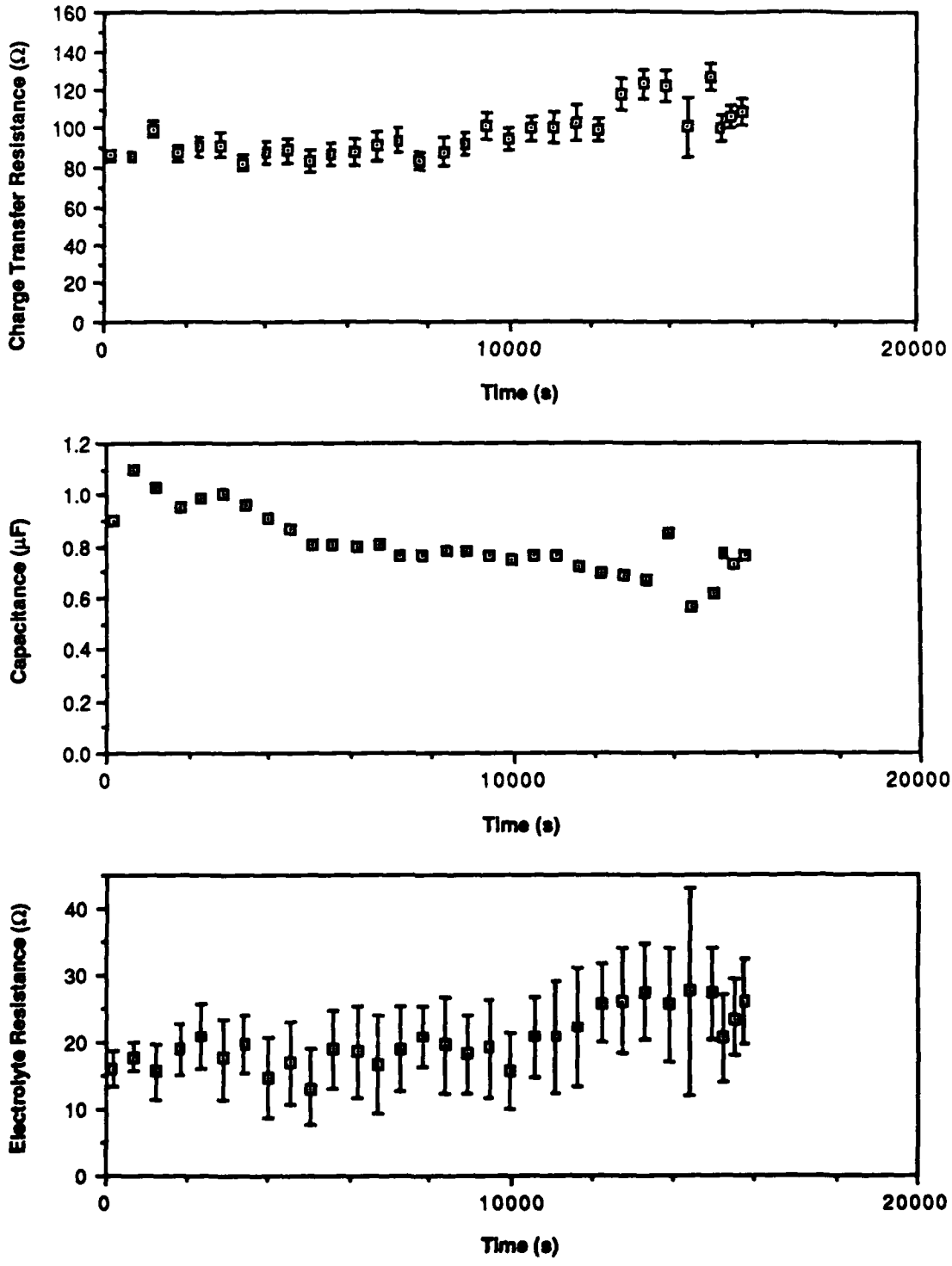

Figure 5.5: Electrical analog values representing best fit to impedance data as a function of time. Electrolyte was added to the corrosion cell at t = 0. The above data is for 6N purity Zn in 3.0 M HCl. The same electrodes were used for this data as for the data of figure 5.3. No error bars were calculated for the capacitance.

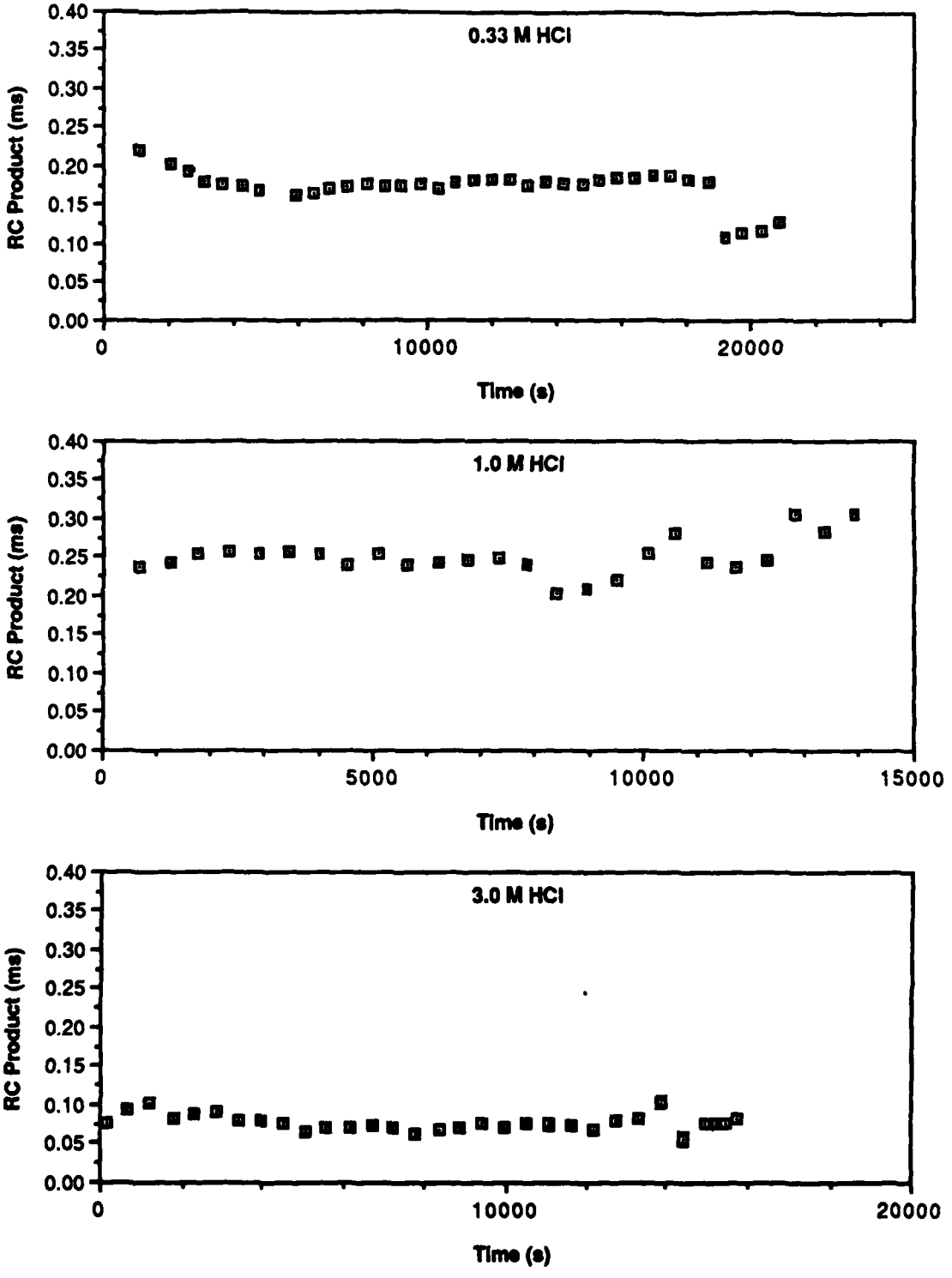

Figure 5.6: The RC product as a function of time for the reactions depicted in figures 5.3, 5.4, and 5.5. The top graph corresponds to figure 5.3, the middle to the 5.4, and the bottom to 5.5.

In more a vigorous reaction, e.g. 4N85 Zn (i.e. Zn with 15 impurities per 10^6 atoms) in 3.0 M HCl, the impedance of the cell deviates from ideal by progressively larger amounts as the reaction proceeds. Distortion of the impedance characteristics is attributed to extreme roughening of the surface. A high degree of surface topography was visible with microscopic examination of such surfaces. Both theoretical[105,106] and experimental[107] studies of the impedance as a function of surface roughness demonstrate a strong, and to large degree unpredictable, link between interfacial impedance and surface topography.

However there is another factor which is important: the analysis of the electrochemical cell assumed identical surfaces. If those surfaces have different impedances and different $R_{ct}C_d$ products, then the total cell impedance will be distorted from the ideal semicircle. The distortion will take the form of elongating the semicircle form of the real-imaginary plot. However, the sum of the total cell charge transfer resistance $(R_{ct1} + R_{ct2})$ will still be determined by the low frequency intercept of the real axis. Since the analysis is done for low frequency, and the value of importance is the total charge transfer resistance, some distortion of the impedance characteristic due to unequal impedances could be tolerated if it could be easily distinguished from distortion due to severe surface roughening. The relative consistency of the RC products in figure 5.6 indicate that distortion due to different RC products should not be a problem.

5.2 NOISE MEASUREMENTS

Experiments to determine the source(s) of interaction current fluctuations in the corrosion of Zn in HCl provide the focus of the following section. Measurements have determined the following:

- Overall fluctuation amplitude.
- Interaction current noise versus interfacial voltage noise.
- Current noise power as a function of frequency.
- Variable load analysis of noise source(s).
- Current noise amplitude versus average current amplitude.
- Current noise amplitude versus cell impedance at 100 kHz.
- Current noise amplitude versus cell impedance at 1 kHz.
- Current noise power as a function of R_{ct}.

Presentation of the results of these experiments, and their interpretation, constitute the rest this chapter.

The important results, as they pertain to understanding the corrosion of Zn in HCl, can be summarized as follows. Large current spikes appear to be the dominant source of noise. These spikes occur when bubbles release from the surface, exposing active cathodic regions. The surge in hydrogen reduction which results is throttled either by a gas film forming on the active site or by mass transport. The exposed cathodic site is sufficiently active to drop the impedance of the interface significantly. Neither electrolyte resistance nor electrode area fluctuations are important sources of noise in the interaction current.

5.2.1 Fluctuation Amplitude

The analysis of chapter three assumed that the fluctuations of the interaction current are much less than the corrosion current. This section addresses that concern for the reaction of Zn in HCl. The characteristics of the interaction current fluctuations in the time domain are also discussed.

Fluctuations of the interaction current were measured for 6N purity electrodes in the 0.33 M, 1.0 M and 3.0 M concentration HCl. The amplitude was quantified by determining the standard deviation of the interaction current over 5.7 second intervals and averaging that value over the total data set to determine the "average" standard deviation. The 5.7 second interval corresponded to the length of the data segment used for the power spectra analysis of the data. Thus, the interval over which the average deviance is calculated equals the interval used for subsequent data analysis. Results for the data are shown in table 5.3.

Table 5.3: Deviance of Interaction Current

Concentration of HCl (M)	Corrosion Current (A)	Standard Deviation (A)	Ratio σ/i_c	Shot Noise to 30 Hz (A)
0.33	$5.3\pm0.3 \times 10^{-6}$	2.7×10^{-8}	0.005	1.0×10^{-11}
1.0	$7.6\pm2.8 \times 10^{-6}$	5.7×10^{-7}	0.08	1.2×10^{-11}
3.0	$5.1\pm0.4 \times 10^{-5}$	3.1×10^{-6}	0.06	3.1×10^{-11}

The fluctuation amplitude is surprisingly large compared to the corrosion current. For comparison, the shot noise amplitude for a current the magnitude of the corrosion current (with a unit charge of 2e) is listed in the last column. The shot noise amplitude has been calculated for a bandwidth of 30 Hz, the approximate bandwith of the data aquisition electronics. The observed noise is three to five orders of magnitude

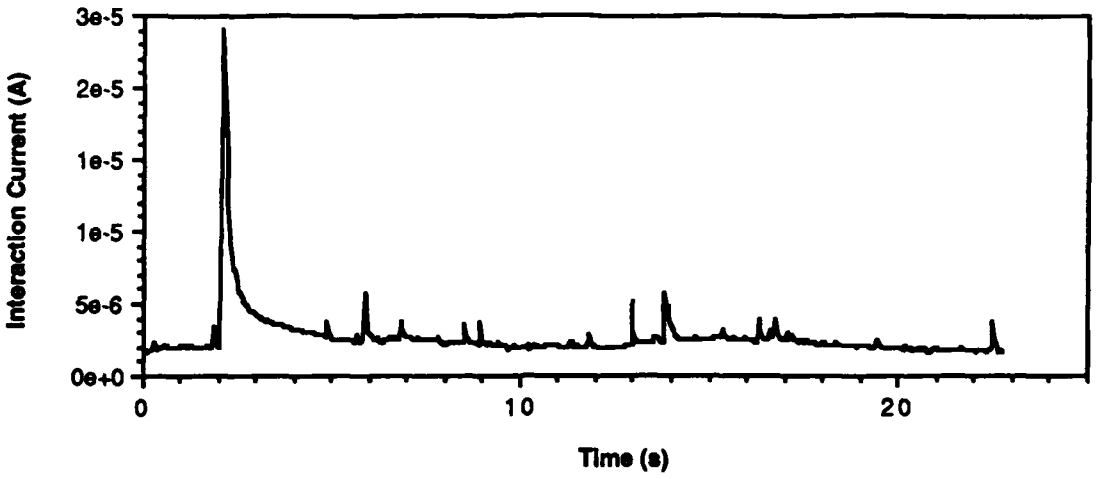

Figure 5.7: Current spikes in the reaction of Zn in 3.0 M HCl. The spike at two seconds provides an especially large example. Smaller spikes, e.g. the event at 14 seconds are more typical. Although the spikes in this example are all of the same polarity, generally spikes are observed with either polarity.

above the rate noise levels predicted for the interface.

The results clearly indicate that the fluctuation amplitude is sufficiently low for the analysis of chapter three to apply for the 0.33 M HCl data. However, the fluctuation level is dangerously close to being too large for the 1.0 and 3.0 M HCl reactions. This concern is amplified by visual inspection of the data accumulated on the interaction current. The time series data is dominated by "spikes." A particularly large spike is illustrated in figure 5.7. The amplitude of this event exceeded one half the corrosion current. In general the amplitude of the spike events was lower, usually less than a sixth of the corrosion current for the 1.0 and 3.0 M reactions. However, the presence of the spikes emphasizes the necessity to interpret the data with care.

Closer examination of interaction current data in figure 5.7 reveals a second noise process which appears as a slow undulation of the "steady-state" current. The term steady-state current is used here to describe the current in the intervals between spikes. The spikes are

distinct events which occur with a rate of roughly 0.5 s^{-1}. The variation of the steady-state current is more gradual in nature. Figure 5.10 shows the steady-state fluctuation more clearly.

The two proposed noise sources which yield power levels significantly larger than the shot noise level are hydrogen bubble evolution and catalyst number fluctuation. The rate of the respective events which drive these two mechanisms are substantially different. The events which drive hydrogen evolution noise are the growth and detachment of bubbles, while the events driving catalyst number fluctuation are the arrival and removal of impurities. The number of impurities atoms on a 1mm diameter zinc surface (6N purity) is on the order of 10^7. The number of hydrogen bubbles is orders of magnitude lower, a value of 10^2 being a reasonable number. If both processes have similar time constants, then on the order of 10^5 impurity events occur for every hydrogen bubble event. Consequently one might expect that events resolved on time scales of tenths of seconds will be more likely to be associated with gas evolution. General drifts of the steady-state current would, on the other hand, be more likely to result from the superposition of many small events, e.g. impurity number fluctuation.

5.2.1.1 Time Constant of Interaction Current Spikes

Visual examination of the spike in figure 5.7 reveals a sharp onset, followed by what appears to be an exponential decay. To determine the time constant of the decay, the following procedure was used. First, the steady-state current value is subtracted from the spike. The natural logarithm of the corrected interaction current is then plotted against time. By fitting a line to the resulting data, the time constant is

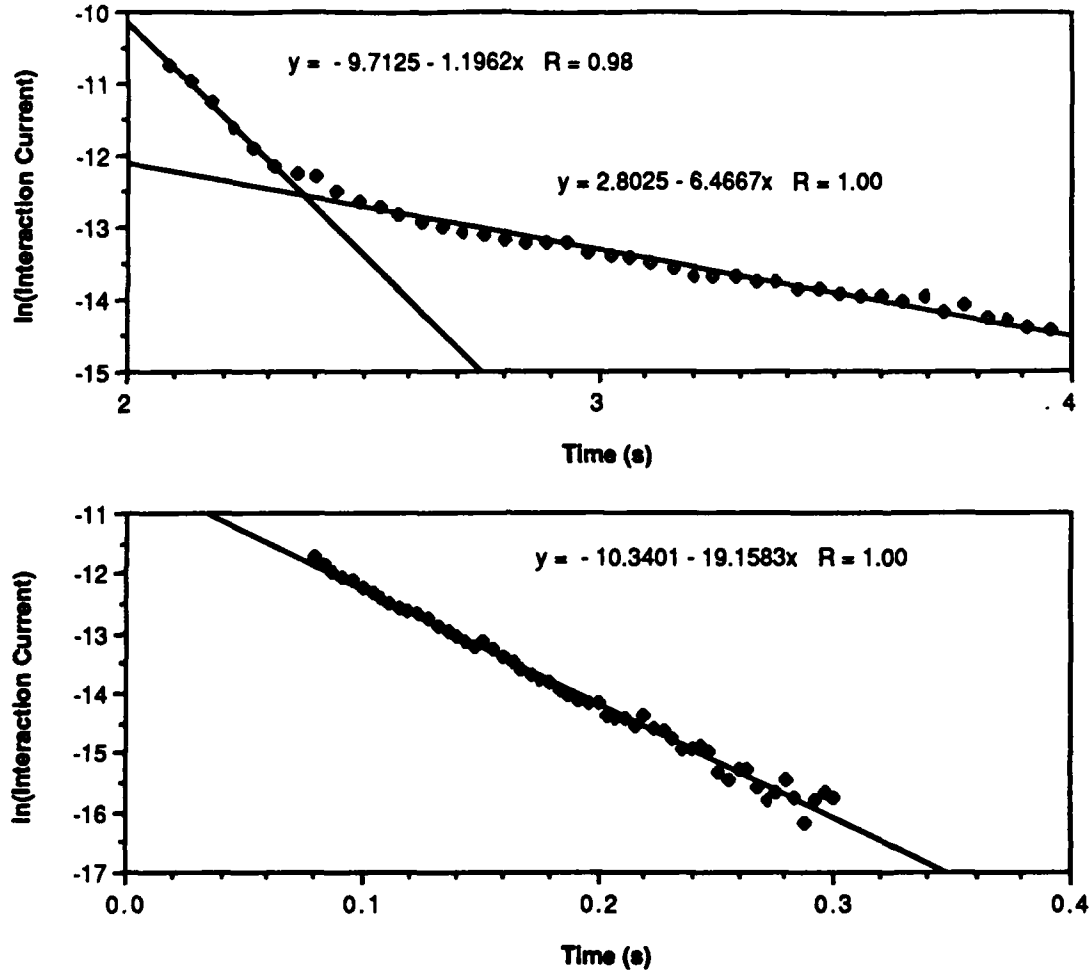

Figure 5.8: Plots of the decay portions of spikes observed for 6N purity Zn in 3.0 M HCl. After subtracting the steady-state current, the logarithm of the interaction current is plotted against time. The linear fit to the resulting plot is given in each figure. The time constant is given by the negative reciprocal of the quoted slope. Figure a) depicts the same large spike as in figure 5.7, while figure b) depicts another large spike observed in the same run.

determined.

Figure 5.8a illustrates the decay portion of the large spike in figure 5.7. It appears to have two time constants, 0.15 seconds and 0.84 seconds. A similar plot for another large spike observed during the same corrosion run is depicted in figure 5.8b. A very good fit is obtained with a time constant of 0.05 seconds. Visual inspection of the data confirms that a range of time constants are observed, even with the

smaller spikes.

The time constant is too fast to be related to double layer charging effects (time constants of the interface were determined to be on the order of 0.1 ms earlier in this chapter). Bubble growth, as was seen by Gabrielli et al.[43], is an unlikely explanation also. The growth of a bubble would result in a gradual rise, with an abrupt drop, rather than the other way around. The most likely event associated with the spike is bubble release from the surface. This was confirmed by tests in which the electrochemical cell was jarred to detach a bubble, resulting in an observed current spike.

To summarize the conclusions of this section:

- While amplitudes of observed current fluctuations appears to be generally low enough for the analysis of chapter three to be valid, spikes observed in the data may cause problems in the 1.0 and 3.0 M reactions.
- The largest spikes observed have amplitudes comparable to the corrosion current.
- The spikes consist of an abrupt rise, followed by an exponential decay.
- Decay time constants range from 0.05 to 1 seconds.
- The time constants are too slow to be associated with double layer charging.
- The spikes are associated with the detachment of bubbles.

5.2.2 Simultaneous Measurement of Current and Voltage

Simultaneous measurement of the interaction current and the average

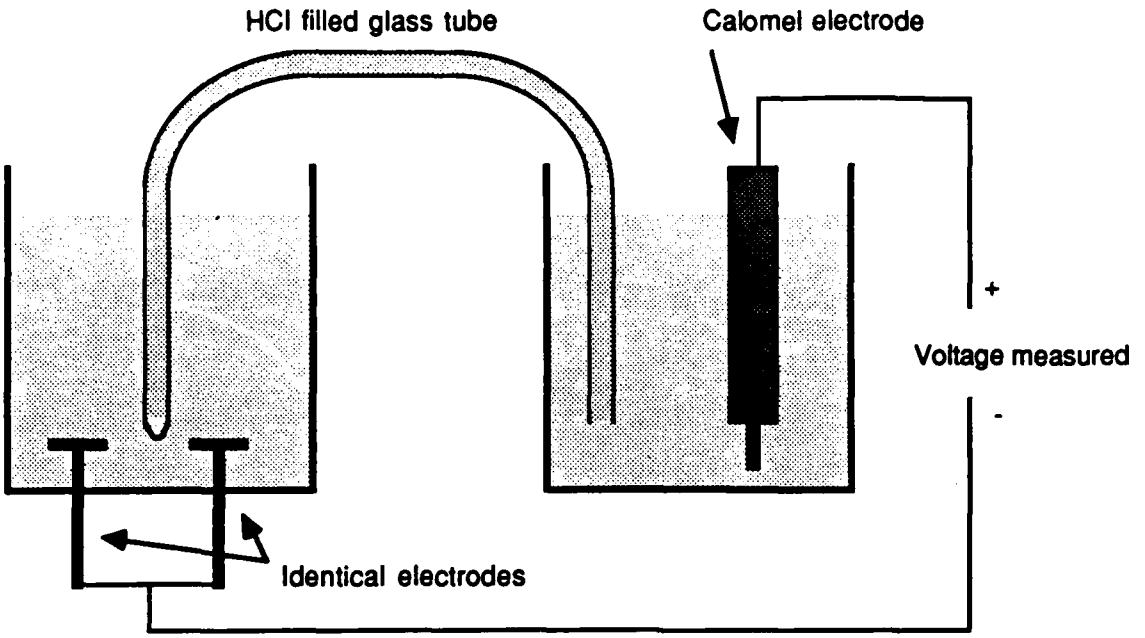

Figure 5.9: Experimental arrangement used to measure average potential drop across electrochemical interfaces of identical electrodes. Both electrolyte volumes were filled with HCl. The calomel electrode was isolated from the Zn in HCl cell to prevent the introduction of impurities to the Zn in HCl corrosion cell (the cell on the left).

voltage across the electrochemical interfaces was accomplished by incorporating a calomel electrode into the corrosion cell. The interconnect resistance (i.e. the external load) between the two electrodes was set to zero for these experiments, so that the Zn electrodes were always at the same potential. A voltage probe (a capillary filled with HCl) was placed directly between the two interfaces, so that the voltage, V_m, measured from the capillary to the Zn electrodes was equal to $(V_1+V_2)/2$, where V_1 and V_2 are the potentials across electrodes 1 and 2 respectively. Figure 5.9 illustrates the experimental arrangement.

Results of the simultaneous current-voltage measurement are shown in figure 5.10. Voltage spikes are associated with the observed current

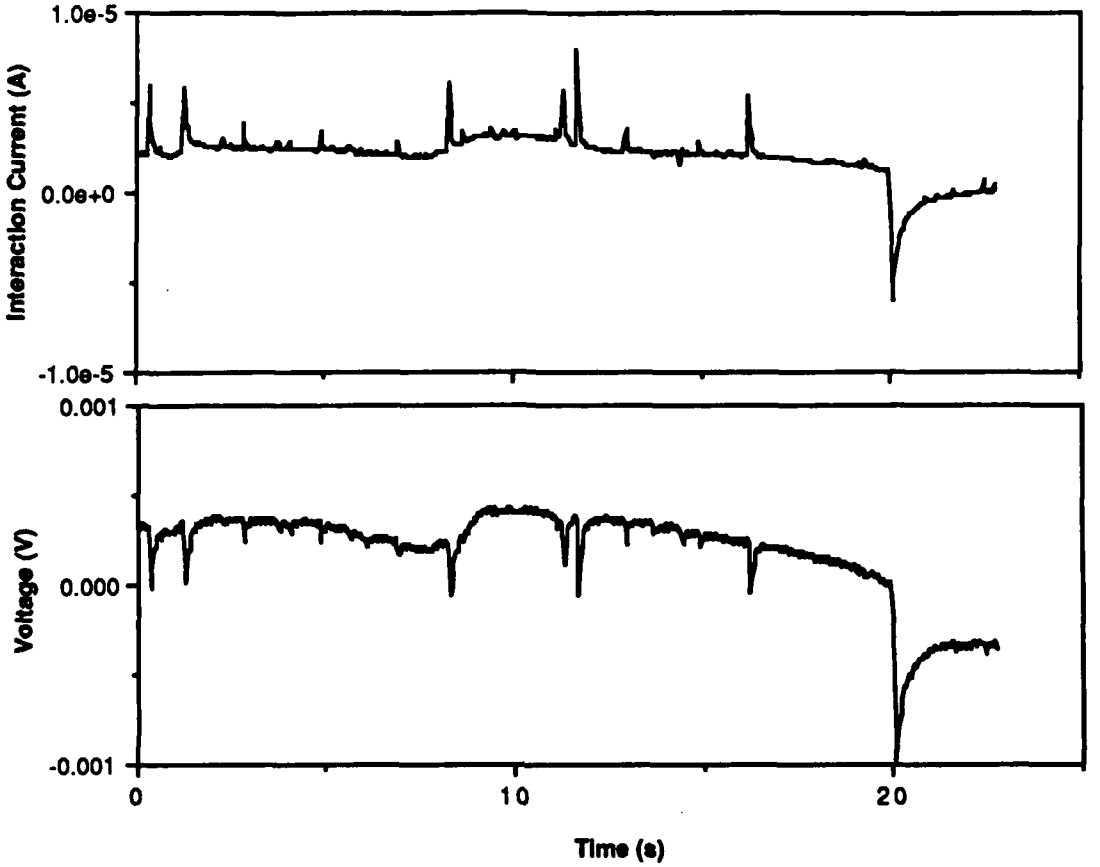

Figure 5.10: Simultaneous current and voltage measurements of 6N purity Zn reacting in 3.0 M HCl. Note that the spikes in the interaction current curve are of both polarities, while the spikes in the voltage measurement are all the same polarity. Also note that the steady state current drift is reflected in the voltage data.

spikes. The voltage spikes observed for the Zn in HCl are always of negative polarity, implying the spike represents either an increase in the cathodic rate or a decrease in the anodic rate. Since the events are associated with bubble release, which in turn exposes additional electrode surface and induces electrolyte convection, a decrease in the anodic rate does not seem plausible. Therefore the current spikes are most likely associated with increases in the rate of hydrogen reduction.

The acceleration of the cathodic process could result from convection

of electrolyte induced by bubble release. If convection accelerates the cathodic process, then the cathodic process must be throttled by diffusion. This seems unlikely since no evidence for diffusion control was found in the impedance spectra. Furthermore, the time dependent portion of a current flowing to an electrode under diffusion control decays as $1/\sqrt{t}$ [108] (this is true independent of whether the electrode is planar or spherical). Decay of the observed spikes has been proven to be exponential.

Exposure of an active cathodic region on the surface by the departing bubble is an alternative explanation for the sudden increase in cathodic rate. One might expect to find bubbles in the vicinity of an active cathodic site, since the concentration of dissolved hydrogen gas will be higher in these regions. Furthermore, impurities are already believed to play a substantial role in the cathodic process (see chapter four), and provide a candidate for the proposed sites. Decay of the current spike could then be attributed to buildup of a gas film layer on the active site. Gas films at hydrogen evolving electrodes have been previously proposed by Kuhn and Stevenson[38].

Buildup of a gas film layer can be used to explain the exponential decay of current. The rate of coverage of surface area by the film should be roughly proportional to the rate of production of hydrogen gas. Since the production of hydrogen gas is determined by the cathodic current, one can write:

$$\frac{dA_\beta}{dt} = -k\, i_\beta$$

Here A_β is the area of the active cathodic region, and i_β is the cathodic

current supported by the area. The constant k relates the change in area (due to coverage by the gas film) to the cathodic current. If the cathodic current is proportional to the exposed area, then the equation becomes:

$$\frac{di_\beta}{dt} = -\frac{1}{\tau} i_\beta$$

This clearly has as its solution a decaying exponential. The time constant of the current spike decay, τ, will depend on the cathodic rate of the exposed site, and the efficiency with which evolved hydrogen molecules are incorporated into the gas film. The range of time constants observed could be explained by observing that different impurities are present in the Zn used for the experiments. Thus the active sites, if they are impurities, might have a range of compositions.

There are other possibilities for active cathodic sites on a zinc surface. As has been previously discussed, defects will create a high degree of mophology in their immediate vicinity, providing large numbers of sites for proton adsorption. Thus defects might also provide a region more favorable to proton reduction.

5.2.2.1 Polarity of Current and Voltage Spikes

An interesting aspect of the simultaneous current and voltage measurements is that the polarity of the voltage spikes is independent of the polarity of the current spikes. This can be explained in terms of the circuit model described in chapter three.

The polarity independence of voltage and current spikes can be understood by incorporating current sources in parallel with both

interfaces into the circuit model of figure 3.4. Current source $I_1(t)$ is at surface 1, and source $I_2(t)$ is at surface 2. For both sources, a positive value directs current into the electrolyte. Then the interaction current can be written (once again ignoring double layer charging):

$$i_c = \frac{R_{ct1} I_1 - R_{ct2} I_2}{R_{aq} + R_{ct1} + R_{ct2}}$$

The voltages across the interfaces are:

$$V_1 = R_{ct1} I_1 - \frac{R_{ct1}\left(R_{ct1} I_1 - R_{ct2} I_2\right)}{R_{aq} + R_{ct1} + R_{ct2}}$$

$$V_2 = R_{ct2} I_2 + \frac{R_{ct2}\left(R_{ct1} I_1 - R_{ct2} I_2\right)}{R_{aq} + R_{ct1} + R_{ct2}}$$

Setting $R_{ct1} = R_{ct2} = R$, one has for V_m and i_c:

$$V_m = \frac{R\left(I_1 + I_2\right)}{R_{aq} + 2R}$$

$$i_c = \frac{\left(I_1 - I_2\right)}{R_{aq} + 2R} \quad .$$

Current injection events of the same polarity will generate a voltage signal of similar polarity regardless of which electrode generates the event. However the resulting interaction current signal can be of either sign depending on the electrode which is source of the perturbation. Thus a current source model is capable of generating voltage and current spikes

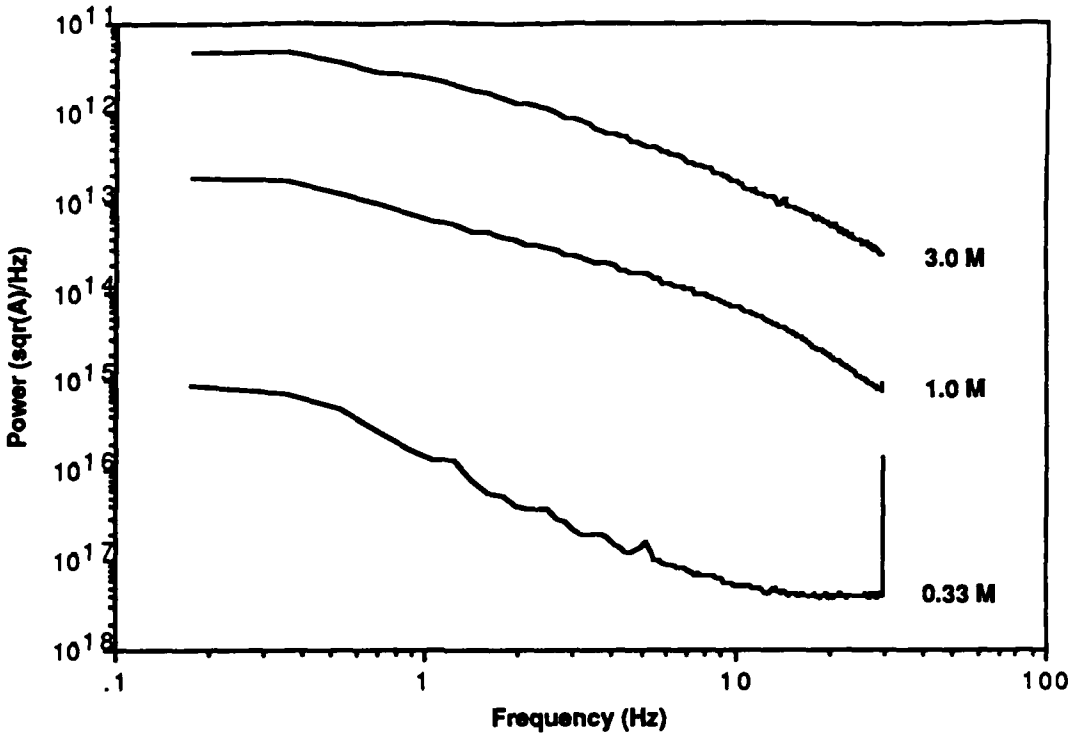

Figure 5.11: Power spectra of interaction current fluctuations for three different electrolyte concentrations. Data was obtained using a slightly noisier potentiostat than the one described in chapter four. Consequently, the background noise level contaminated the data for the 0.33 M HCl run above about 10 Hz. Aliasing of 60 Hz power-line pickup generated the spike at 30 Hz (the sample rate was 90 Hz). Each plotted spectrum represents the averaging of at least 850 individual spectra obtained over a time period of more than four hours.

of either the same or opposite polarity, by invoking sources at both interfaces.

5.2.3 General Spectral Characteristics

The characteristics of the power spectra depends on electrolyte concentration, electrolyte purity, Zn purity, and other factors relating to the reaction rates. Figure 5.11 depicts the noise level measured for 6N purity Zn corroding in various concentrations of HCl. Since increasing the HCl concentration leads to higher corrosion rates, the general conclusion which can be drawn from figure 5.11 is that higher corrosion

rates generate a greater noise amplitude. One would expect this to be the case since higher corrosion rates imply greater event rates, which in turn imply more noise.

Spectra of the interaction current can be characterized as having a $1/f^{\alpha}$ frequency dependence. The general trend for the spectra in figure 5.11 is for α to be small at low frequencies and large at high frequencies, ranging from zero to two. The spectrum of the 0.33 M HCl data is an exception to this generalization because the corrosion cell noise power drops below the potentiostat noise above 10 Hz. The potentiostat noise was slightly higher for this experiment than indicated in chapter four because a 3140 op-amp (National Semiconductors) was used instead of the OP-27. The flat part of the 0.33 M HCl spectrum (i.e. above 10 Hz) should be ignored. Between 0.3 Hz and 10 Hz both the 1.0 M and 3.0 M reaction drop with $\alpha \approx 1$, with the 3.0 M reaction being slightly steeper. Above 15 Hz both the 1.0 M and the 3.0 M data have an $\alpha \approx 2$, with the 1.0 M reaction being slightly steeper. The 0.3 M reaction drops with $\alpha \approx 2$ between 0.3 Hz and 3 Hz.

The models presented in chapter two generally predict either Lorentian or Lorentian-like spectra. Both the hydrogen evolution model by Gabrielli et al.[43], and the catalyst fluctuation model proposed by the author predict a flat spectrum at low frequencies and $1/f^2$ at high frequencies. While the data does not appear to be a particularly good fit to a Lorentzian, its general characteristics are observed.

A model developed by McWhorter[109] for explaining 1/f noise in the electrical properties of germanium may help explain the data (see also van der Ziel[110]). McWhorter illustrated that 1/f spectral characteristics may result from a superposition of Lorentians with different time

constants. A Lorentzian spectrum can be written as:

$$S_i(\omega) = 2\pi\overline{\Delta i^2}\frac{\tau}{1 + \omega^2\tau^2}$$

where the time constant is τ. Note that this has the same form as spectral distribution derived for the catalyst number fluctuation. For catalyst number fluctuation the time constant is given by $N\lambda/r_\alpha$ which is the average residence time of an impurity on the surface. In Gabrielli's model the time constant is the average period of bubble nucleation.

To obtain a 1/f spectra, McWhorter postulated a distribution of time constants. The probability a particular event has a time constant of τ is $g(\tau)$. Then the spectrum can be written:

$$S_i(\omega) = 2\pi\overline{\Delta i^2}\int_0^\infty \frac{g(\tau)\,\tau\,d\tau}{1 + \omega^2\tau^2}$$

With a choice of $g(\tau) = 1/(\tau \ln(\tau_1/\tau_0))$ for $\tau_0 \le \tau \le \tau_1$ and $g(\tau) = 0$ otherwise, one has for the spectrum:

$$S_i(\omega) = \frac{2\pi\overline{\Delta i^2}}{\omega \ln\left(\tau_0/\tau_1\right)}\left[\tan(\omega\tau_1) - \tan(\omega\tau_0)\right]$$

Thus, the power spectra is flat for ω much less than $1/\tau_1$, falls as $1/f^2$ for ω much greater than $1/\tau_0$, and falls as 1/f between these two demarcations.

Analysis of the current spikes has already determined a range of time constants for the decay of the spikes. The model therefore fits the

experimental evidence. Thus the regions of the spectrum with $\alpha \approx 1$ can be explained by incorporating a model with a range of time constants. For the 1.0 M data the τ_0 would be about 0.02 seconds, and τ_1 about 0.5 seconds.

The model for describing the mechanism underlying the power spectra is as follows:

- The current spikes are the dominant contribution to the power spectra.
- The power spectra of such spikes will have a Lorentzian-like form, with the time constant of the spectra roughly equal to the time constant of the current spike.
- The spikes have a distribution of time constants.
- The resulting power spectrum is the superposition of many Lorentzian-like spectra.

The general trend of the observed power spectra is for the onset of $1/f^2$ noise to occur at low frequencies as the concentration of HCl drops. Thus longer time constants are observed as the concentration drops, which is expected from the model proposed for gas film coverage of cathodic sites. The lower proton concentrations will lead to lower current densities at the cathodic sites, prolonging the period of buildup of the gas film.

5.2.4 Variable Load Noise Analysis

Variable load analysis can be used to extract the charge transfer resistance and to determine if the dominant current fluctuations are

passive or active in origin. As described in chapter three, resistance or area fluctuations, being passive, follow $1/R_t^4$ at high values of R_t, while fluctuations in the anodic or cathodic rate of one of the surfaces follow $1/R_t^2$.

Noise power as a function of total external load is plotted in figures 5.12 for two different frequency bandwidths. A summary of the run parameters are listed below:

- The data set aquired with the SQUID magnetometer.
- Measurements made in mu-metal shields.
- 6N purity zinc (sample LC-9) in 1.0 M HCl.
- Pretreatment included exposure to nitric acid just prior to run.
- Total time to accumulate data: 2 hrs.

Etching of the electrode in nitric acid deviates from the preparation technique described in chapter four. While nitric acid was very effective in removing surface impurities, it also removed several μm of Zn, complicating the measurement of the average corrosion rate as described earlier in this chapter. Consistent experimental results were obtained using the less destructive preparation techniques described in chapter four, and these were used for all of the other data in this thesis.

Two variable load plots are shown in figure 5.12. One plots average power density in the bandwidth from 0 to 2.8 Hz against applied load, while the second plots power density from 36.6 to 39.4 Hz. Least squares fits to the data are shown for both passive and active fluctuations. The parameters of the fit are noise amplitude and effective charge transfer

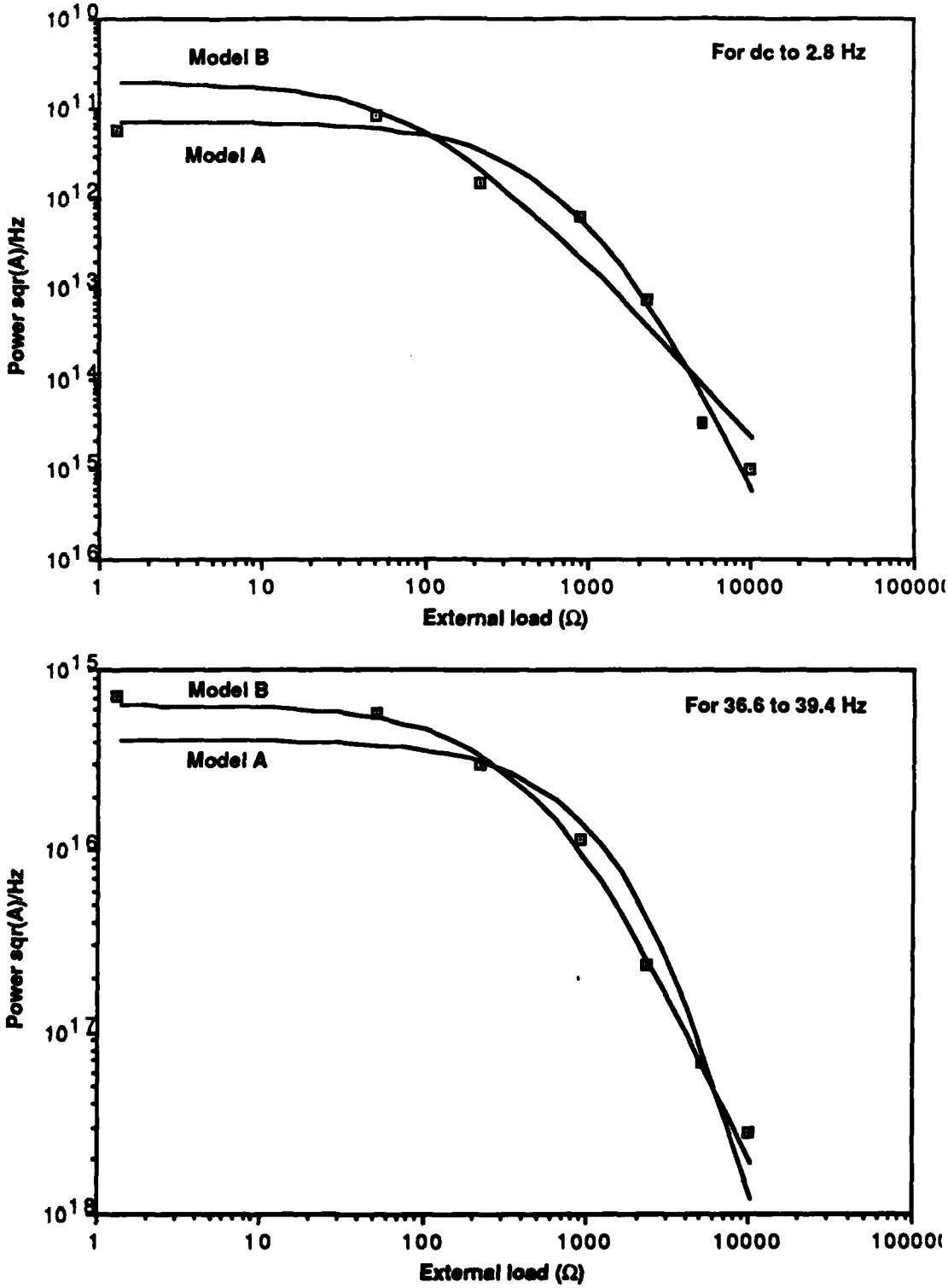

Figure 5.12: Power as a function of external load. Curve A represents the best fit for active fluctuations, and curve B the best fit for passive fluctuations to the plotted data. Power for the top graph was determined between 0 and 2.8 Hz, while power for the bottom graph was determined between 36.6 and 39.4 Hz.

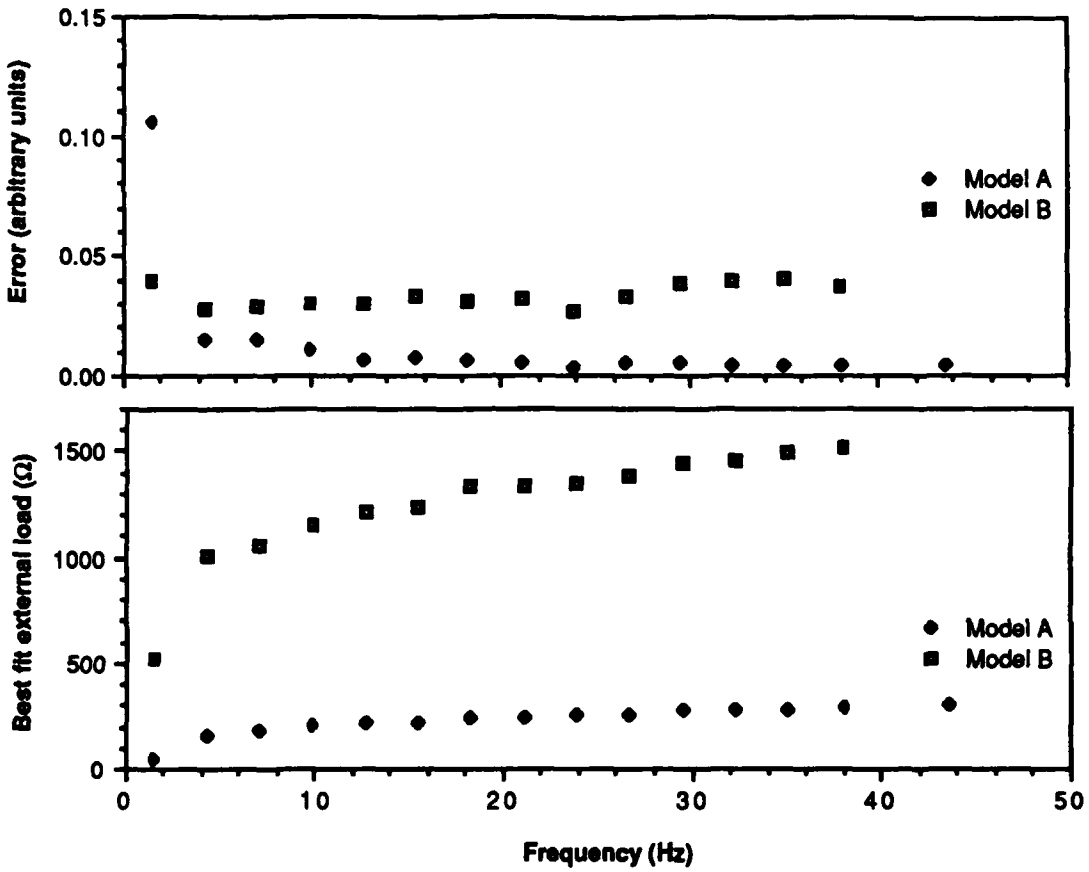

Figure 5.13: Error and best charge transfer resistance fits for active fluctuation model (model A) and passive fluctuation model (model B). Impedance measurements of the same surface yielded a charge transfer resistance of 690 Ω. The error quoted is of the least squares fit to the data, and is in arbitrary units.

resistance. For the lowest bandwidth, passive fluctuations give a slightly better fit. However the large amount of scatter of the data makes interpretation difficult. For all bandwidths above the lowest, active fluctuations provide a better fit. The higher bandwidths also exhibit a relatively low degree of scatter. The best charge transfer fit to the high frequency data is 290 Ω, which is less than half the 690 Ω value determined by impedance measurement.

The optimum charge transfer resistance depends on the bandwidth used for determining the noise power. In general, lower charge transfer resistance values are observed when the bandwidth is centered at lower

frequency. Figure 5.13 shows the "best fit" values for R_{ct} as a function of frequency using both a passive fluctuation and an active fluctuation model. Also shown is the relative error in the least squares fit of the data to the respective model. The active fluctuations fit best for all but the lowest bandwidth. At the lowest bandwidth, the error for either fit is relatively high.

Variable load analysis consistently generates charge transfer resistances which are too low compared to the impedance data. This is true not only for the data shown, but also other data taken by the author. The least underestimation measured in any run was 30%, but the factor of two calculated for the data above is more typical. The reasons for this are not clear. One possible explanation is that the charge transfer resistance of the interface drops during a current spike. Since most of the noise power derives from current spikes, the effective charge transfer resistance "seen" by the spike will be lower than the average charge transfer resistance (i.e. that measured via impedance techniques). This implies the cathodic sites exposed by bubble release are sufficiently active that they can substantially change the overall charge transfer characteristics of the interface.

5.2.5 Current Noise Power versus Average Current

The data presented in the previous section indicates the possibility that passive fluctuations may play a role at low frequency. An additional test to determine the viability of passive fluctuations is suggested by the analysis of chapter three of area or electrolyte resistance fluctuations. A feature common to these two noise mechanisms is that the current fluctuations are proportional to the average value of the

interaction current. This can be understood since both mechanisms simply modulate an already existing interaction current.

Rewriting the results of chapter three, the current fluctuation amplitude due to fluctuations in R_t can be written:

$$\overline{\Delta i_c^2} = \left(\frac{i_c}{R_{ct1} + R_{ct2} + R_t}\right)^2 \overline{\Delta R_t^2}$$

The parallel formula for area fluctuations (e.g. on electrode 1) is:

$$\overline{\Delta i_c^2} = \left(\frac{i_c R_{ct1}}{R_{ct1} + R_{ct2} + R_t}\right)^2 \frac{\overline{\Delta A_1^2}}{A_1^2}$$

Here $\Delta A_1/A_1$ is the fractional change of area on electrode 1. The formula for area fluctuations on electrode two can be obtained simply by exchanging the subscripts "1" and "2".

Assuming that the fluctuations which drive the noise ΔR_t and ΔA are independent of the interaction current, the observed noise power should be proportional to the square of the average interaction current level. This is an experimentally accessible measurement. Experiments to measure $S_i(f)$ versus average i_c were run for 0.33 M, 1.0 M, and 3.0 M HCl.

A plot of noise power versus average current is depicted in figure 5.14 for the reaction of 6N purity Zn in 3.0 M HCl. For this particular figure, the noise power was determined between 0 and 2.8 Hz. The bandwidth was chosen to be the same as gave evidence for passive fluctuations in the previous section. No relationship between the two variables is visible. Plots using the spectral power in different

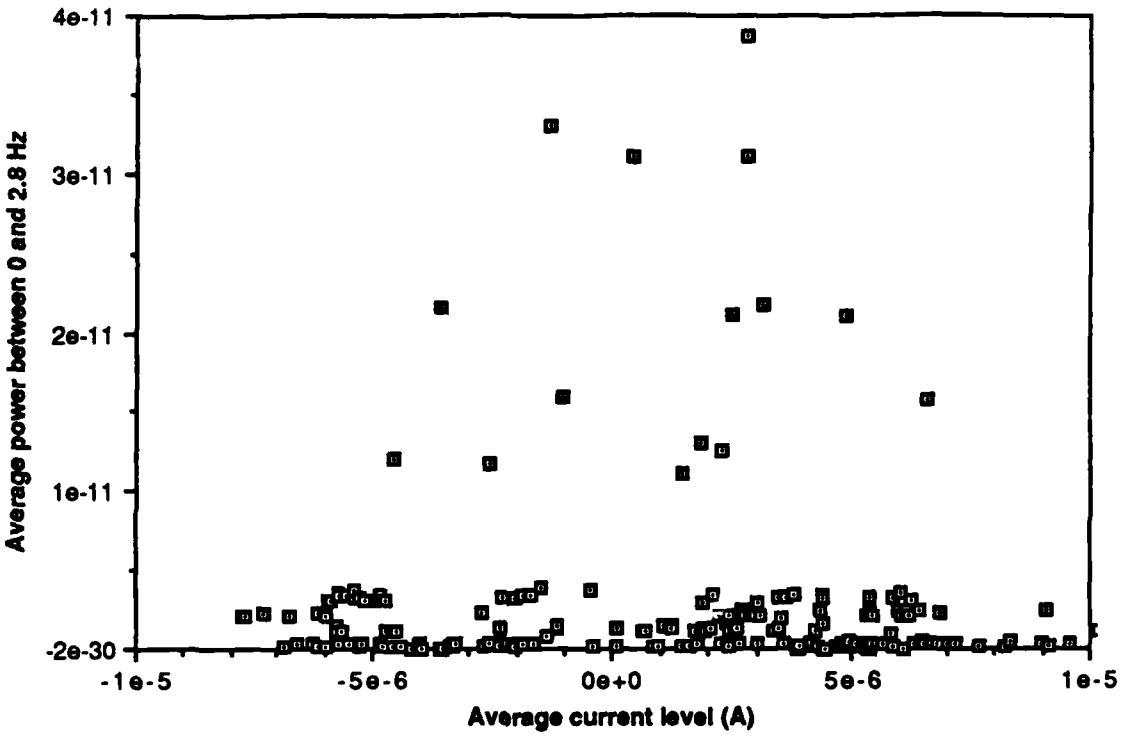

Figure 5.14: Total power in the frequency range from 0 to 2.8 Hz plotted against the average value of the interaction current. The time series segments used to calculate each data point are 5.7 seconds long.

bandwidths and/or with different concentrations of HCl all show similar lack of correlation. This result strongly contradicts area or electrolyte conductivity fluctuations as likely explanations for the observed noise.

5.2.6 Electrolyte Conductivity versus Interaction Current

A final test of electrolyte conductivity fluctuations was the simultaneous measurement of the cell impedance at 100 kHz and the interaction current. This was attempted by applying an 3 mV rms signal across the cell with the potentiostat, while holding the DC voltage at zero. The 100 kHz current output of the potentiostat was monitored by a lockin amplifier with a time constant of 30 ms. The output of the lockin (proportional to the cell admittance) and the current output of the

potentiostat below 30 Hz were both aquired using the computer data aquisition system. Since the cell impedance at 100 kHz is dominated by the electrolyte, this experiment effectively measured electrolyte resistance and interaction current at the same time.

The interaction current was measured using the potentiostat. The data aquisition was 90 Hz, and a 30 Hz low pass filter preceded the D/A system, as with earlier experiments in which the interaction current was measured alone.

A substantial drawback to the the experiment stems from the application of the 3 mV signal. At 100 kHz this results in roughly 180 μA of current though the cell, as compared to the corrosion current, which was on the order of 75 μA. Consequently, there is a large probability that the interaction current is significantly perturbed by the application of the 100 kHz signal. Unfortunately, reducing the amplitude of the voltage also reduces the signal to noise ratio, making resistance fluctuations quite difficult to resolve. On the positive side, if bubble related events drive the fluctuations, then these events may still occur since bubble growth and detachment continues even under application of the signal.

Typical output from a simultaneous measurement of impedance and interaction current for 6N purity Zn in 3.0 M HCl is shown in figure 5.15. There does not appear to be much correlation. To test the data rigorously, the coherence function of the two data sets was calculated using the techniques outlined in chapter four. Results of the coherence function calculation are in figure 5.16. Only at very low frequency is there any indication that coherence between the two signals might exist.

Although the results of this test are suspect, due to the large

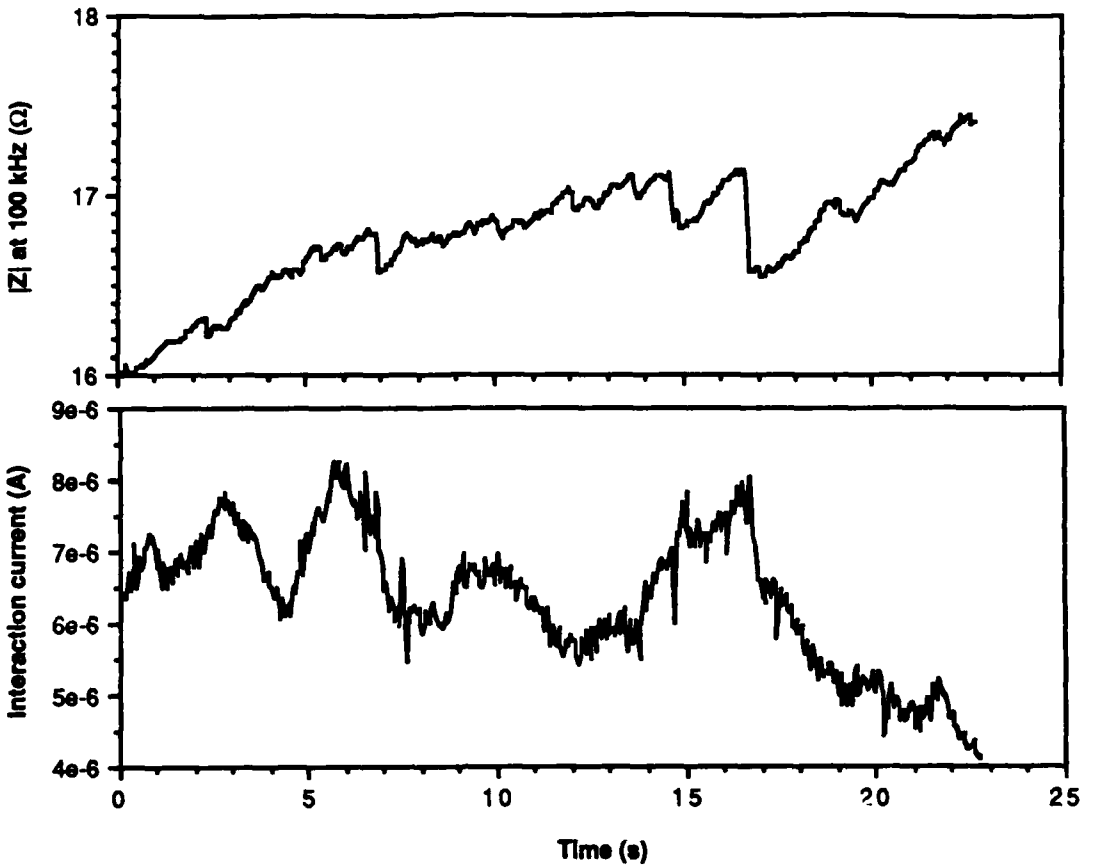

Figure 5.15: Simultaneous measurement of the interaction current and the high frequency impedance of the electrochemical cell. For the reaction of 6N Zn in 3.0 M HCl. The impedance is dominated by the electrolyte conductivity at 100 kHz.

currents with which the interface was perturbed, they do tend to indicate that aqueous resistance fluctuations can be only a small contribution. A particularly interesting point is that the amplitude of the measured resistance fluctuations is only about 5%. This is not large enough to account for significant fluctuations of the interaction current.

The experimental apparatus was by replacing the corrosion cell was replaced with a switch which was turned between 8 Ω and 50 Ω at random intervals (on the order of twice per second). The potentiostat was set to a small voltage so that a change in the current output of the potentiostat was observed when the switch was changed. This experiment produced a

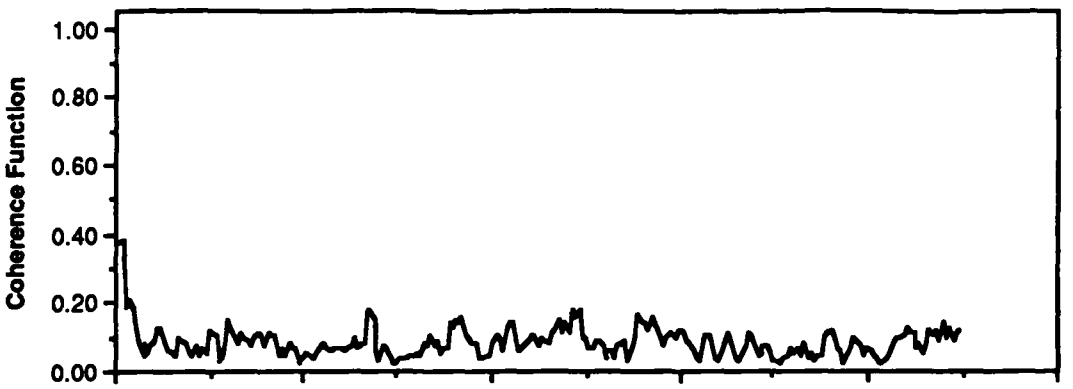

Figure 5.16: Coherence function for interaction current and high frequency impedance.

completely correlated resistance and "interaction current". The coherence function resulting from this test did not drop below 0.85 throughout the entire frequency range, proving that the lockin measurement is capable of detecting correlation between resistance fluctuations and the interaction current.

5.2.7 Cell Impedance versus Interaction Current

The cell impedance and interaction current were measured simultaneously, using a method identical to that used for the electrolyte conductivity and interaction current measurement. To measure cell impedance, a low frequency was used, in this case 1 kHz. The impedance measured by the lockin is sum of the the electrolyte resistance, and the impedance of the two interfaces. At 1 kHz the impedance contribution from the electolyte is 12 % that of the combined interface impedance.

Figure 5.17 shows simultaneous 1 kHz impedance versus interaction current plots for 6N Zn in 3.0 M HCl. A 8 mV signal was applied for this experiment, resulting in a current of about 60 μA. This is roughly comparable to the expected 50 μA corrosion current. The lockin amplifier was used with an integration time of 0.1 seconds which corresponds to a

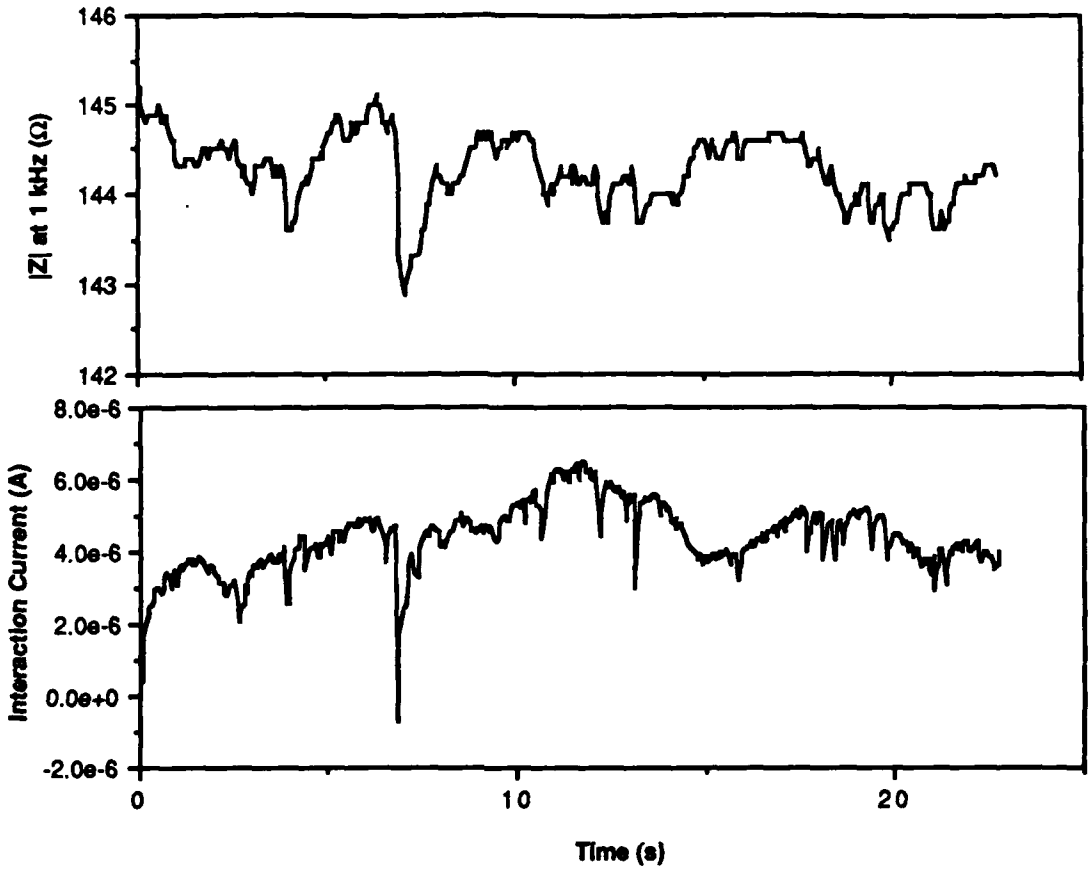

Figure 5.17: Simultaneous measurement of the interaction current and the high frequency impedance of the electrochemical cell. The impedance is dominated by the electrolyte conductivity at 100 kHz.

low pass filter of roughly 2 Hz.

There appears to be some correlation between current spikes and decreases in the cell impedance. Because of the effective 2 Hz low pass filtering of the impedance data, the decreases in impedance may be significantly more pronounced than are shown in figure 5.17. This lends some credence to the model advanced to explain the lower charge transfer resistances observed by the variable impedance technique. That model postulated that the current spikes are sufficiently large that the cumulative charge transfer resistance of the cell is reduced.

The coherence function between the interaction current and the

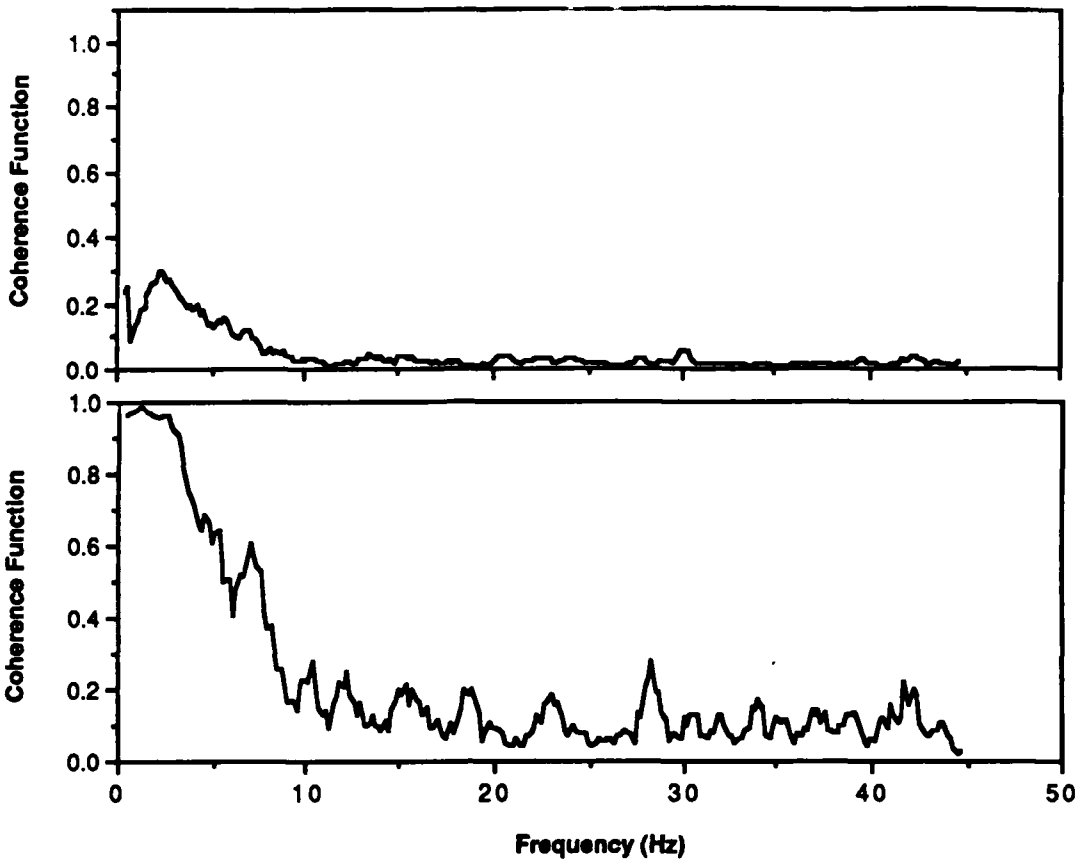

Figure 5.18: Coherence function for interaction current and cell impedance measured at 1 kHz (top), and for randomly switched resistor (bottom). Because of the large time constant used in the lockin, the impedance data is strongly filtered above about 2 Hz. Thus the bottom graph indicates that under ideal conditions coherence between the interaction current and the cell impedance can not be detected above 5 to 10 Hz.

impedance was calculated and is shown in figure 5.18. There appears to be about 20% coherence between the two observables up to about 5 Hz. The lack of correlation at higher frequencies is probably due to the instrumentation, as is described below.

The coherence function generated by measuring the randomly switched resistor arrangement is also shown in figure 5.18. The experimental set-up was configured the same way for the switching resistor test as for the experiment on the corrosion cell, including identical lockin settings. The coherence function for the switched resistor test indicates that

because of the filtering effect of the lockin amplifier on impedance measurement, the coherence measurement is only good below about 5 Hz.

5.2.8 Scaling of Noise Power with Charge Transfer Resistance

Scaling of noise power with reaction rate provides a valuable clue to the nature of the noise mechanism. For a process in which the events occur randomly and are statistically independent (i.e. a Poisson process), the relationship between the noise power and the rate of events can be written:

$$S_r(\omega) \propto a^2 r$$

The constant a is the event amplitude. The assumption of statistically independent events is physically reasonable, and makes the problem tractable.

In the Zn in HCl corrosion system, the events which generate the noise signal are most likely associated with hydrogen bubbles growing and/or detaching from the surface. Provided bubble sizes do not change significantly with concentration, higher corrosion rates will result in faster bubble growth and more bubbles nucleating and detaching per unit time. Thus the rate of bubble events should be proportional to the corrosion current. Recalling that R_{ct} varies inversely with the corrosion current, one expects the following relationship:

$$S_i(\omega) \propto 1/R_{ct}$$

This assumes the size of the event remains constant. Similar arguments can be made for other noise processes at an electrode (e.g. shot noise).

The argument that bubble size should not depend on concentration is

fairly straightforward but should be reviewed. The detachment of a bubble from a surface is determined primarily by the balance between its buoyancy and the surface tension of the electrolyte. The surface tension of HCl decreases by only 1.5% between 0.33 M and 3.0 M[111]. The density of the HCl increases 5% through the same concentration range[112]. Consequently, the size at which a bubble detaches should not be substantially affected by concentration.

Noise power as a function of charge transfer resistance is depicted in figure 5.19. Results from six runs at three different HCl concentrations (0.33 M, 1.0 M and 3.0 M) are plotted. The functional dependence of $S_n(\omega)$ on R_{ct} has the following form:

$$S_I(\omega) \propto (R_{ct})^{-4}$$

Clearly this is a much stronger dependence than one would expect from the previous discussion. The faulty assumption is most likely that the event amplitude is constant as a function of concentration.

The proposed mechanism for the current spike is exposure of active cathodic sites by departing hydrogen bubbles. The size of a current spike will be roughly proportional to the proton concentration in the electrolyte, given the same active site. Bringing all of the elements together, the current noise power should have the following form:

$$S_I(\omega) \propto \frac{C_o^2}{R_{ct}}$$

This accounts for some, but not all of the excess dependence of noise power on R_{ct}. The number of approximations which have been made in the

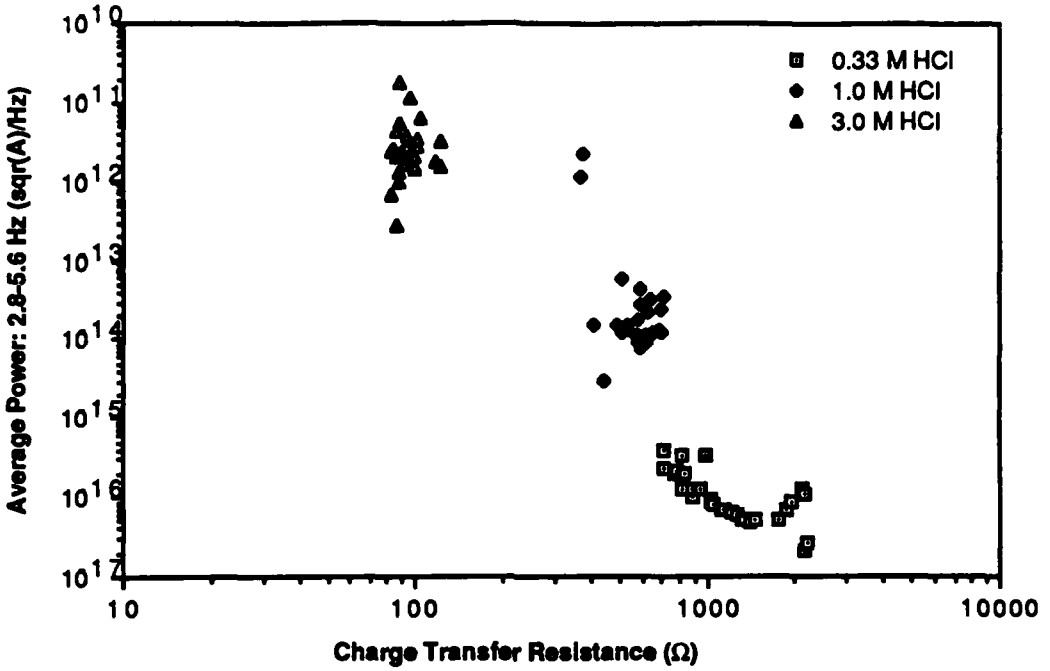

Figure 5:19: Power versus observed charge transfer resistance for 6N purity Zn in 0.33, 1.0, and 3.0 M HCl.

derivation precludes any pretense at precision.

The above discussion is replete with assumptions. However, the general idea of arriving at a stronger dependence of S_i on R_{ct} by incorporating the concentration dependent amplitude of noise events is clear. The strong implication of the analysis is that not only the rate, but also the amplitude of the fluctuation events will change with changing corrosion rate.

CHAPTER 6: CONCLUSIONS

This thesis had two objectives: to develop new methods for the study of electrochemical noise processes, and to use these methods to understand the noise mechanisms of a simple electrochemical system. Specifically,

- A mathematical treatment was developed to provide a link between fundamental noise processes and the interaction current flowing between the two electrodes, i.e. the fluctuation relationships.
- A technique of variable load analysis has been introduced which provides a means to measure the charge transfer resistance.
- Variable load analysis has also been demonstrated to offer the capability to distinguish between passive fluctuations and active fluctuations
- An electrochemical cell incorporating two identical electrodes was designed for studying electrode processes at open circuit potentials.
- Experimental results for measurements of the noise generated by the corrosion of Zn in HCl are presented.

One general conclusion is fairly unambiguous. There is no strict relationship which exists between noise power and corrosion rate. Experimentally, a correlation is observed when the same electrode is used for all experiments, and identical surface preparation techniques are used for each run. However, when different purity zinc is used, the noise levels can change an order of magnitude while the corrosion rates remain roughly the same. Consequently, noise power alone cannot be used to

measure corrosion rate.

The charge transfer resistances as measured by the variable load technique typically agree with standard impedance measurements to within a factor of two. Of the two measurements, the values obtained via variable load analysis were 30 to 50% lower. The explanation for the error advanced by the author centers on the discrete nature of the noise source (i.e. the current spikes). The variable load technique is sensitive to the interface parameters only during intervals the noise source is active (i.e. during a spike). However, the modification of the reaction rates which generate the current spike also appear to drop the cumulative charge transfer resistance of the cell. Thus the cumulative charge transfer resistance "sampled" by variable load analysis is lower than the steady-state value. Since the impedance measurement is sensitive to the average impedance of the cell, the variable load technique yields lower values. Therefore the author suggests even better agreement should be obtained for systems in which the fluctuations are less discrete or of smaller amplitude.

The ability to distinguish passive from active fluctuations has been unambiguously demonstrated. The variable load technique gives a quantitative method of differentiating between the two classes of noise sources. However, because the variable load technique requires noise measurements at different values of external load, it is especially susceptible to variations in the overall noise level of the cell which might occur during the course of the measurements. If the noise source is passive, changes in noise power might be driven by shifts in the steady-state level of the interaction current (passive fluctuations scale

with the interaction current). The measurements on Zn in HCl were difficult because the noise levels themselves fluctuate from minute to minute. Consistent results were obtained for this thesis by averaging over several hours of data.

The variable load technique also provides the capability for separating the contribution of an active noise source from that of a dominant passive noise source, although this was not demonstrated experimentally. The capability derives from the $1/R_t^4$ dependence of noise power on total load resistance observed by passive sources. This relation holds for external loads greater than the cumulative charge transfer resistance of the electrochemical cell. Active sources have only a $1/R_t^2$ dependence. Thus at sufficiently high values of external load, the dominant passive fluctuations will be attenuated sufficiently that active fluctuations will become the major contribution.

The observation that the contributing noise source may depend on the external load is a result of general importance for noise measurement in electrochemical systems. It is entirely possible that two experiments designed to measure the same noise source in a given electrochemical system will actually be sensitive to different noise sources. Thus the effective external load of the experimental apparatus as seen by the interface(s) under measurement must be considered in the interpretation of experimental data.

Plotting average current level versus noise level provides an unambiguous method to test whether the noise scales with the square of the steady-state interaction current. The fluctuation relations derived in chapter three indicate that such a correlation is a strong indication of

passive fluctuations.

The Fourier transform techniques used by the author provide the ability to segregate noise sources in the frequency domain. Both variable load measurement and the measurement of noise versus interaction current level can be accomplished using different bandwidths for determining noise power. Thus if two noise sources are dominant in different frequency ranges, it should be possible to resolve them.

6.1 Noise Processes in the Dissolution of Zn in HCl

To satisfy the second objective, dissolution of Zn in HCl was studied experimentally. This is a system with relatively simple reaction mechanisms. However, the evolution of hydrogen bubbles add considerable complexity. Convection induced by bubble release appears to be a dominant source of noise. Specifically,

- Current spikes are observed, the largest of which have amplitudes comparable to the corrosion current magnitude.
- Time constants of the spikes range from 0.02 to 0.05 seconds.
- Polarity of the voltage component of the spikes indicates a surge in the cathodic process, i.e. hydrogen evolution.
- The event triggering the spike is bubble detachment from the surface.
- Neither electrode area fluctuation nor electrolyte conductivity fluctuation contribute significantly to the noise signal.
- Variable load analysis indicates a best fit for active fluctuations.

- Variable load analysis yields a smaller resistance value than does impedance measurement by 30-50%.

The model constructed by the author to explain these results is tight and consistent. The current spike is initiated with the release of a hydrogen bubble from the electrode surface. The area of the electrode exposed by the departing bubble has low hydrogen overpotential compared to the rest of the surface. The region reduces hydrogen sufficiently rapidly that a gas film forms over the surface of the cathodically active region, rapidly throttling the process. The time constant observed is associated with the progressive coverage of the cathodic site by the gas film.

One might expect hydrogen bubbles to nucleate preferentially above regions with low potentials for hydrogen evolution since they produce high concentrations of H_2. The regions of low hydrogen overpotential could be impurities, defects in the crystal lattice, or grain boundaries. The author is unaware of evidence for the last two in the literature, but they should be considered since they satisfy two criteria: first, they are anomalous regions on the surface, and second, they should have high densities of dangling bonds to serve as proton adsorption sites. Impurities offer perhaps the best explanation. Large clusters of impurity atoms might be expected, even in a high purity material, since impurities are known to migrate preferentially to grain boundaries.

The noise mechanism proposed above can explain the lack of correlation between noise and corrosion rate. For example: a surface with many "weak" hydrogen reduction sites could maintain the same average cathodic current as a surface with a few "strong" sites. The signal from

the first surface would consist of many small current spikes, while the signal from the second would consist of a few large spikes. Consequently the surface with a few strong sites would produce higher noise levels while maintaining the same corrosion rates.

6.2 RESEARCH OPPORTUNITIES

Many possibilities exist for expanding on this work using identical electrode systems for understanding electrochemical noise processes. Study of noise processes in other systems, especially those not dominated by hydrogen evolution, is an obvious next step. Also, a useful extension of the present work would be to rederive the fluctuation relations incorporating the effects of double layer charging and diffusion limited transport.

In the following sections two experiments are reviewed which would expand on the capabilities initiated in this thesis. Integrating identical electrodes into a rotating electrode system is proposed as a method by which the observed gas evolution noise could be suppressed. An experimental geometry which would provide for the measurement of the interaction current between two identical electrodes, while applying a net current to the system, is proposed as a method to greatly extend the electrochemical regimes accessible to the noise analysis methods investigated here.

6.2.1 Rotating Electrode Noise Measurements

Incorporating the two-electrode corrosion cell into a rotating disk

electrode offers several advantages for noise measurement.

A rotating disk electrode consists of a disk, with the electrode surface(s) embedded in its face, which is rotated around the disk's axis. Fluid convection for this system has been extensively studied, and is simple compared to other convectional systems. The existence of a hydrodynamic boundary layer near the electrode surface provides a region across which the reactants must diffuse. This produces well defined boundary conditions for diffusion processes since the electrolyte beyond the diffusion layer is generally assumed to have bulk concentrations of the various species. The relationship between rotation frequency (ω) and the diffusion layer thickness (δ) has been determined, and is:

$$\delta = 1.61\, D^{1/3}\, \omega^{-1/2}\, \upsilon^{1/6}$$

Here υ is the viscosity of the electrolyte. Diminishing the diffusion layer thickness will increase the rate of diffusion across the interface. Thus neither hydrogen bubble nor concentration gradient driven convection should occur, given sufficient rotation speed.

A specific problem which could be solved using a rotating disk system is that of gas evolution. The dominance of gas evolution noise prevented study of some of the possible noise sources suggested in chapter two (e.g. catalyst number fluctuation and morphology related noise). By eliminating hydrogen bubble formation, other, more subtle noise processes could be detected and investigated.

Rotation speed is yet another experimental parameter which one can vary while making noise measurements. One should be able to measure noise versus diffusion layer thickness during a single run. This would allow

one to test whether noise mechanisms in a given system were influenced by mass transport properties near the electrode. Experimental parameters which can be varied without replacing the electrode or changing the electrolyte characteristics are especially useful since concerns about variations in such parameters as the electrode microstructure and impurity concentration will be greatly diminished.

There are at least two potential problems which could complicate this experiment. Both hydrodynamic instabilities associated with the rotating electrode, and the electrical connection between the rotating electrode assemble and the laboratory instrumentation, could generate their own noise. Clearly a great deal of care should be exerted to ensure that the rotation of the electrode is smooth and vibration free to avoid the first problem. The second problem could be eliminated by assembling a preamplifier on the rotating electrode and passing the amplified signal to the laboratory electronics.

6.2.2 Two-Electrode Impressed Current Measurements

A relatively simple modification of the present experimental apparatus would allow fluctuations in the interaction current to be measured during application of a net current to the cell. The advantage of such an experiment is that the interface could be driven into regimes outside those selected by the equilibrium currents or corrosion currents of the electrode itself. This could simplify noise analysis tremendously by allowing experiments in a regime in which a single reaction process dominates the current contribution.

The proposed experimental arrangement and the equivalent circuit are

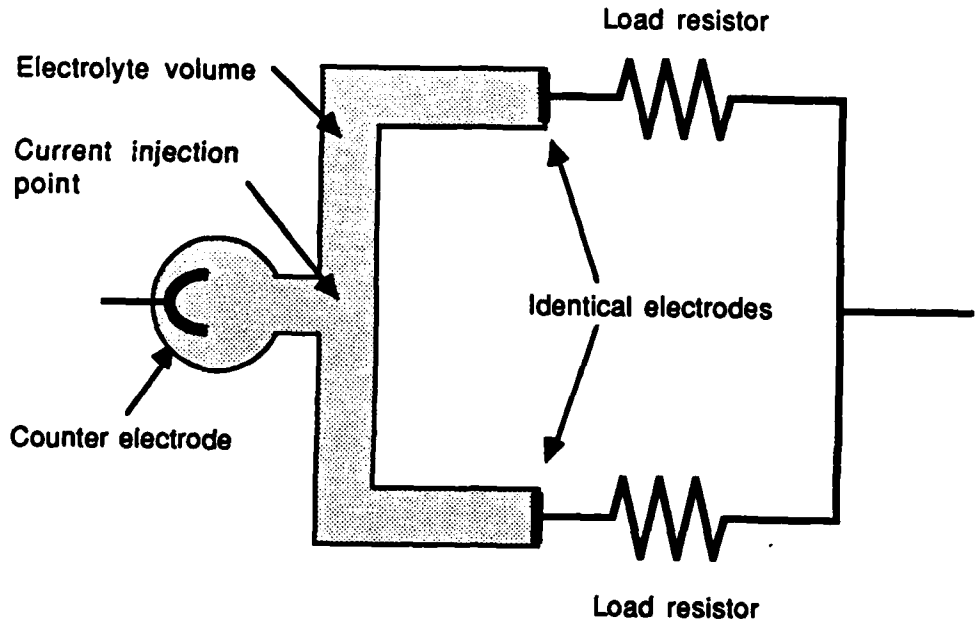

Figure 6.1: Design for measuring interaction current between two identical electrodes (also refered to as the working electrodes) while applying a net current to the system. The load resistors on each of the working electrodes should be equal.

illustrated in figure 6.1. A counter electrode has been added to the system for current injection on the electrolyte side. The electrochemical cell should be completely symmetric with respect to the working electrodes (the electrodes between which the interaction current flows). This should ensure that the electrolyte resistance is the same between the counter electrode and each of the working electrodes. The system also uses two identical load resistors. The external current source is attached to the counter electrode and between the two load resistors, and a driving current, i_d, is applied to the cell. The equivalent circuit for the cell is illustrated in figure 6.2.

Only slight modification of the analysis in chapter three is required for derivation of fluctuation relations for the proposed cell. Take the

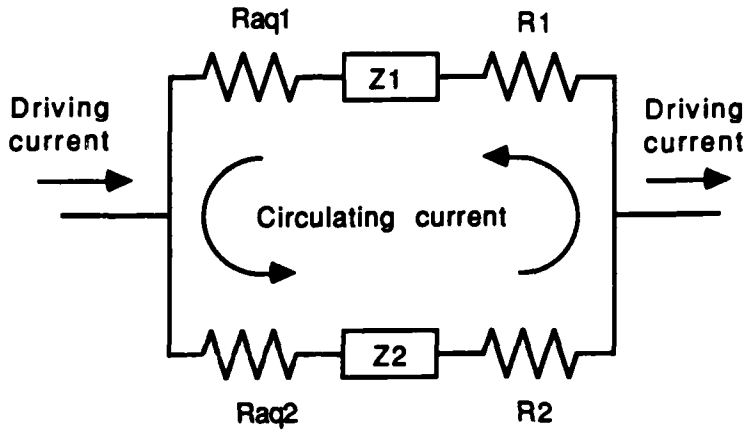

Figure 6.2: Equivalent circuit for the biased identical electrode cell. The interfaces are represented by impedances Z_1 and Z_2. The cell should be constructed so that the aqueous resistance, R_{ct1} and R_{ct2}, are equal. The load resistances, R_1 and R_2, should be equal also.

total current through electrode one as i_1 and the current through electrode two as i_2. Then writing i_1 and i_2 in terms of i_c and i_d, one has:

$$i_d + i_c = i_{a1}e^{\gamma_a(V_1 - V_{a1})} - i_{b1}e^{-\gamma'_b(V_1 - V_{b1})}$$

$$i_d - i_c = i_{a2}e^{\gamma_a(V_2 - V_{a2})} - i_{b2}e^{-\gamma'_b(V_2 - V_{b2})}$$

$$V_1 + i_d(R_{aq1} + R_{aq2} + R_1 + R_2) + i_d(R_{aq1} - R_{aq2} + R_1 - R_2) - V_2 = 0$$

The values R_{aq1} and R_{aq2} are the aqueous resistance between the current injection point and the respective working electrodes. Note that the current injection point is not the counter electrode. The current injection point is the midpoint of the electrolyte channel between the two electrodes, at the junction with the channel from the counter electrode (see figure 6.1). This can be understood since $R_{aq1}+R_{aq2}$ must equal the

total resistance between the two electrodes.

Mathematical manipulation identical to that of chapter three will yield the fluctuation relations for the biased system. One consequence of the biasing current will be to amplify passive fluctuations such as fluctuations in the aqueous resistance near one electrode.

Use of an electrochemical cell like that proposed above could facilitate the study of noise mechanisms in electrochemical processes such as electrocrystallization, or pitting under conditions of impressed current. Gas evolution could be investigated in the absence of corrosion processes, e.g. on platinum electrodes. In short, the proposed cell should allow the techniques advanced in this thesis to be brought to bear on broad and exciting range of electrochemical processes.

APPENDIX A: HIGHLY ASYMMETRIC RANDOM TELEGRAPH SIGNAL

The random telegraph wave has two states, which shall be referred to as "up" and "down" in the following discussion. The transitions follow a Poisson distribution. The probability of an up transition is p_u, and is p_d for a down transition. The highly asymmetric random telegraph has a much higher probability of transition for one direction than the other. To determine the power spectrum of such a signal, one must first determine the autocorrelation function.

Writing the random telegraph wave as x(t), the autocorrelation function of the random telegraph wave is $\langle x(t)x(t+\tau)\rangle$. For x = 0 in the down state and x = A in the up state, the autocorrelation function can be determined by evaluating:

$$\langle x(t)x(t+\tau)\rangle = A^2\, P(u,\, 0)P(u,\, \tau|\, u,\, 0)$$

Here P(u, 0) is the probability of the random telegraph wave being in state "up" at time 0. This is just equal to $p_u/(p_u + p_d)$. P(u, τ| u, 0) is the probability of x(τ) being up, given that it was up at time 0. If $p_d \gg p_u$, then the probability x(t) will stay in the up state from time 0 to t is much larger than the probability it will changeover one or more times, and return to the up state at time τ. Thus P(u, t| u, 0) is approximately $\exp(-p_d\tau)$. The autocorrelation function can therefore be written:

$$\langle x(t)x(t+t)\rangle = \frac{A^2 p_u}{p_u + p_u} \exp(-p_d|\tau|)$$

Here the absolute value of τ is used since the autocorrelation function must be even. Applying the Wiener-Khintchine theorem to obtain the power spectrum, $S_x(\omega)$, yields:

$$S_x(\omega) = \frac{1}{\pi}\int_{-\infty}^{\infty} \frac{A^2 p_u}{p_u + p_u} \exp(-p_d|\tau|) \exp(-i\,\omega\,\tau)\, d\tau = \frac{A^2 p_u}{p_u + p_u} \frac{2\,p_d}{p_d^2 + \omega^2}$$

REFERENCES

1) Tyagai, V. A., and Lukyanchikova, N. B., *Surf. Sci.*, 12, 331 (1968)

2) Cardon, F., and Gomes, W. P., *Ber. Bunsengesell Phys. Chem.*, 74, 436 (1970)

3) Cardon, F., *Physica*, 52, 144 (1971)

4) Bellingham, J. G., MacVicar, M. L. A., Nisenoff, M., and Searson, P. C., *J. Electrochem. Soc.*, 133, 1753 (1986)

5) Iverson, W. P., *J. Electrochem. Soc.*, 115, 617 (1968)

6) Bertocci, U., and Krugger, J., *Surf. Sci*, 101, 608 (1980)

7) Bertocci, U., and Yang-Xiang, Y., *J. Electrochem. Soc.*, 131, 1011 (1984)

8) Hladky, K, and Dawson, J. L., *Corros. Sci.*, 21, 317 (1981)

9) Hladky, K, and Dawson, J. L., *Corros. Sci.*, 22, 231 (1981)

10) Bellingham, J. G., MacVicar, M. L. A., and Nisenoff, M., *IEEE Trans. on Mag.*, MAG-23, 477 (1987)

11) Gabrielli, C., Huet, F., and Keddam, M., *Electrochem. Acta*, 31, 1025 (1986)

12) Van Kampen, N. G., "Stochastic Processes in Physics and Chemistry", North-Holland, Amsterdam, p. 237 (1981)

13) Tyagai, V. A., *Electrochim. Acta*, 16, 1647 (1971)

14) Keizer, J., *J. Chem. Phys.*, 63, 398 (1975)

15) Keizer, J., *J. Chem. Phys.*, 64, 1679 (1976)

16) Gabrielli, C., Huet, F., and Keddam, M., *Electrochim. Acta*, 31, 1025 (1986)

17) Langevin, P., *C. R. Acad. Sci. Paris*, 146, 530 (1908)

18) Uhlenbeck, G. E., and Ornstein, L. S., *Phys. Rev.*, 36, 823 (1930)

19) Tyagai, V. A., and Lukyanchikova, N. B., *Surface Sci.*, 12, 331 (1968)

20) Barker, G. C., *J. Electroanal. Chem.*, 21, 127 (1969)

21) Tyagai, V. A., *Electrochim. Acta*, 18, 229 (1973)

22) Barker, G. C., *Pure Appl. Chem.*, 15, 239 (1967)

23) van Vliet, K. M., *J. Math. Phys.*, 12, 1981 (1971)

24) van Vliet, K. M., *J. Math. Phys.*, 12, 1998 (1971)

25) Kiezer, J., *J. Chem. Phys.*, 63, 5037 (1975)

26) Musha, T., and Sugita, K., *J. Phys. Soc. Japan*, 51, 3820 (1982)

27) Musha, T., Sugita, K., and Kanelo, M., in "Noise in Physical Systems and 1/f Noise", Savelli, M., Lecoy, G., and Nougier, J. P. editors, Elsivier, Amsterdam, p. 398 (1983)

28) de Vos, A., van den Berg, R. J., and de Goede, J., *Phys. Lett.*, 102A, 320 (1984)

29) van den Berg, R. J., and de Vos, A., *Phys. Lett.*, 92AP, 203 (1982)

30) van den Berg, R. J., de Vos, A., and de Goede, J., *Phys. Lett.*, 87A, 98 (1981)

31) Feher, G., and Weissman, M., *Proc. Nat. Acad. Sci.*, 70, 870 (1973)

32) Kolb, H. A., and Woermann, D., *J. Chem. Phys.*, 80, 3781 (1984)

33) Brodd, R. J., and Leger, V. E., in "Encyclopedia of Electrochemistry of the Elements", ed. A. J. Bard, Vol. 5, Dekker, New York, p. 2 (1976)

34) Leistra, J. A, and Sides, P. J., *J. Electrochem. Soc.*, 134, 2442 (1987)

35) Dees, D. W., and Tobias, C. W., *J. Electrochem. Soc.*, 134, 1702 (1987)

36) Dees, D. W., and Tobias, C. W., *J. Electrochem. Soc.*, 134, 369

(1987)

37) Hine, F., Yasuda, M., Nakamura, R., and Noda, T., *J. Electrochem. Soc.*, 122, 1185 (1975)

38) Kuhn, A. T., and Stevenson, M., *Electrochim. Acta*, 27, 329 (1982)

39) Janssen, L. J. J., and Barendrecht, E., *Electrochim. Acta*, 28, 341 (1983)

40) Sides, P. J., and Tobias, C. W., *J. Electrochem. Soc.*, 127, 288 (1980)

41) Duckovic, J., and Tobias, C. W., *J. Electrochem. Soc.*, 134, 331 (1987)

42) Sides, P. J., and Tobias, C. W., *J. Electrochem. Soc.*, 129, 2715 (1982)

43) Gabrielli, G., Huet, F., Keddam, M., and Macias, A., in "Surfaces, Inhibition, and Passivation", McCafferty, E., and Brodd, R. J., Editors, The Electrochemical Society, Penington, NJ, p. 507 (1986)

44) Kannangara, D. C. W., and Conway, B. E., *J. Electrochem. Soc.*, 134, 894 (1987)

45) Haung, K., "Statistical Mechanics", John Wiley & Sons, New York, p. 332 (1963)

46) Gilmer, G. H., *Science*, 208, 355 (1980)

47) Temkin, D. E., *Sov. Phys. Crystalogr.*, 14, 344 (1969)

48) Solov'ev, V. V., and Borisov, V. T., *Sov. Phys. Dokl.*, 17, 8 (1972)

49) Gilmer, G. H., *J. Cryst. Growth*, 42, 3 (1977)

50) Cahn, J. W., *Acta Met.*, 8, 554 (1960)

51) Honig, J. M., "The Solid Gas Interface", ed. Flood, E. A., Dekker, New York, (1967)

52) Gilmer, G. H., *J. Cryst. Growth*, 49, 465 (1980)

53) Blyholder, G., in "Modern Aspects of Electrochemistry", Bockris, J. O'M. and Conway, B. E., editors, Plenum Press, New York, p. 1 (1976)

54) Delahay, P., *J. Phys. Chem.*, 70, 2373 (1966)

55) Holub, K., Tessari, G., and Delahay, P., *J. Phys. Chem.*, 71, 2612 (1967)

56) Delahay, P., and Holub, K., *J. Electroanal. Chem.*, 16, 131 (1968)

57) Macdonald, D. D., and Urquidi-Macdonald, M., *J. Electrochem. Soc.*, 132, 2316 (1985)

58) Urquidi-Macdonald, M., Real, S., and Macdonald, D. D., *J. Electrochem. Soc.*, 132, 2316 (1985)

59) Pourbaix, "Atlas of Electrochemical Equilibria in Aqueous Solutions", Pergamon Press, New York (1966)

60) Shreier, L. L., "Corrosion", George Newnes Limited, London

61) Grauer, R., and Feitknecht W., *Corros. Sci.*, 7, 629 (1967)

62) Stumm, W. S., and Morgan, J. J., "Aquatic Chemistry, An Introduction Emphasising Chemical Equilibrium in Natural Waters", John Wiley & Sons, Inc., New York (1981)

63) Roetheli, B. E., Cox, G. L., and Littreal, W. B., *Metals & Alloys*, 3, 73 (1932)

64) Bressen, J., and Wiart, R., *J. Appl. Electrochem.*, 9, 43 (1979)

65) Epelboin, I., Ksouri, M., Lejay, E., and Wiart, R., *Electrochim. Acta*, 20, 603 (1975)

66) Epelboin, I., Ksouri, M., and Wiart, R., *J. Electroanal. Chem.*, 65, 373 (1975)

67) Epelboin, I., Ksouri, M., and Wiart, R., *J. Electrochem. Soc.*, 122,

1206 (1975)

68) Epelboin, I., Ksouri, M., and Wiart, R., *J. Electroanal. Chem.*, 58, 433 (1975)

69) Epelboin, I., Ksouri, M., and Wiart, R., *J. Less Common Metals*, 43, 235 (1975)

70) Sorenson, D. T., Davidson, A. W., and Klinberg, J., *J. Inorganic Nucl. Chem.*, 13, 64 (1960)

71) James, W. J., Straumanis, M. E., and Johnson, J. W., *Corrosion*, 23, 15 (1967)

72) Straumanis, M. E., and Wang, Y., *Corrosion*, 22, 132 (1967)

73) Johnson, J. W., Sun, Y. C., and James, W. J., *Corros. Sci.*, 11, 153 (1971)

74) James, W. J., and Stoner, G. E., *J. Am. Chem. Soc.*, 85, 1354 (1963)

75) Kim, J. T., and Jorné, J., *J. Electrochem. Soc.*, 127, 8 (1980)

76) Uhlig, H. H., "Corrosion and Corrosion Control", John Wiley & Sons, New York, p. 28 (1985)

77) Abdou, A. H., *Phil. Mag.*, 45, 105 (1954)

78) Bressan, J., and Wiart, R., *J. Appl. Electrochem.*, 9, 43 (1979)

79) Horn, F. H., *Phil. Mag.*, 43, 1210 (1952)

80) Erdey-Gruz, T., "Kinetics of Electrode Processes", Adam Hilger, London (1972)

81) Kuhn, A. T., Yusof, J., B., and Hogan, P., *J. of Appl. Electrochem.*, 9, 765 (1979)

82) Vondracek, R., and Izak-Krizko, J., *Annales de Chimie et de Physique*, 44, 376 (1925)

83) Troquet, M., and Pageitti, J., *Mat. Chem. and Phys.*, 14, 193 (1986)

84) Troquet, M., and Pageitti, J., *Electrochim. Acta*, 27, 197 (1982)

85) Troquet, M., Labbe, J. P., and Pageitti, J., *Corr. Sci.*, 21, 101 (1981)

86) Troquet, M., and Pageitti, J., *Electrochimica Acta*, 21, 101 (1981)

87) Hauser, A., "The Corrosion of a Zinc Rotating Electrode in One Molar Hydrochloric Acid", Masters Thesis, Dept. of Chem Engineering, U. of Calif., Berkeley (1984)

88) Jaklevic, R. C., Lambe, J., Silver, A. H., and Mercereau, J. E., *Phys. Rev. Lett.*, 12, 159 (1964)

89) Jaklevic, R. C., Lambe, J., Mercereau, J. E., and Silver, A. H., *Phys. Rev.*, 140, A1628 (1964)

90) Zimmerman, J. E., Beall, J. A., Cromar, M. W., and Ono, R. H., *Appl. Phys. Lett.*, 51, 617 (1987)

91) Nakane, H., Nishino, T., Hirano, M., Takagi, K., and Kawabe, U., *Jap. J. of Appl. Phys.*, 26, L1581 (1987)

92) Biomagnetic SQUID System, 2nd Order Gradiometer, Manufactured by Biomagnetic Technologies Inc., San Diego, CA

93) Romani, G. L., Williamson, S. J., and Kaufman, L., *Rev. Sci. Instrum.*, 53, 1815 (1982)

94) Ott, H. W., "Noise Reduction Techniques in Electronic Systems", Wiley, New York, p. 157 (1976)

95) Shideler, R. W., and Bertocci, U., *J. of Research of NBS*, 85, 211 (1980)

96) Harris, F. J., *Proc. IEEE*, 66, 51 (1978)

97) Welch, P. D., *IEEE Trans. Audio and Electroacoust.*, AU-15, 70 (1967)

98) Geckinli, N. C., "Discrete ourier Transformation and Its Application

to Power Spectra Estimation", Elsevier, Amsterdam, p. 47 (1983)

99) Bendat, J. S., and Piersol, A. G., "Random Data", Wiley, New York, p. 362 (1986)

100) Kendig, M. W., Meyer, E. M., Lindberg, G., and Mansfeld, F., *Corros. Sci.*, 23, 1007 (1983)

101) Mansfeld, F., *Corrosion*, 38, 301 (1982)

102) Mansfeld, F., *Corrosion*, 36, 301 (1981)

103) Hladky, K., Callow, L. M., and Dawson, J. L., *Br. Corros. J.*, 15, 20 (1980)

104) Gabrielli, C., "Identification of Electrochemical Processes by Frequency Response Analysis", Solartron

105) Halsey, T. C., *Phys. Rev. A*, 36, 5877 (1987)

106) Bates, J. B., Chu, Y. T. and Stribling, W. T., *Phys. Rev. Lett.*, 60, 627 (1988)

107) Armstrong, R. D., and Burnham, R. A., *J. Electroanal. Chem.*, 72, 257 (1976)

108) Bard, A. J., and Faulkner, L. R., "Electrochemical Methods", John Wiley & Sons, New York, p. 501 (1980)

109) McWhorter, A. L., "1/f Noise and Related Surface Effects in Germanium", Lincoln Lab. Rpt. No. 80, Boston (1955)

110) van der Ziel, A., "Noise in Solid State Devices and Circuits", John Wiley & Sons, New York, p. 125 (1986)

111) Bockris, J. O'M., and Reddy, A. K. N., "Modern Electrochemistry 2", Plenum Press, New York, p. 692 (1970)

112) Weast, R. C., and Astle, M. J., ed., "CRC Handbook of Chemistry and Physics", 63rd ed., CRC Press, Boca Raton, p. D-240 (1982)